Chapter 15

The Law of Inertia as Drawn by CFLE Theory

"In fact, if an observer inside an accelerated Einstein's chamber released an apple having a negative gravitational mass, the apple would 'fall upward' (in respect to the space ship), and, as observed from outside, would move with an acceleration twice that of the space ship without being subject to any outside forces. Thus we will be forced to choose between Newton's Law of Inertia and Einstein's Principle of Equivalence — a very difficult choice indeed!"

George Gamow (1904–1968)

15.1 Force Line Arrangement to Ensure (Ensue) Inertia for Real Life

Figure 15-1-1 gives an example of a situation that can be easily experienced in real life. The figure part A shows the gravitational force line arrangement when a car moves with constant speed, much like the magnetic field in classical electrodynamics.

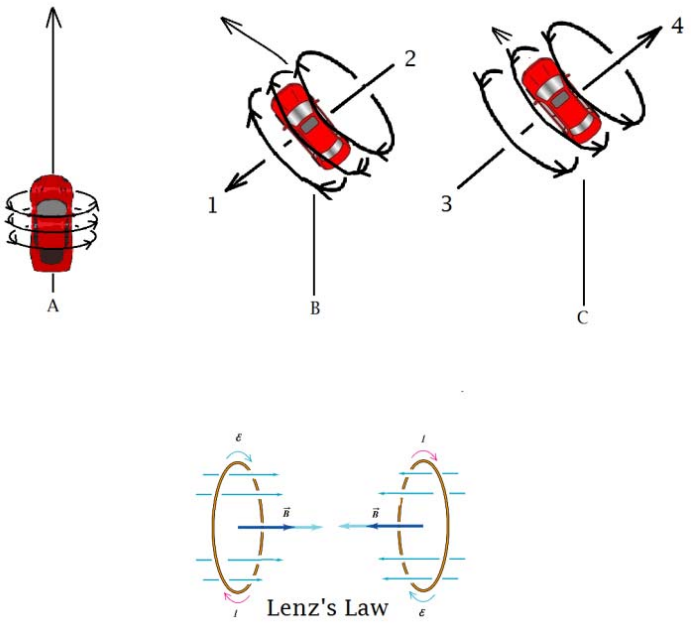

Figure 15-1-1

The figure part B is the force line arrangement when a car starts rotation to the left side, where there should be a centripetal point. Now the vehicle's acceleration is influenced by the acceleration from point 2 to point 1, and much like the case of action and reaction, a new force line arrangement state called "inertia" occurs from point 3 to point 4. Such gravitational situation corresponds to "Lentz's law" in classical electromagnetic theory. However, the real situation and the situation in Figure 15-1-1 of "Lentz's law" are different. The circular movement that Lentz's law expresses is the current of the electric charge, and its force line is newly generated as the magnetic force line that tries to offset this electric charge current. What this electromagnetic phenomenon explains is that in order to ensure the exclusions principle with macro-scale energy, conservation law must be followed. Thus, for a gravitational force that has force lines, the same law of inertia and law of energy conservation should exist according to the correspondence property of every force line element.

15.2 Force Line Arrangement to Ensure Inertia for Photon Radiation

When acceleration is initiated, the force line arrangements that occur when particles collide with resistant material in space are as shown in Figure 15-2-1. Here, because the gravitational force lines crowd the magnetic plane, the perfect spherical shape is changed to an oval. (However, in order to clearly demonstrate the direction of movement, a cylinder form is used in the following figures.)

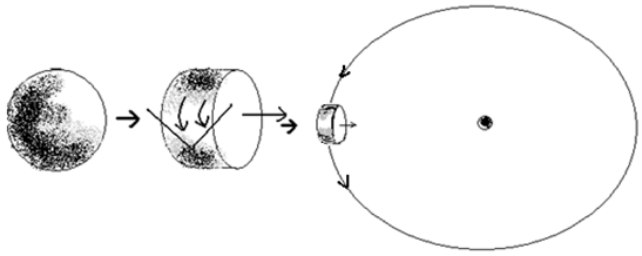

Figure 15-2-1

This magnetic field is called the "first acceleration magnetic field."

From this stage, the particle becomes more accelerated, and the force line arrangement resulting from resistance of accelerating particles against resistant material is shown in Figure 15-2-2.

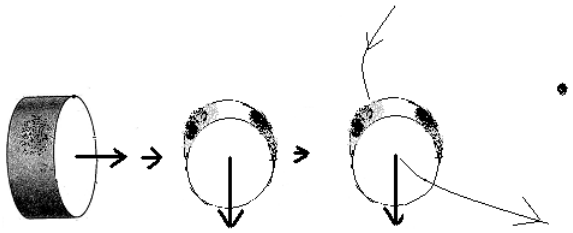

Figure 15-2-2

This force line arrangement occurs to ensure orbital movement of the particle. Therefore, this magnetic field is called the "orbital magnetic field" or "second accelerations magnetic field." That is, this magnetic field is none other than the magnet field B of classical electrodynamics. From this stage, as the particle becomes more accelerated, a further new force line arrangement results because of inertia, as shown in Figure 15-2-3.

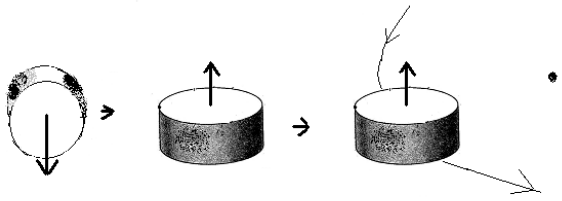

Figure 15-2-3

This field is called the spin magnetic field or the third accelerations magnetic field. This force line arrangement of the particle can expend the increasing acceleration energy through rotation of the orbital plane itself. From this stage of further particle acceleration, another force line arrangement will result because of inertia. This is shown in Figure 15-2-4.

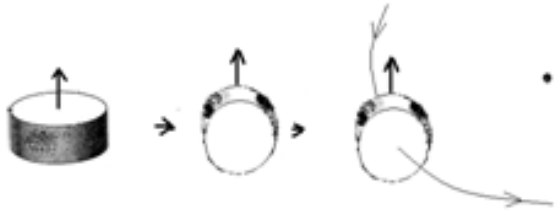

Figure 15-2-4

This field is called the reversal spin magnetic field. When the particle accelerates even more, another force line arrangement due to inertia occurs, as shown in Figure 15-2-5.

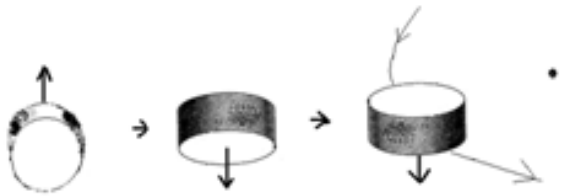

Figure 15-2-5

This field is called the reverse orbital magnetic field. Finally, with greater particle acceleration, a final force line arrangement develops, as in Figure 15-2-6.

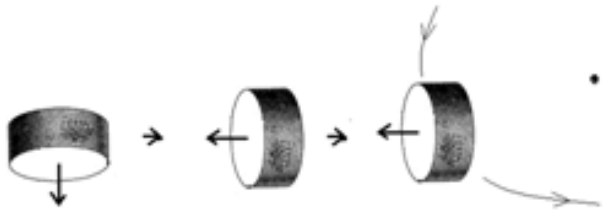

Figure 15-2-6

That is, the particle tries to move in the anti direction of acceleration. This final resistance is observed as the original inertia. Without knowledge about these changes of force line arrangements, an observer tends to think that "there should be a centrifugal force," in other words, "inertial force and centrifugal force should be the same and are an apparent force." However, because of all these force line arrangements, CFLE theory treats such centrifugal force and inertial force as physically existing real forces, not apparent forces. However, as the accelerations force becomes stronger at each stage, the particle must be able to accept and bear such exertion. Therefore, the particle has to newly arrange its force lines to adapt to the increasing acceleration. Because such exerted-upon particle sends out contradictorily arranged force lines that are oriented anti direction against acceleration, this

"presented force line" is observed as electromagnetic wave radiation. Such a phenomenon can be considered with the viewpoint of gauge theory. That is, because of the change in momentum ($p = mv$), as a wave packet, the particle wants to maintain gauge symmetry, and so it sends away the changed momentum and related force line to outside of its system in the form of the observed radiation.

15.3. Force Line Arrangement to Ensure Inertia for Establishing Quantization

During the process of particle acceleration, photons are emitted from the accelerating particle. After such photon emission, and once the particle has adapted to the outside situation and no longer needs to emit photons, the particle reaches a stable state in which the quantum state is balanced. Figure 15-3-1 shows this process.

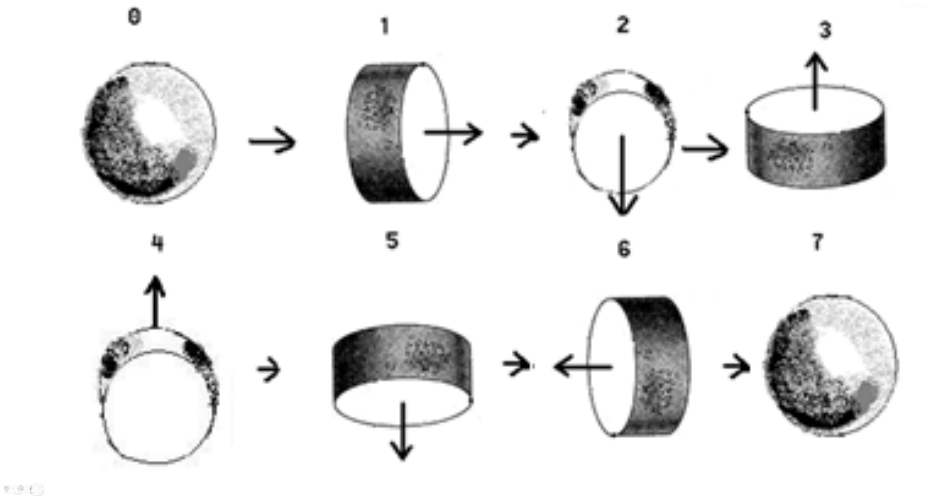

Figure 15-3-1

That is, after the 6 steps comes the photon radiation step. However, once the energy state reaches a balanced state, no further photon emission is needed after step 6 and the process restarts from the first step. The particle repeats steps 1 through 6 without photon radiation for a long time. The first step is like an aphelion, and the sixth step is like a perihelion. Therefore, almost every usual orbital form becomes universally ellipse. Such physical quantization steps by inertia are an important reason for the success of quantum theory. So far, however, the successes of present quantum theory are proven and emphasized

only through the mathematical process, but the physical process cannot be shown. But now, CFLE theory can explain the physical process and highlight the limitation of quantum theory successfully.

15.4 Force Line Arrangement to Ensure Inertia for Spin and Helicity

§15.3 discussed the quantization process by inertia with force lines. In the third step, the spin magnetic field occurs, as shown in Figure 15-4-1.

Figure 15-4-1

However, from the same spin magnetic field, a particle can use two different directions of rotation, as shown in Figure 15-4-2.

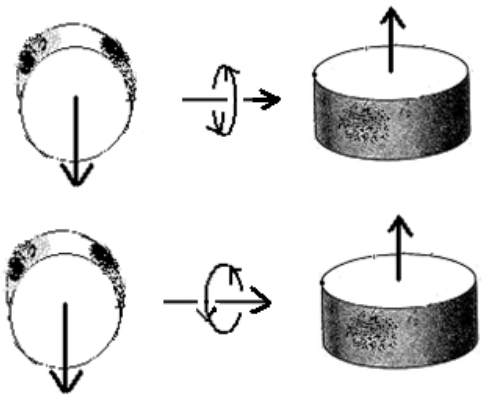

Figure 15-4-2

This force line arrangement can occur in degrees of freedom of force line elements.

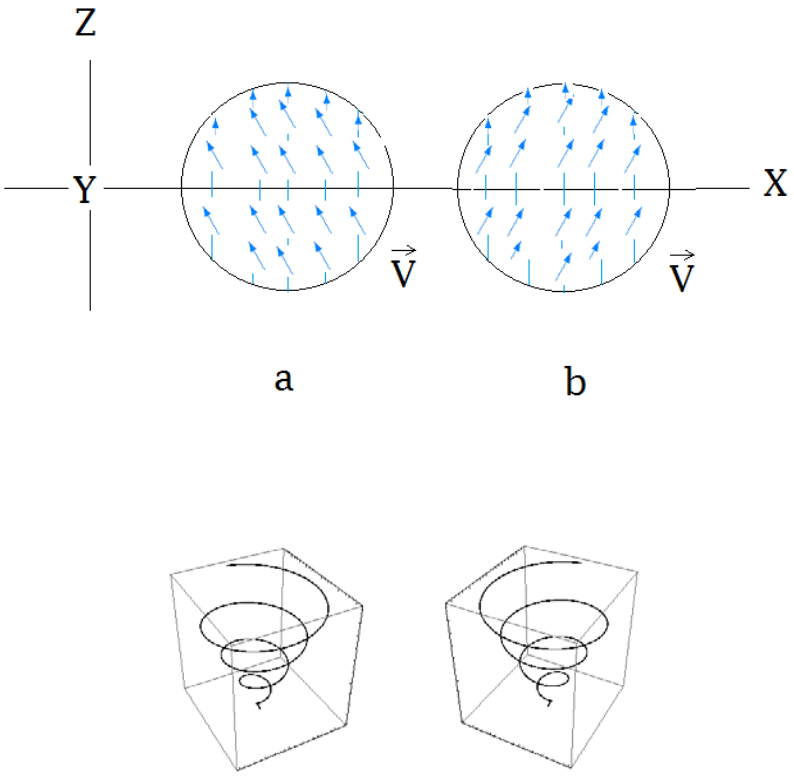

Figure 4-4-13

15.5 Force Line Arrangements to Ensure Inertia for Quantization of the Big-Bang and Big-Crunch

Quantization by force line arrangement can be used for expansion and contraction of the universe. Because every object has gravitational force lines, the force line arrangement steps discussed in §15.3 can apply to free-fall and recoil, as seen in Figure 15-5.

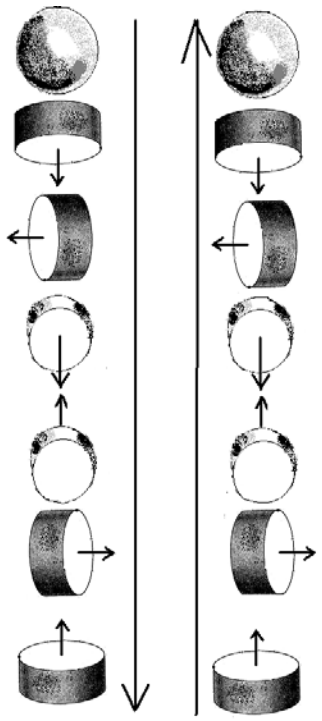

Figure 15-5

This force line arrangement occurs step by step to reached the aphelion (maximum expansion), with the first step starting as free-fall (contraction of the universe), and finishing as a step 8 (maximum contraction). In this phase, each object emits its force lines as photons.

Conclusion: end of the big bang is changed to big crunch by inertia.

15.6. Quantum Theoretical Background of Orbital Movement in CFLE Theory

In 1913, Niles Bohr established an atomic model that agreed well with observed facts postulated by quantum theory. In 1926, E. Schrödinger developed another atomic model using the wave equation, because there were serious discrepancies in the background of the Bohr atomic model. At that time, physicists pondered the stability of the atom. According to classical electrodynamics, because of acceleration by the electromagnetic force, the electrons that are revolving around the protons should fall into the protons with radiation of an electromagnetic wave, but instead the electrons stay for a long time in their orbit without photon radiation. Thus, physicists could not understand the

nature of the atom. Sir Isaac Newton was faced with the same problem 300 years earlier, and unfortunately he could not solve this problem, despite solid attempts to do so. Two hundred years later, Albert Einstein too was faced with the same problem, and the solution eluded him, despite his attempt to solve the mystery of the general quantum theoretical nature with the cosmological constant $k = \Lambda$. Because modern physics had abandoned the force line that was introduced by Michael Faraday, and even also abandoned the physical real inertial force, current physics cannot solve the same problem that expanded to gravitational phenomena.

CFLE theory, however, successfully solves this problem by introducing the force line and its force line element, and by inertia from force lines. When the force line is curved, the previous steps are changed, as seen in Figures 15-6-1 through 15-6-3.

Figure 15-6-1. Under flat force lines

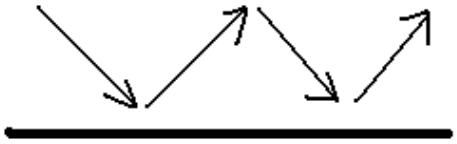

Figure 15-6-2. Under middle curved force lines

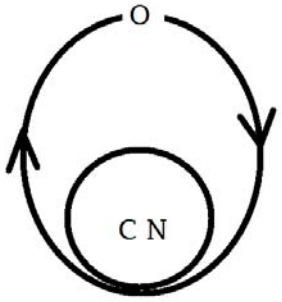

Figure 15-6-3. Under strong curved force lines

Figure 15-6-1 shows that normal freefall and reaction. Figure 15-6-3 shows that freefall path in strong curved frame of reference. O is the as aphelion of atomic orbit, and CN is the positive center of nucleus. Even case of simple freefall has to move in sphere shape path.

In figure 15-6-3 there are also oddities concerning the geometrical properties intrinsic spin. If an ordinary spinning body is rotated in space through 360^o it returns to its original configuration. A particle with spin$\frac{1}{2}$, however, will not do this. If such particle is rotated through 360^o it assumes a quantum state with measurably different physical properties. To return the particle to its initial state it is necessary to rotate it through720^o. In other words, a spin $\frac{1}{2}$particle requires a double rotation relative to $'everyday'$ objects before it $'comes\ back\ to\ its\ staring\ state'$. Therefore, g factor of spin $\frac{1}{2}$ state should be$g = 2$. Because this double rotation free-fall of photon near the sun should be double.(cf.§20.3)

15.7 The Uncertainty Principle, Mass Screening Theory, Inertial Law, and CFLE Theory

In 1924, De Broglie introduced the mater–wave concept for an object, and Davisson and Germer proved the existence of the mater-wave in 1927. Therefore, every object cannot escape application of the uncertainty principle. According to this principle, every object should be explained as a wave packet. From this uncertain position and uncertain momentum of an object, an observer cannot measure these parameters infinitely at the precise same time. Namely, $\Delta MV\Delta X \geq \hbar$.

This is none other than Heisenberg's uncertainty principle. However, speed V ought to be constant by inertial law in order to satisfy the relativity theory. Whether observing a particle in the micro world or a galaxy in the macro world, inertial law should be used, and the Heisenberg uncertainty principle can be changed as follows:

$$\Delta M\Delta X \geq \frac{\hbar}{V} \qquad 15\text{-}7\text{-}1$$

This is not just an ordinary mathematical transposition, because the formula after this transposition should be called mass screening theory. Because of the inertial law of the force line elements theory, the right side of the equation is always constant, leaving ΔX and ΔM to have inversely proportional quantities. Thus, the ΔX mass screening property and the inertia property should occur at the same time. To satisfy such condition, ΔX should be formed with real force line elements, and only then can we unify the relativity and quantum theories and inertial law and uncertainty principle as one theory by CFLE theory. Therefore, the

property of mass uncertainty degree ΔM and the property of position uncertainty degree ΔX as functions of velocity V (as discussed in §4) are properties of force lines and their force line elements.

When the V in the Heisenberg uncertainty principle ($\Delta MV\Delta X \geq \hbar$) cannot transpose from the left side to the right side, the Heisenberg uncertainty principle, inertial law, and theory of relativity become isolated theories to one another. Therefore, this formula $\Delta M\Delta X \geq \frac{\hbar}{V}$ is called the unified mass screening theory.

15.8 Solving Mystery of Solar Looping and Coronal Mass Ejection by CFLE theory

The correspondence property of every force line element asserts that inertia should occur for huge objects too. According to quantum theory and CFLE theory, the formation of inertia occurs in a series of steps that can be graphically expressed as in Figures 15-8-1 through 15-8-6, depicting the revolution of Earth.

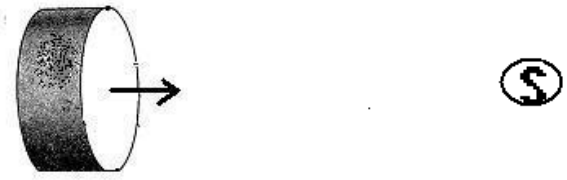

Figure 15-8-1. First step: acceleration gravitomagnetic field state

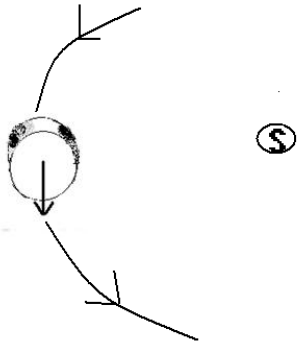

Figure 15-8-2. Second step: orbital gravitomagnetic field state

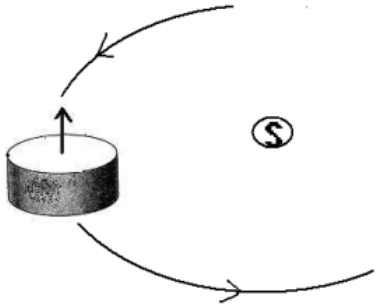

Figure 15-8-3. Third step: spin gravitomagnetic field state

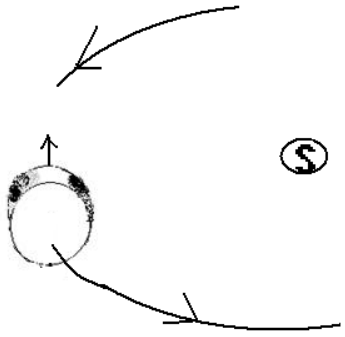

Figure 15-8-4. Fourth step: inertia anti orbital gravitomagnetic field state

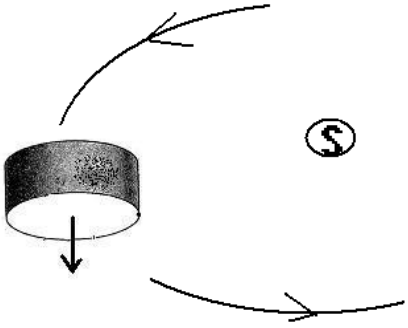

Figure 15-8-5. Fifth step: inertia anti spin gravitomagnetic field state

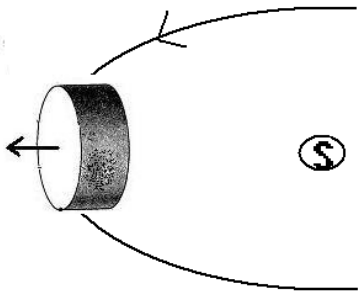

Figure 15-8-6. Sixth step: inertia anti acceleration gravitomagnetic field state

Such inertia can occur on Earth and the sun's rotation, as expressed in figures 15-8-7 through 15-8-12 (where Earth is shape as a cylinder form for clearer depiction of the force lines.)

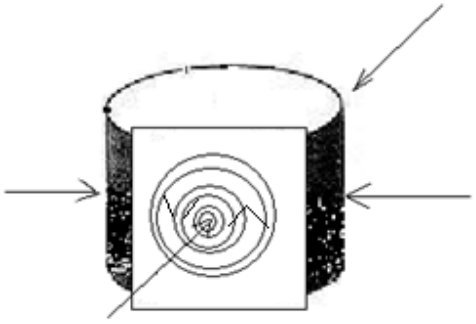

Characteristics: volume decrease, radius contraction

Figure 15-8-7. First step: rotation acceleration gravitomagnetic field state

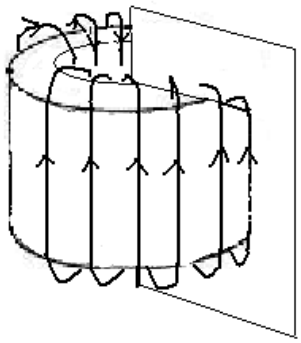

Figure 15-8-8. Second step: rotation orbital gravitomagnetic field state

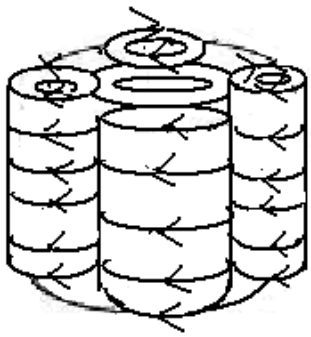

Characteristics: Rotation speed increase

Figure 15-8-9. Third step: rotation spins gravitomagnetic field state.

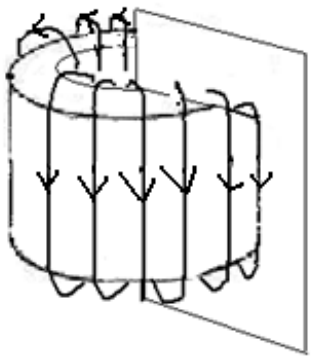

Characteristics: Rotation speed decrease. Energy emission

Figure 15-8-10. Fourth step: inertial anti orbital gravitomagnetic field state

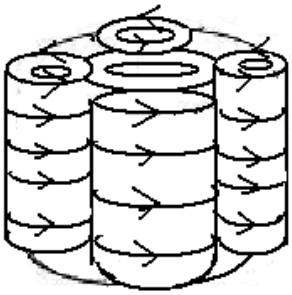

Characteristic: Heat radiation

Figure 15-8-11. Fifth step: inertia anti spin gravitomagnetic field state

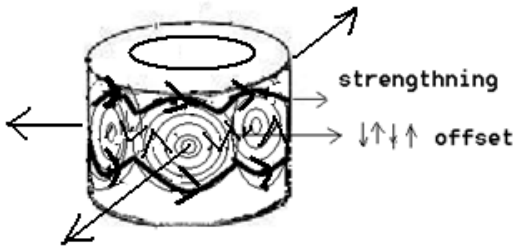

Characteristics: Volume increase, radius increase, atmosphere increase

Figure 15-8-12. Sixth step: inertial anti acceleration gravitomagnetic field state

After this state, the process repeats itself from the first step. Because of the strong rotation gravitomagnetic field, magnetic reversal by revolution of Earth cannot occur. However, an inertial anti acceleration gravitomagnetic field state can be expressed (see Figure 15-18-13).

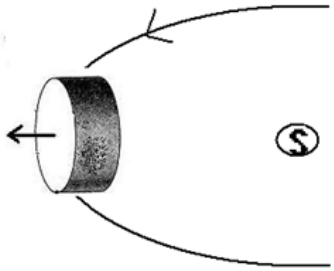

Figure 15-8-13

At this time, inertial force by anti acceleration cannot fall down the axis of the rotation, but the component of the inertial force remains on the inertial plane, as shown in Figure 15-8-14.

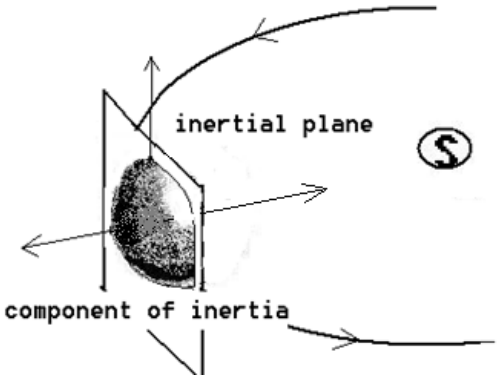

Figure 15-8-14

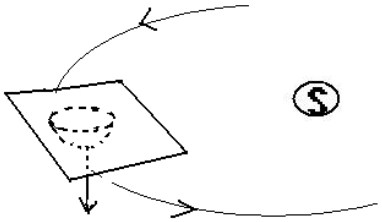

Figure 15-8-15. First step: change of inertial plane

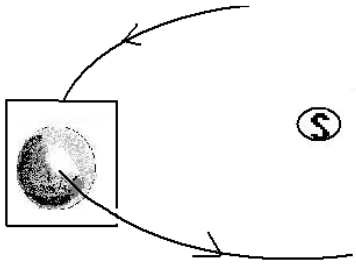

Figure 15-8-16. Second step: change of anti orbital state plane

Phenomena that occur by such inertial forces on Earth include the continental drift, El Nino, and magnetic hall in the sky over Brazil. On the sun, corresponding phenomena include sunspot generation, its polarity change, magnetic loop generation, protuberant generation, generation of flare energy, occurring of filaments, pulsation of the sun and stars, etc. In the CFLE theory, momentum is

$p = mv$

changed to

$$F = \frac{d}{dt}(P) = \frac{d}{dt}(mv)$$

$$= v\left(\frac{dm}{dt}\right) + m\left(\frac{dv}{dt}\right)$$

$$= iv + ma \qquad 15\text{-}8\text{-}1$$

Because in the Newtonian theory there is no mass change, the first term of the right side is equal to zero; that is,

$iv = 0$

Therefore, there is only

$$F = ma \qquad 15\text{-}8\text{-}2$$

In the classical theory of relativity, because $F = iv + ma$ is only a property of empty space, there can exist charge current or mass current. But, in CFLE theory, the first term of the right side of Eq. 15-8-1 ($\frac{dm}{dt} = i$) can be considered as a "mass current," as in the "charge

current" of classical electrodynamics. This "mass current" can be used in real physical situations, which is a defining difference between the classical theory of relativity and the CFLE theory of relativity.

The mass current of rotation of Earth and the mass current of revolution of Earth can be expressed with a simple figure (Figures 15-8-17 and 15-8-18).

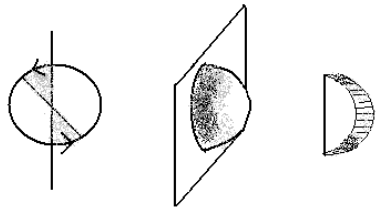

Figure 15-8-17. $\frac{dm}{dt} = i_{\text{rotation}}$

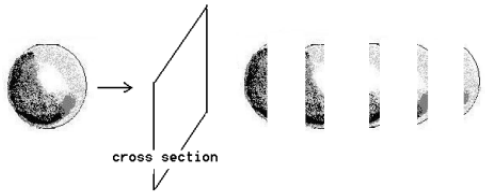

Figure 15-8-18. $\frac{dm}{dt} = i_{\text{revolution}}$

The moment, during unit time, when the mass passes the unit cross-section is called the revolutions pack (Figure 15-8-18). The mass pass cross-section during rotation is called the rotations pack (Figure 15-8-17). Now, using a simple figure (Figure 15-8-19) of the rotations pack and revolutions pack, the process of inertial force formation can be shown.

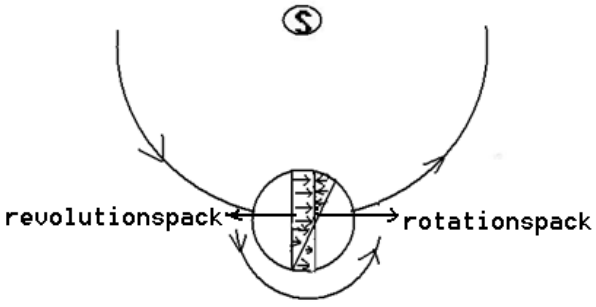

Figure 15-8-19

At this moment, on the centripetal side of Earth (Pacific Ocean), the rotations pack collides with the revolutions pack. Because this collision creates undue energy, such excess energy flows to the centrifugal side (Atlantic Ocean). Figure 15-8-20 depicts this process.

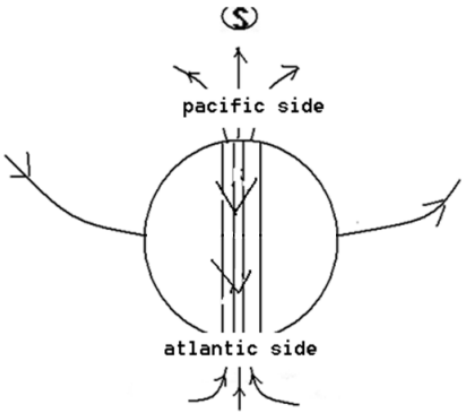

Figure 15-8-20

In the case of the sun, this is the cause of coronal mass ejections (CMEs), as shown in Photo 15-8-1.

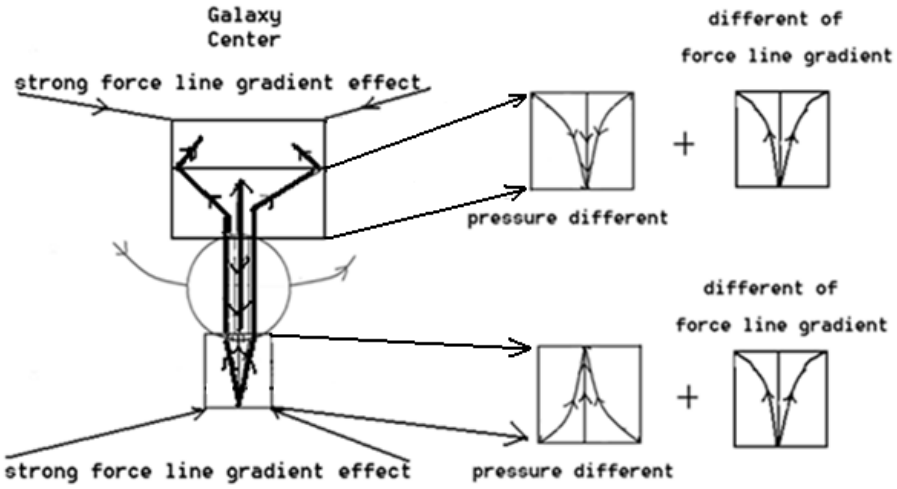

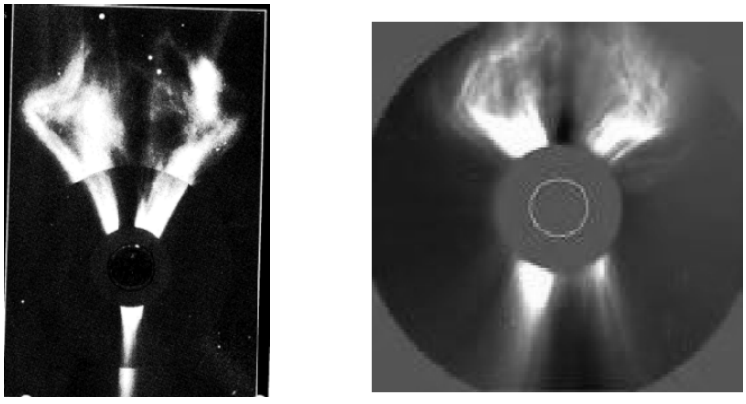

(A) Example of one same spin **(B) Example of two different spins**

Photo 15-8-1. **(Source: SOHO, NASA/ESA)**

The inertial force line arrangement on the inertial plane can be expressed by Figure 15-8-21 (where hexahedrons are used instead of spheres for clearer description).

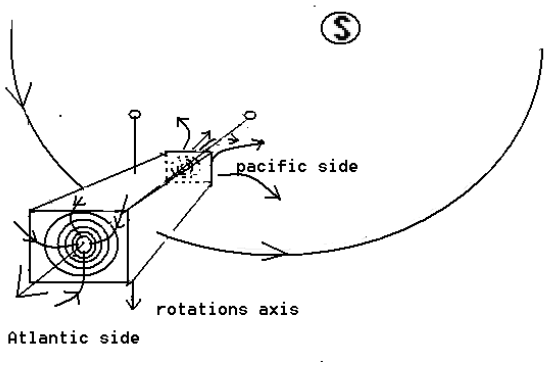

Figure 15-8-21

At this point, the inertial force tries to fall down the rotation axis and attempts to change the anti spin gravitomagnetic field state (Figure 15-8-22).

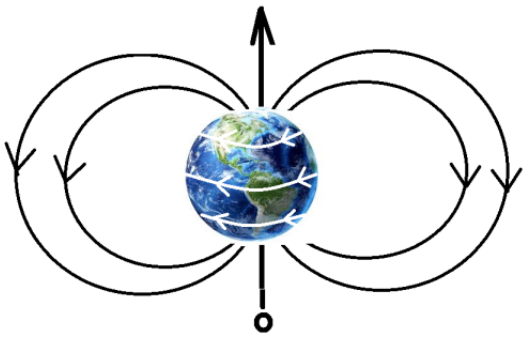

Figure 15-8-22

This situation implies that Earth will fall down by inertial force and the anti-spin state change. However, because of the action-reaction law, the inertial plane rotates to the anti-spin state, and the inertial force does not really cause Earth to fall down (see Figure 15-8-23).

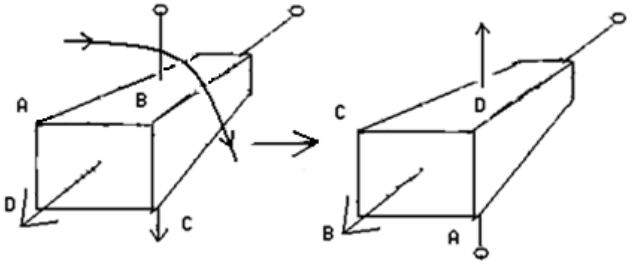

Figure 15-8-23

However, the inertial force has another component, the anti-rotation state. Although the inertial force tries to change the rotation direction of Earth, it cannot really do so, and instead it changes the inertial plane itself by interaction with Earth (Figure 15-8-24).

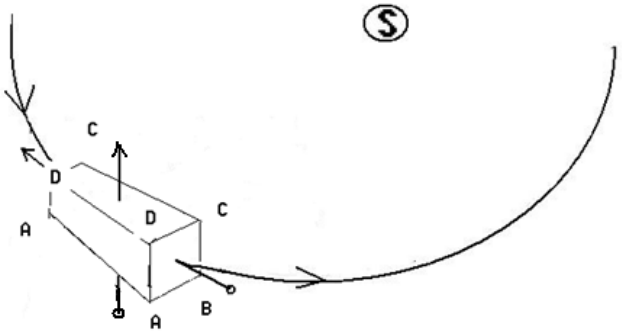

Figure 15-8-24

The inertial force has still one last component to initiate, the anti-start state (Figure 15-8-25).

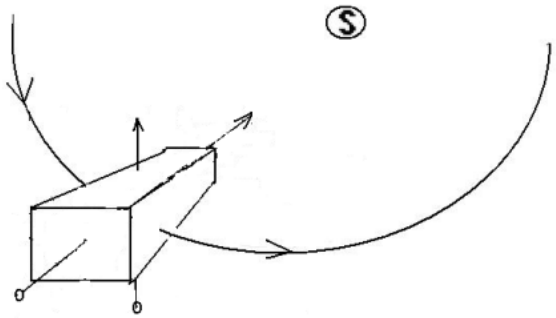

Figure 15-8-25

However, the inertial plane of rotation changes as seen in Figures 15-8-26 through 15-8-31.

A: *Rotation Accelerations Gravitomagnetic Field State*

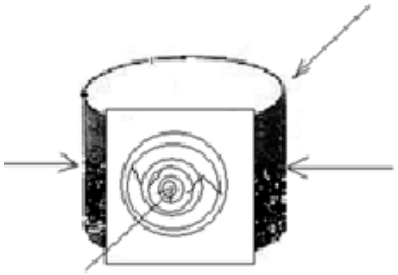

Figure 15-8-26. Reason of energy flow for fast continental drift or sunspot and CME

B: *Rotation Orbital Gravitomagnetic Field State*

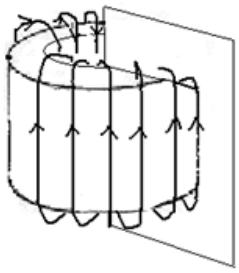

Figure 15-8-27. Characteristics: Vertical circle loop

C: *Rotation Spins Gravitomagnetic Field State*

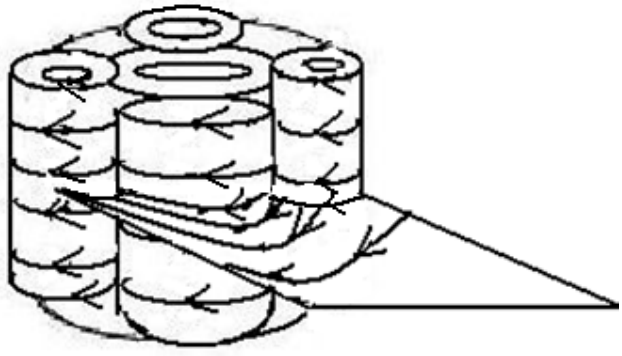

Figure 15-8-28. Characteristics: El Nino or Loop

D: *Inertial Anti Spin Gravitomagnetic Field State*

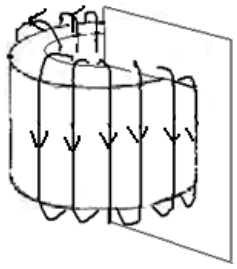

Figure 15-8-29. Characteristics: La Nina or loop and strong CME

E: *Inertial Anti Orbital Gravitomagnetic Field State*

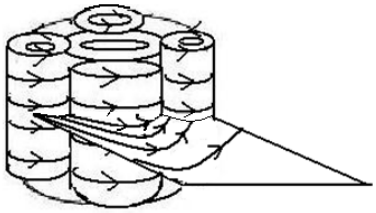

Figure 15-8-30. Characteristics: Vertical circle loop

F: *Inertial Anti Acceleration Gravitomagnetic Field state*

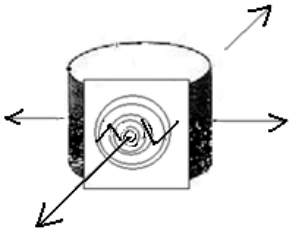

Figure 15-8-31. Characteristics: slow continental drift or anti sunspot

At state A, filaments appear because of the force line running as shown in Figure 15-8-32.

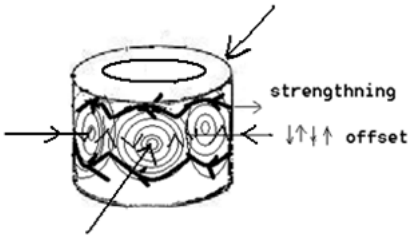

Figure 15-8-32. Characteristics: mottels and filaments

On the sun's surface, there are lots of force line distributions (Figures 15-8-33 and 15-8-34).

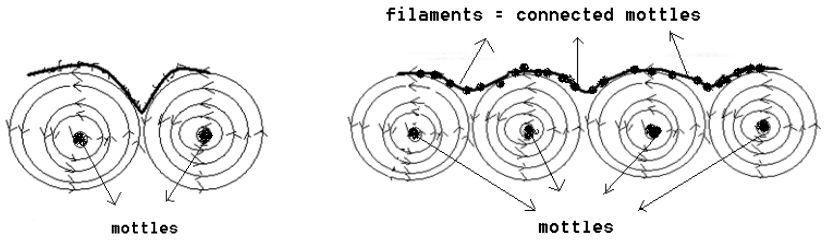

Figure 15-8-33

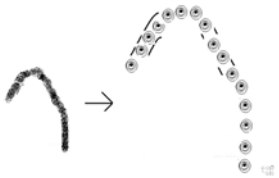

Figure 15-8-34

The real shape of mottles and filaments on the sun's surface are shown in the panels in Photo 15-8-2.

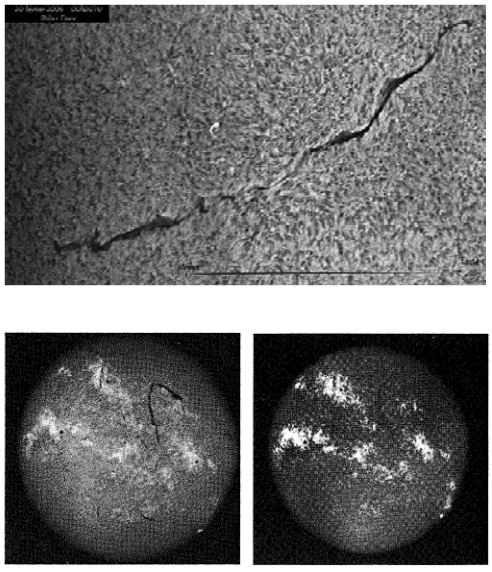

Photo 15-8-2 (Source: *Top panel*: SOHO, NASA/ESA. *Bottom panels*: Kiepenheuer, K. O. 1953. *The Sun*, p. 433. G. P. Herausg, Editor. Reproduced with permission from University of Chicago Press © 1953.)

Between states A and states B, and states F and states A, there occur rings that form a protuberant.

The force line arrangement of states A is shown by Figure 15-8-35.

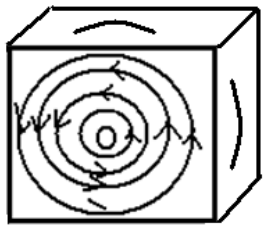

These force lines distribute on the sun's surface

Figure 15-8-35

At the start of states B, the rotated plane of force lines distribution is as shown in Figures 15-8-36.

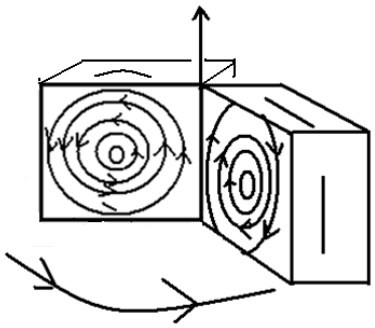

Rotation of inertial plane and related loop generating

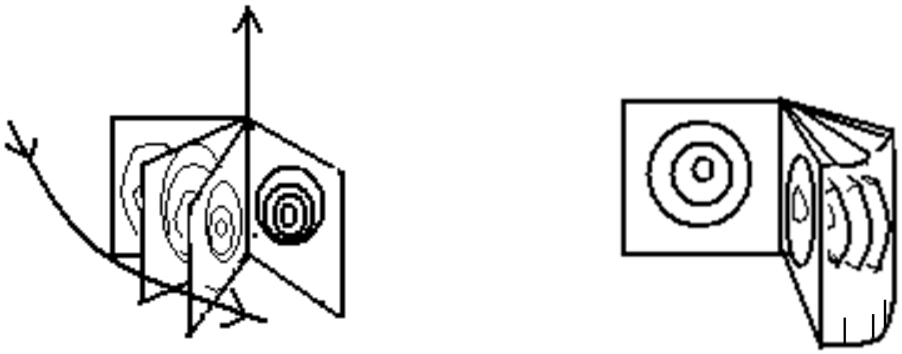

Figure 15-8-36

The real observed form of a solar loop as seen through a solar telescope is shown in Photo 15-8-3.

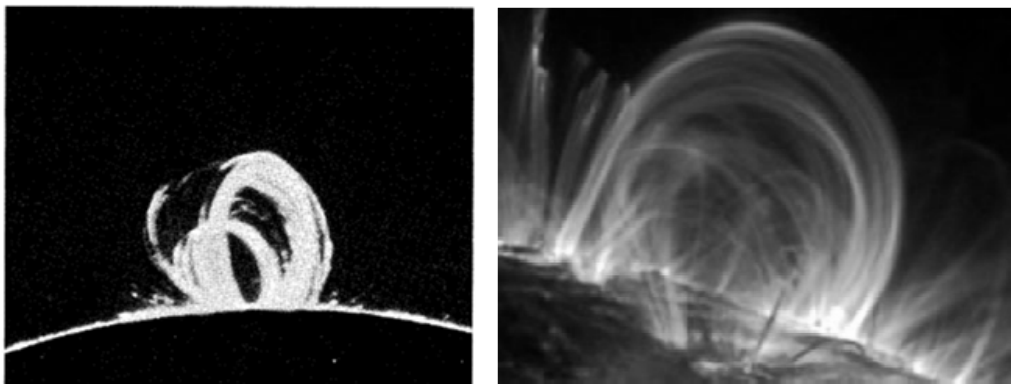

Photo 15-8-3 (Source: *Left panel*: Sacramento Peak Observatory, Geophysics Research Directorate, AFCRC. *Right panel*: SOHO, NASA/ESA)

In other word inertial process of revolution and rotation interact as interaction between orbital angular momentum and spin angular momentum

Orbital potential and revolution potential is changed by inertial process and is interacted during the given cycle. During this inertial process solar rotation energy is radiated as flare, coronal mass ejection etc by speed up of solar rotation (by this speed up of solar rotation is same as usual glitch of pulsar). That is physical essence of solar activity with gravito magnetic force line. Here important point is that this gravito magnetic force line is not electromagnetic force line. This gravito magnetic force line that's strength is same as electromagnetic force line strength, is direct visible and observable evidence of gravito magnetic force line.

Next step of force line change is 3 of Figure 15-8-37.

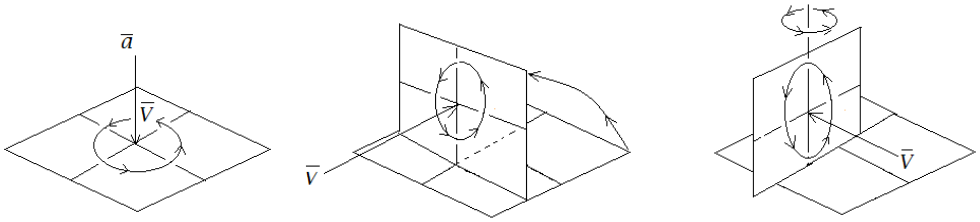

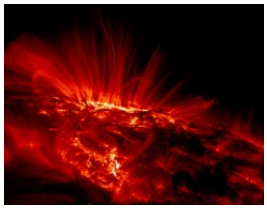

1

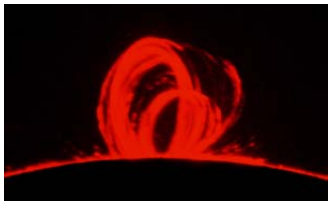

2

3

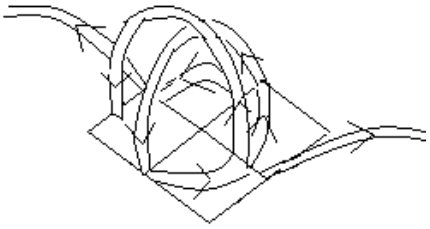

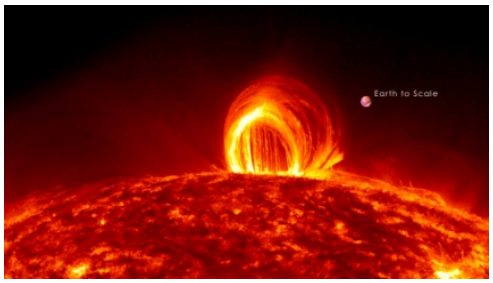

1+2+3

Figure 15-8-37

However, when energy increase by inertial interaction is huge, form of gravitomagnetic force line cannot be kept and become coronal mass ejection as 4, 5, and 6 of Figure 15-8-38

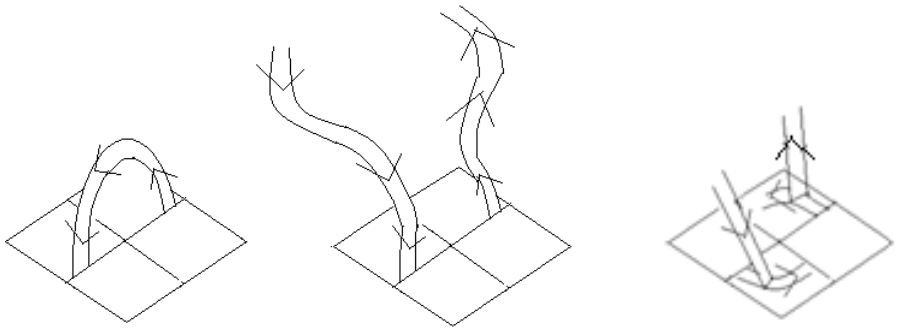

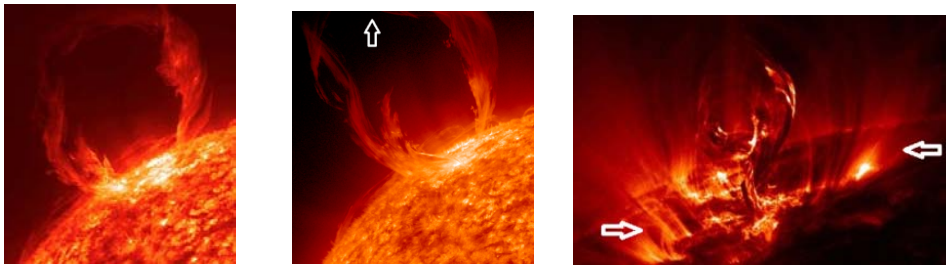

4 5 6

Figure 15-8-38

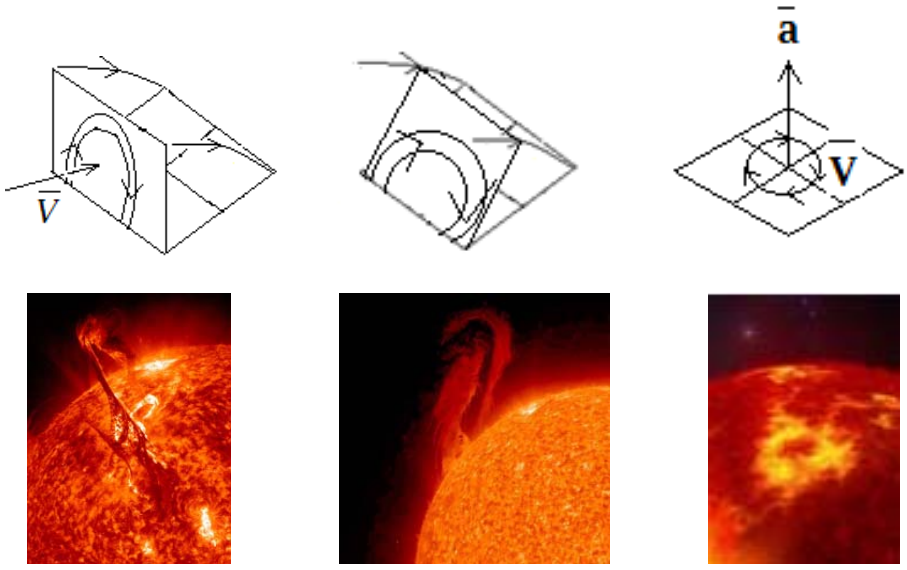

7 8 9

Figure 15-8-39

Last step of gravito magnetic force line change is 7, 8 and 9 of Figure 15-8-39.

Each step of gravito magnetic force line change from 1 to 9 correspond each rotation state from A to F.

Because relativistic physics abandons the real gravitational force line and its force line element, relativistic physics cannot even try to explain such phenomena.

However, because CFLE theory has force line and its elements, CFLE theory can explain quantum wave mechanically such phenomena as

$$\Psi_{\text{total}} = \psi_{\text{orbital}} \cdot \psi_{\text{spin}} \qquad 5\text{-}2\text{-}1$$

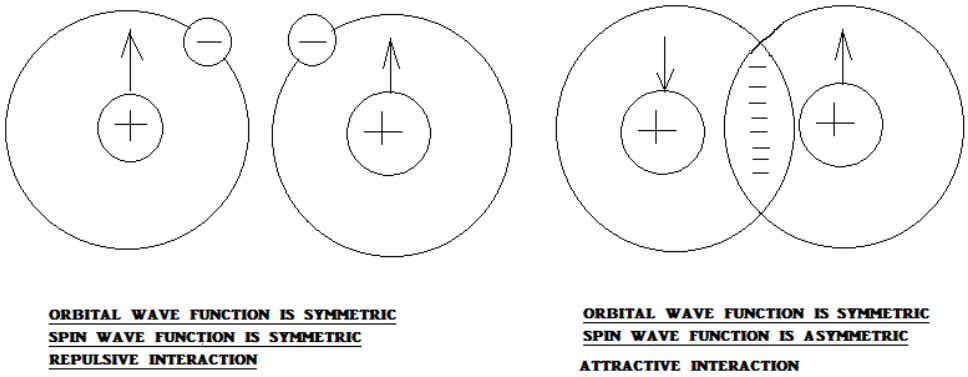

Figure 5-2-1

when the spin wave function is asymmetrical, the orbital function can be symmetrical. This is what makes the covalent bond of a H_2 molecule possible, despite it being composed of only a pair of 1 proton plus 1 electron. Without such spin asymmetry and orbital symmetry between H atoms, there would only be repulsive action according to the Pauli principle, as demonstrated in Figure 5-2-1.

Now, such physical quantum wave mechanical essence can apply to huge astronomical mechanical objects by CFLE theory.

In case of spin wave function is symmetric, left proton correspond

Galactic center, left electron correspond one of stars (the sun) around galaxy, right electron and proton correspond constituent particles of the star (the sun). According to probability of wave function, revolution speed and rotation speed is changed. Therefore, two angular momentum interact as $\Psi_{\text{total}} = \psi_{\text{orbital}} \cdot \psi_{\text{spin}}$.

According to $\Psi_{\text{total}} = \psi_{\text{orbital}}\psi_{\text{spin}}$ is radiated changed energy of revolution angular momentum or energy of rotation (spin) angular momentum.

That is quantum wave mechanical reason of sun's activity and pulsar's glitch activity.

The continental drift of Earth occurs as in Figure 15-8-35 (with Figure 15-8-36 depicting the inertial axis), from the centripetal side [Pacific Ocean side, 0°, 160°] to the centrifugal side [Atlantic Ocean side, 0°, 20°]. Because the excess undue energy causes the mass of this area to flow from the Pacific side to the Atlantic side, the Atlantic Ocean becomes wider. According to the force line arrangement of the inertial plane of inertial force, the force lines well up under the sea level of the Indian Ocean and west Pacific Ocean (Figure 15-8-39)

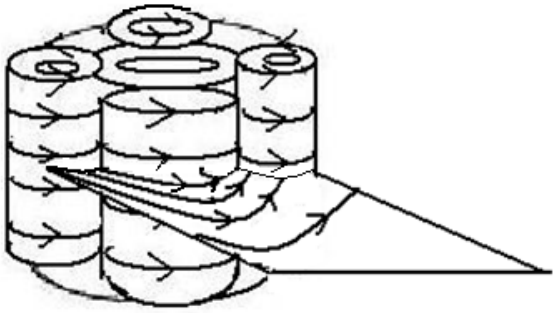

Indian Ocean west Pacific **Peru side east Pacific**

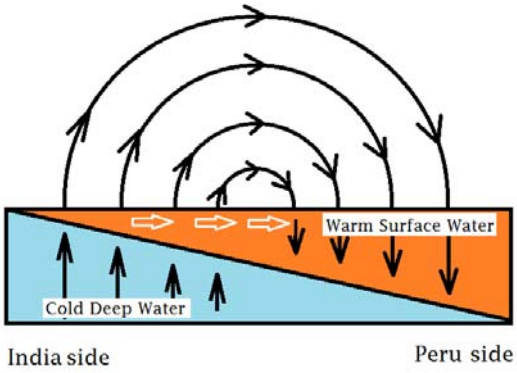

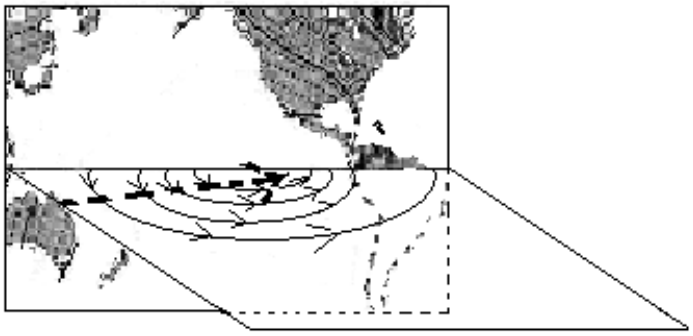

Figure 15-8-40

That is the real reason of the El-Ninõ. Originally, warm water at the ocean surface stays on the entire Pacific Ocean, but according to state D, the inertial plane of the inertial force lies such that the force lines arrangement pushes up the cold water under the sea level on the Peru side (east Pacific Ocean), as shown in Figure 15-8-40.

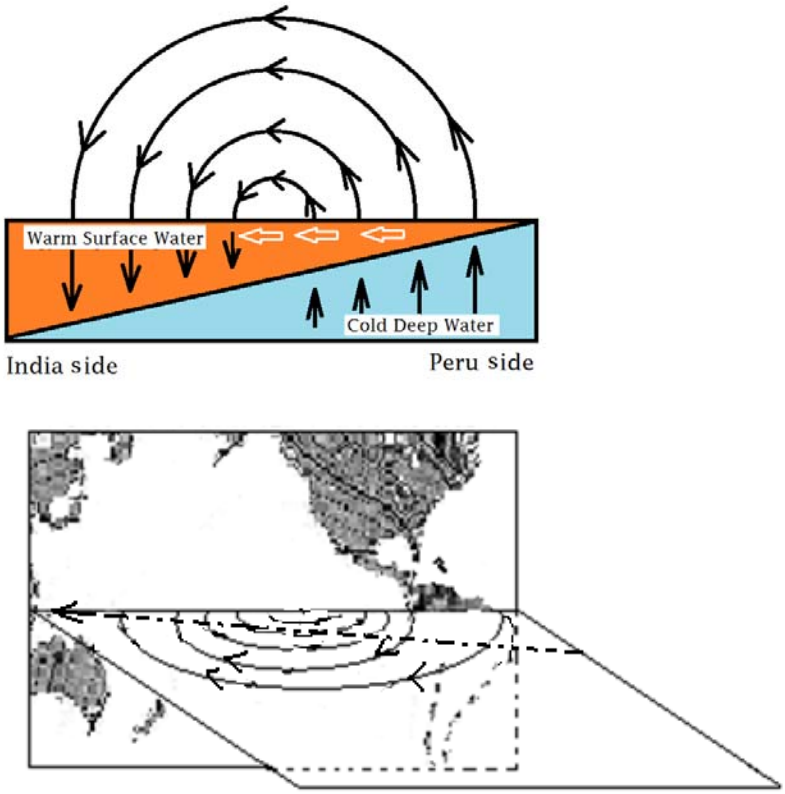

Figure 15-8-41

Thus the warm water of the ocean surface flows to the west Pacific Ocean which is called the La Ninã, since according to the change of force lines arrangement the sea water of the ocean moves too. Although the sun and Earth are of different sizes and have different component materials, they should share the same phenomena because of the correspondence property of all force line elements. The corresponding phenomenon of Earth's continental drift is the sunspot phenomenon of the sun. The correspondence inertial plane is shown in Figure 15-8-41. The real form of the sun's surface is shown in Photo 15-8-4.

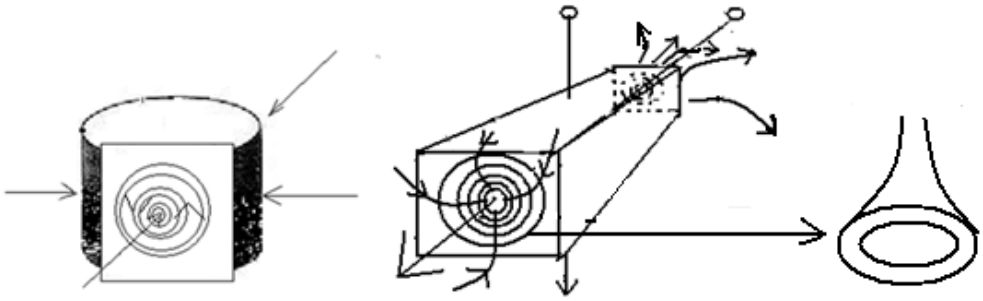

Figure 15-8-42

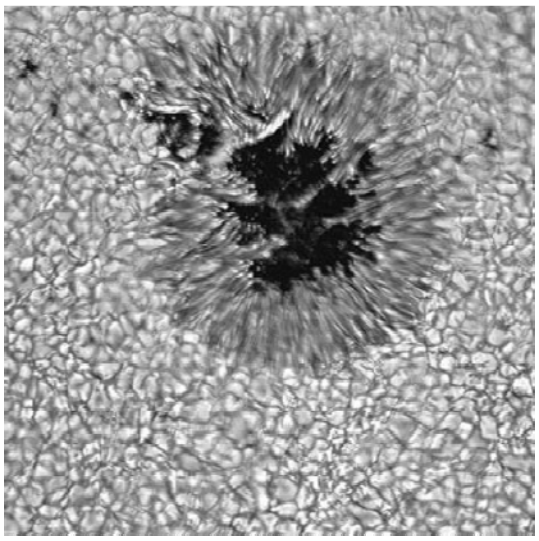

Photo 15-8-4 (Source: SOHO, NASA/ESA)

Because the sun is formed by gases, its mass current is very strong, despite that the same inertial force is similar, and related downward pressure of the area with the temperature and decrease of the density of the gas appear. Therefore, the sunspot is observed as being black in color.

This is the real cause of sunspot generation. The start of sunspot increase is called the period of the sun's activity.

The change of the sun's surface and inside of the optical layer is depicted in Figure 15-8-43.

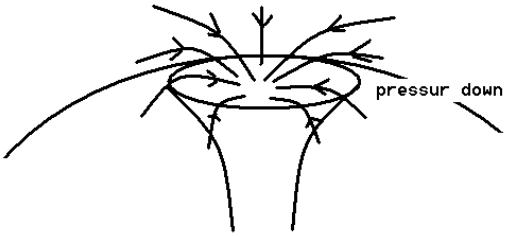

Figure 15-8-43

Between sunspots, mass-magnetic force lines run as in Figure 15-8-44.

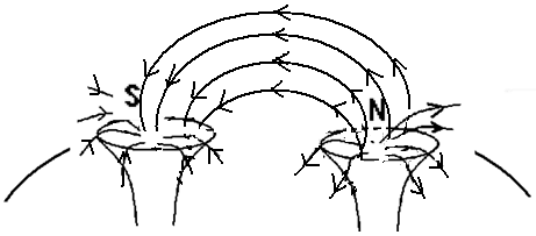

Figure 15-8-44

A variety of phenomena have appeared in the sun's atmosphere. One of them is the dark filament. The cause of the dark filament is the inertial force of the sixth step (Figure 15-8-45). The real form of the sun's surface is shown in Photo 15-8-5.

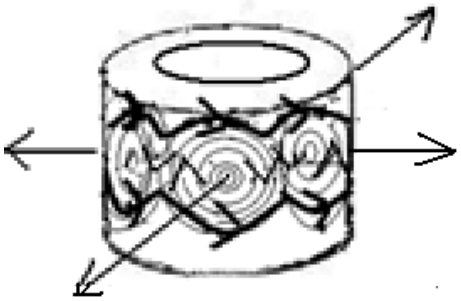

Figure 15-8-45

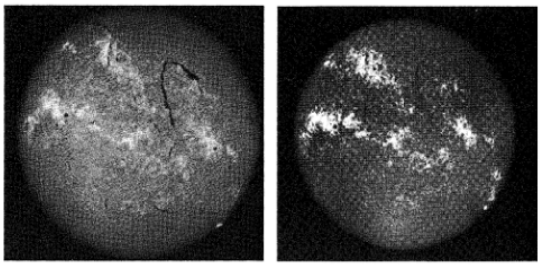

Photo 15-8-5 (Source: Kiepenheuer, K. O. 1953. *The Sun*, p. 433. G. P. Herausg, Editor. Reproduced with permission from the University of Chicago Press © 1953)

The sun's material moves along the force line arrangement caused by inertia, creating the dark filament. On one side of the sun's corona and in the chromosphere appear the coronal loop and protuberance. These sun phenomena are caused by the force line arrangements of steps C and D, respectively (Figures 15-8-45 and 15-8-45).

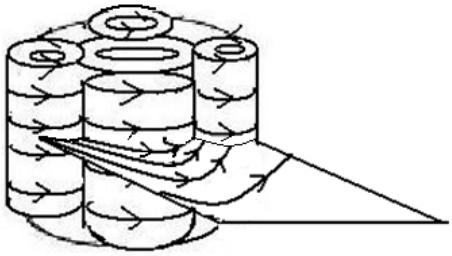

Figure 15-8-46

Because of spin reversal, the force lines run as in Figure 15-8-46. The observed photo about this phenomenon is shown in Photo 15-8-6.

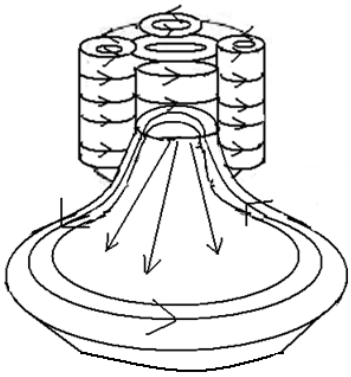

Figure 15-8-47

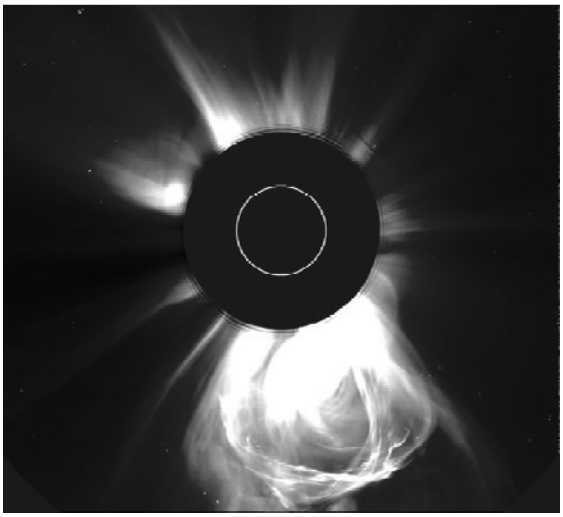

Photo 15-8-6 **(Source: SOHO, NASA/ESA)**

Coronal mass ejections are caused by the excess energy current mass of the sun running according to the force line arrangement of Figure 15-8-47. Photo 15-8-7 shows an actual coronal mass ejection.

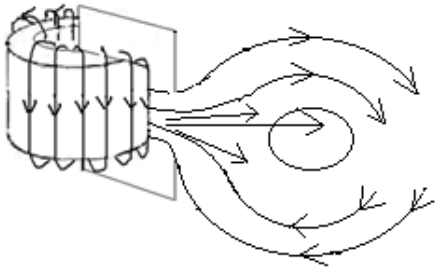

Figure 15-8-48

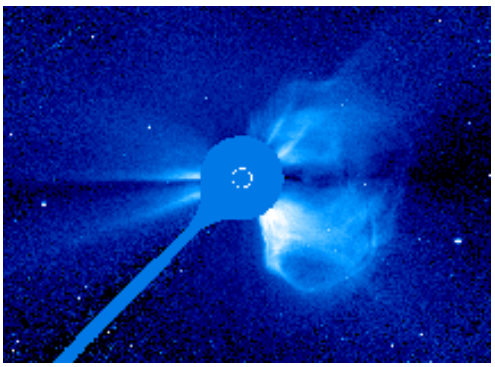

Photo 15-8-7 (Source: SOHO, NASA/ESA)

In Figure 15-8-48 and Photo 15-8-7, an additional requirement was for the shape of the CME of the strong side to be the reverse of the narrow hurricane shape, because the strong force line curve added revolutions energy and rotations energy. The shape of the collision side is the usual hurricane figure, so this side is the exit side, which is also the exit for the main mass emission.

15.9 Solving Mystery of 11 years Solar Cycle and 158 days Sunspots cycle

So far, the explanations of such phenomena have only been qualitative. But without a quantitative explanation, CFLE theory is meaningless. To summarize all the physical quantities of the sun:

$$M_{\odot} = 1.989 \times 10^{30} \text{ kg} \qquad 15\text{-}9\text{-}1$$

$$R_{\odot} = 6.595 \times 10^{8} \text{ m} \qquad 15\text{-}9\text{-}2$$

$$V_{\text{rev}} = 250 \text{ km /s} \qquad 15\text{-}9\text{-}3$$

$$V_{\text{rot}} = 2 \text{ km/s} \qquad 15\text{-}9\text{-}4$$

$$A_{\odot} = 6.087 \times 10^{20} \text{ m}^2 \qquad 15\text{-}9\text{-}5$$

The total rotation energy is

$$E_{\odot} = 2.4 \times 10^{35} \text{ J} \qquad 15\text{-}9\text{-}6$$

The number of revolutions pack is

$$N_{\odot\text{rev}} = 6.027 \times 10^{5} \qquad 15\text{-}9\text{-}7$$

The number of rotations pack is

$$N_{\odot \mathrm{rot}} = 2.15 \times 10^6 \qquad 15\text{-}9\text{-}8$$

The inertial energy of one rotations pack is

$$E_{\odot \mathrm{in}} = 1.12 \times 10^{29}\ \mathrm{J} \qquad 15\text{-}9\text{-}9$$

The rotation period of the sun by definition of the Carrington for sunspot period is

$$P = 27.2753\ \mathrm{days} \qquad 15\text{-}9\text{-}10$$

For the rotations pack and revolutions pack to collide, they need a common period,

$$P = \frac{(27.28\ \mathrm{days})\ (2.50 \times 10^5\ \mathrm{m/s})}{2.00 \times 10^3\ \mathrm{m/s}}$$

$$= 3410\ \mathrm{days}$$

$$= 9.336\ \mathrm{years} \qquad 15\text{-}9\text{-}11$$

Because the keplerian missing factor $f_k = 1.202$ for revolution of galactic center is, the effective period of this inertial resonance is

$$P = (9.336\ \mathrm{years})(1.202)$$

$$= 11.22\ \mathrm{years} \qquad 15\text{-}9\text{-}12$$

The actual observed value is

$$P \approx 11\ \mathrm{years} \qquad 15\text{-}9\text{-}13$$

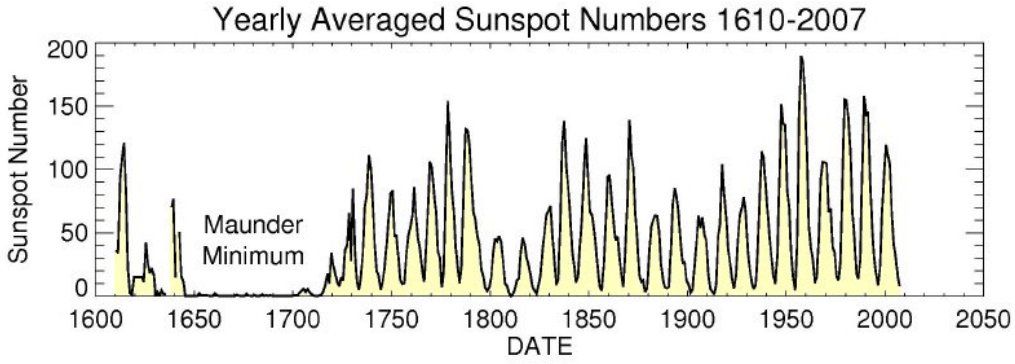

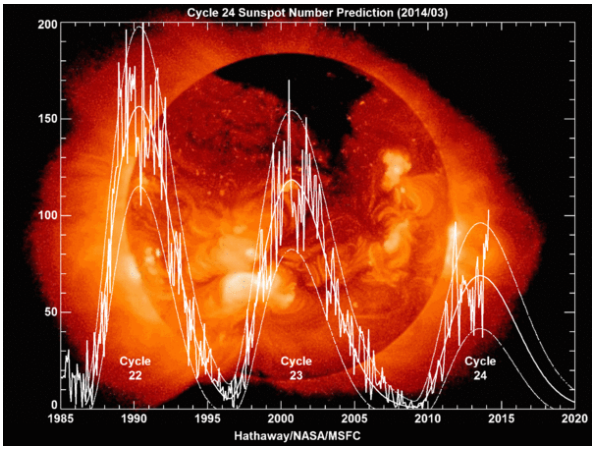

The current prediction for Sunspot Cycle 24 gives a smoothed sunspot number maximum of about 69 in the late Summer of 2013. The smoothed sunspot number reached 68.9 in August 2013 so the official maximum will be at least this high.

Figure 15-9-1

Because the predicted value agrees well with the observed value, the quantitative accuracy of CFLE theory is proven.

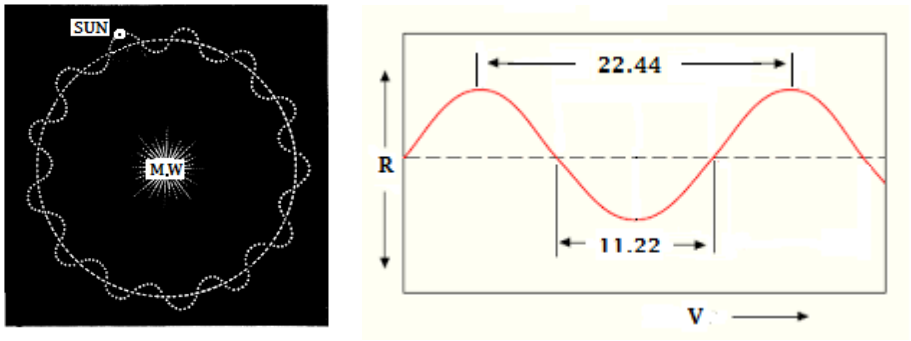

Figure 15-9-2

Therefore, the magnetic reversal period of a sunspot by CFLE theory is

P = (11.22 years) (2)

= 22.44 years

≈ 22 years 15-9-14

The actual observed value is

$T \approx$ 22 years 15-9-15

Such orbit behavior of the sun can explain why sunspot number between one period and next period is almost repeated increase and decrease.

The near 158 day periodicity was first detected in γ- and X-ray flare data (Rieger et al. 1984; Dennis 1985) taken from the *Solar Maximum Mission* and *GOES* satellites in solar cycle 21. During the same solar cycle, it was also found in flares producing energetic interplanetary electrons (Dröge et al. 1990), proton flares (Bai & Cliver 1990), and microwave flares (Bogart & Bai 1985; Kile & Cliver 1991). By combining data from solar cycles 20 and 21, it has also been detected in Hα flares (Ichimoto et al. 1985), microwave flares (Bogart & Bai 1985; Kile & Cliver 1991), and the solar flare index (Özgüc & Ätaç 1989), whereas it has been found in proton flares during solar cycles 19 and 20 (Bai & Cliver 1990).

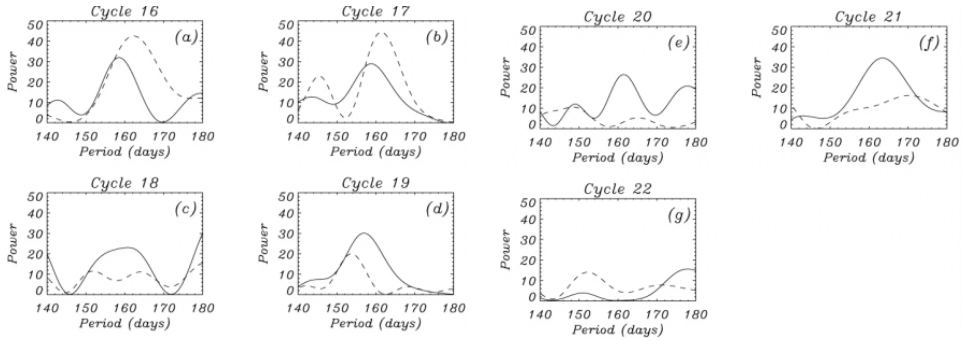

Raw Lomb-Scargle periodograms for sunspot areas (*continuous line*) and group sunspot numbers (*dashed line*) for (*a*) solar cycle 16, (*b*) solar cycle 17, (*c*) solar cycle 18, (*d*) solar cycle 19, (*e*) solar cycle 20, (*f*) solar cycle 21, and (*g*) solar cycle 22. To generate these plots, the first 600 days and the last 1200 days from each cycle have been removed prior to computing the periodogram. In this way, only the values around the maximum of each cycle, where the periodicity is more intense, are retained. Figure 15-9-3

Exact value of g_{eff} (cf.§7)is

$g_{eff} = 5.793596$ 7-4-2-2

Possible range of force line curve change for nuclear reaction by inertial resonance is from $g = 1$ to $g = 5.793596$ of kaon.

and the rotation period of the sun by definition of the Carrington for sunspot period is

$P = 27.2753$ days 15-9-10

Therefore possible periodicity of sunspot strength by CFLE theory is

$P_t = (27.2753\ days)(5.793596)$

=158.022 days

≈ 158 days 15-9-16

Observed value is

$P_t \approx 158$ days 15-9-17

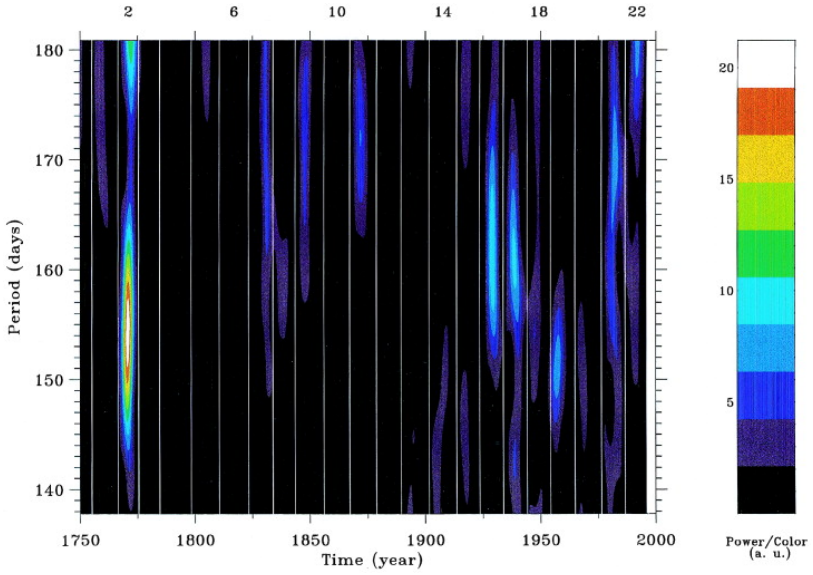

Time/period diagram made using the wavelet analysis of the daily group sunspot numbers. It shows a strong power peak in the 150 ─160 day period range localized around the maximum of solar cycle 2. The wavelet used here is of the Morlet kind and has a width at half-height of 8 nHz in frequency, corresponding to a temporal width of ~1300 days. The power is normalized in order to estimate the significance level. Here, the 95% significance level corresponds to a power value of ~8.3. White vertical lines indicate solar activity minima and some solar cycle numbers are given at the top of the figure.

Figure 15-9-4

Because the observed value and theoretical value again agree quite well, we can have minimum assurance of the previous qualitative discussion of CFLE theory.

When Sun move in galactic orbit, galactic potential is changed as Figure 15-9-2. Because this galactic potential change is changed Sun's Revolution speed.

Because for changed potential to adapt, Sun emit energy for stability of system to keep. That is one reason of sun's activity and polarity change.

Because high degree of free motion of inner material(Gas) of the Sun as Figure 15-9-5, occur local magnetic reversal, Sun spot magnetic reversal as neutron star magnetic reversal and pulsar magnetic reversal.

However, low degree of free motion of inner material (solid) is given as Figure 15-9-6, occur global magnetic reversal as Earth magnetic reversal.

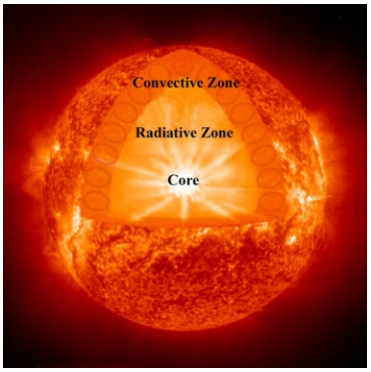

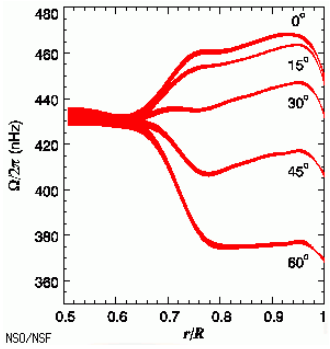

Sun: local magnetic reversal **Tacho cline of the Sun**

Figure 15-9-5

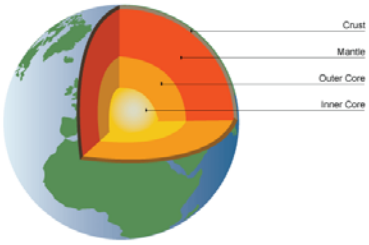

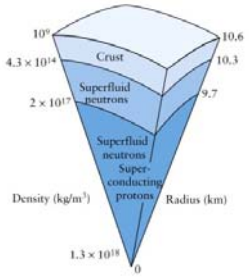

Earth: Global magnetic reversal, Neutron Star: local magnetic reversal

Figure 15-9-6

During the active period of the sun, we can observe flares near sunspots. The energy of a single very large size flare observed per day is

$E \approx 10^{25}$ J

The energy of 10~100 mid-sized flares observed per day is

$E \approx 10^{25}$ J

That of 10~100 very small-sized flares observed per day is

$E \approx 10^{25}$ J

Such flare energies are unthinkably large in the viewpoint of modern thermodynamics. Therefore, to date, modern physics cannot even try to explain such gigantic energy scales of flares. But CFLE theory can explain about flare energy and its energy scale very easy. Because the total rotations energy of the sun is

$E = 2.4 \times 10^{35}$ J

and the number of rotations pack is

$N = 2.15 \times 10^{6}$ 15-9-18

the inertial energy generated by a single collision is

$$E = \frac{2.4 \times 10^{35}\ \text{J}}{2.15 \times 10^{6}}$$

$= 1.12 \times 10^{29}$ J 15-9-19

Because this energy should be emitted over a length of 11.10 years, the inertial energy per year is

$$E = \frac{1.12 \times 10^{29}\ \text{J}}{11.10\ \text{years}}$$

$= 1.01 \times 10^{28}$ J/year 15-9-20

Therefore, on a daily basis, the possible maximum inertial energy emitted is

$$E = \frac{1.01 \times 10^{28}\ \text{J}}{365.2422\ \text{days}}$$

$= 2.765 \times 10^{25}$ J/day 15-9-21

This energy can divided by flare size; that is,

$E = (1 \times 10^{25}\ \text{J}) + (1 \times 10^{25}\ \text{J}) + (0.765 \times 10^{25}\ \text{J})$ 15-9-22

The energy of the first term can be given for one big flare.

The energy of the second term can be given for 10~100 mid-sized flares

Finally, the energy of the third term can be given for 10~100 small flares.

This theoretical division of the energy according to energy size agrees well with observed values, and we obtain here even more assurance about the previous qualitative discussion of CFLE theory.

Because the area of one revolutions pack of the sun is

$$A_{\text{rev}} = \frac{A_{\odot}}{N_{\text{rev}}}$$

$$= \frac{6.087 \times 10^{20}\ \text{m}^2}{6.027 \times 10^5}$$

$$= 1.010 \times 10^{15}\ \text{m}^2 \qquad \text{15-9-23}$$

this is the area in which sunspots can appear, as inertial circles. The radius of this circle is

$$R = \sqrt{\frac{1.010 \times 10^{15}\ \text{m}^2}{\pi}} = 1.793 \times 10^7\ \text{m} \qquad \text{15-9-24}$$

This radius can be expressed as a ratio with the sun's radius. That is,

$$R^{\text{o}} = \frac{R_{\odot}}{R_{rev}} = \frac{69.55 \times 10^7\ \text{m}}{1.793 \times 10^7\ \text{m}}$$

$$= 38.79^{\text{o}}$$

Because The helium ratio of the Sun is H:He = 70:30, and the neutron ratio is P:N = 85:15, so the hydrogen abundance as energy source is

$$HA = \frac{1}{0.85} = 1.176$$

Therefore effective ratio is

$$R^{\text{o}} = \frac{38.79^o}{1.176} = 32.98^o$$

$$\approx 33^{o} \qquad 15\text{-}9\text{-}25$$

This ratio can be used as the maximum appearing latitude of the sunspot when the sun's active period starts.

Therefore, the diameter for this latitude is

$\theta \approx \pm 33°$

The observed value is $\theta = \pm 35°$, as seen in Figure 15-9-3.

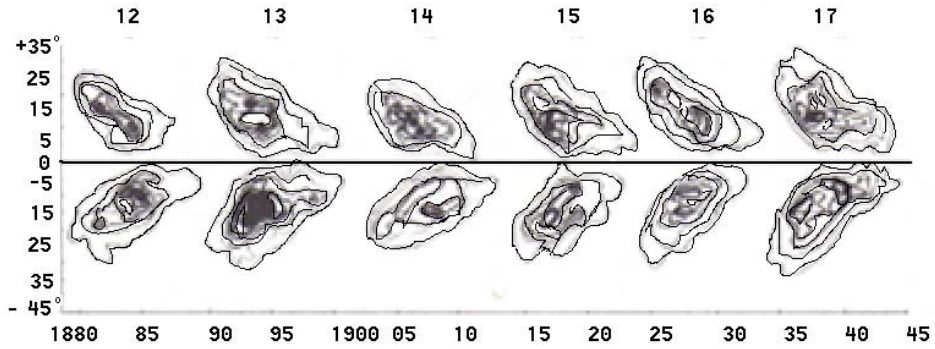

Figure 15-9-7

Essence of this phenomenon is interaction between inertial pole and main pole. Because in the neutron star main pole is very strong, inertial pole move fast to North Pole and South Pole (is called Pole Jumping), and both pole become active zone. Therefore, every astrophysical beam and jet from pulsars and galaxy can radiate.

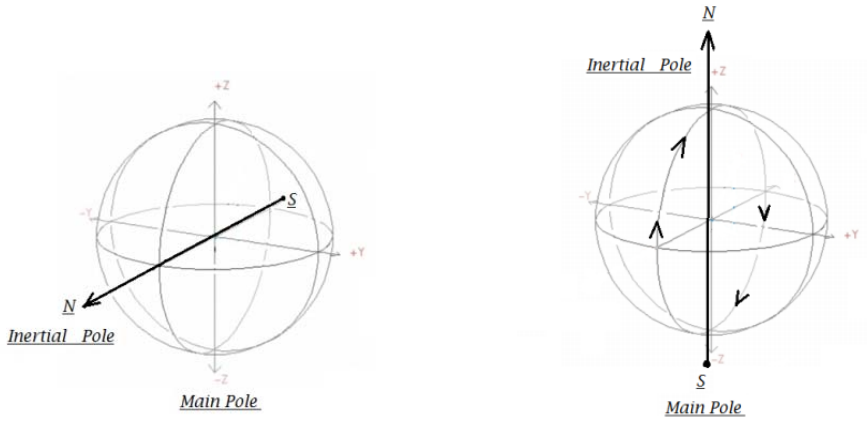

Figure 15-9-8

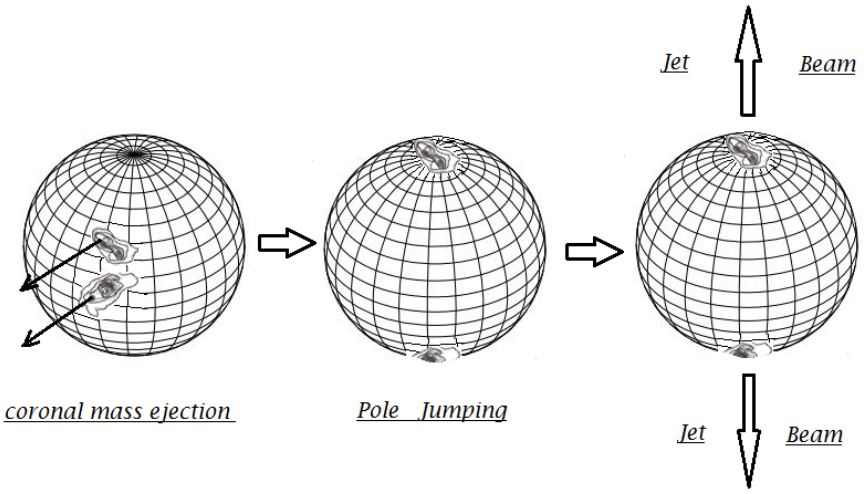

Figure 15-9-9

After pole jumping coronal mass ejection becomes polar beam and polar Jet. That is physical essence of astronomical Beam and Jet.

Following are explanations about the number and size of granules and their meaning. Because each force strength is $N = 1.190208 \times 10^7$, the rotation's acceleration point should be as in Figure 15-8-47-2.

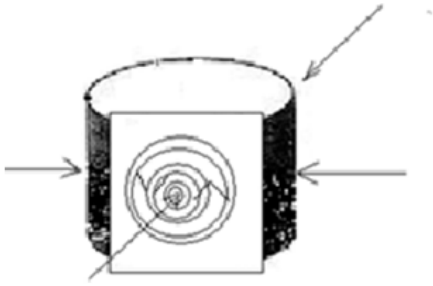

Figure 15-9-10

The ends of the arrows in Figure 15-8-47-2 satisfy this number N. But, because of the correspondence factor of $c_c^2 = (1.5)^2 = 2.25$, and the gravitational permittivity of hydrogen at $g = (6.545979)^2$ being

$Q_g = (0.000579)\ (42.849841) = 0.024810$

$x_g = 1.0248109$

the effective number is

$$d = c_c^2 x^2$$

$$= (1.5)^2 (1.024810)^2$$

$$= (2.25)(1.050) = 2.363$$

$$N = \frac{1.190208 \times 10^7}{2.363}$$

$$= 4.284 \times 10^6 \qquad \text{15-9-26}$$

The observed value is $N \approx 4 \times 10^6$.

Because the sun's surface area is

$$A_\odot = 6.087 \times 10^{20}\ \text{m}^2$$

the unit area of this acceleration of rotation (granule) is

$$A_{\text{rot}} = \frac{6.087 \times 10^{20}\ \text{m}^2}{4.284 \times 10^6} = 1.421 \times 10^{14}\ \text{m}^2$$

The radius of this unit area is

$$R = \sqrt{\frac{A_{\text{rot}}}{\pi}}$$

$$= 6.705 \times 10^6\ \text{m} \qquad \text{15-9-27}$$

Its diameter is

$$D = (6.705 \times 10^6\ \text{m})(2)$$

$$= 1.341 \times 10^7\ \text{m} = 1{,}341\ \text{km} \qquad \text{15-9-28}$$

But, because the helium ratio of the sun is H:He = 70:30, and the related ratio of the neutron is P:N = 85:15, $NR = \frac{1}{0.85} = 1.176$, which means the burning fuel H_1^1 for nuclear fusion is only 85%.

Therefore, the effective diameter of this area is

$$D = \frac{1{,}341\ \text{km}}{(1.176)^2}$$

$= 969.63$ km

$\approx 1{,}000$ km 15-9-29

The observed value is

$D \approx 1{,}000$ km 15-9-30

Because the sun's rotation at this acceleration should run this entire distance of the sun, the life-time of the granules should be

$$T = \frac{969.631 \text{ km}}{2.03 \text{ km/s}}$$

$= 477.651$ s

$= 478$ s

$= 7.96$ min

≈ 8 min 15-9-31

The observed value is

$T = 8$ min 15-9-32

Because the theoretical and observed values agree quite well, the previous qualitative discussion of CFLE theory is validated.

15.10 Solving Origin of Earth Quake Periodicity and Prediction Possibility by CFLE theory

Now, because the rotation speed of Earth is

$V_{rot} = 4.651 \times 10^2$ m/s 15-10-1

and the revolutions speed is

$V_{rev} = 2.987 \times 10^4$ m/s 15-10-2

the inertial interaction period of Earth is

$$P = \frac{(1 \text{ day})\ (2.978 \times 10^4 \text{ m/s})}{4.651 \times 10^2 \text{ m/s}}$$

$= 64.029$ days 15-10-3

Per year, this interaction occurs

$$N = \frac{365.2422}{64.029}$$

$$= 5.704 \text{ times} \qquad 15\text{-}10\text{-}4$$

Because such inertial force influences all of Earth's mass, Earth should be able to spend this energy in any rotations form. It's possible maximum speed is

$$V = \frac{4.651 \times 10^2 \text{ m/s}}{[\frac{(8.640 \times 10^4)(5.704)}{22.975}]}$$

$$= 2.168 \times 10^{-2} \text{ m/year}$$

$$\approx 2.2 \text{ cm/year} \qquad 15\text{-}10\text{-}5$$

where 22.975 is the difference between electricity and gravity (cf. §5).

The observed value is

$$V = 2 \text{ cm/year} \qquad 15\text{-}10\text{-}6$$

Because the rotation energy of Earth is

$$E = 2.137 \times 10^{29} \text{ J} \qquad 15\text{-}10\text{-}7$$

and the number of rotations pack is

$$N = 2.099 \times 10^4 \qquad 15\text{-}10\text{-}8$$

the inertial energy that Earth would have to spend is

$$E = \frac{2.137 \times 10^{29} \text{J}}{2.099 \times 10^4}$$

$$= 1.018 \times 10^{25} \text{ J} \qquad 15\text{-}10\text{-}9$$

Because such collisions occur 5.604 times per year, the possible annual total energy of inertia for the continental drift is

$$E = (1.018 \times 10^{25} \text{ J}) (5.604)$$

$$= 5.705 \times 10^{25} \text{ J} \qquad 15\text{-}10\text{-}10$$

This energy is the varying energy that scientists have been trying to find since Alfred Wegener (1880-1930)'s time to date. The influence of inertial force on Earth's surface can be depicted as in Figure 15-8-48.

The range of influence of the inertial force of the opposite side is expressed in Figure 15-8-49.

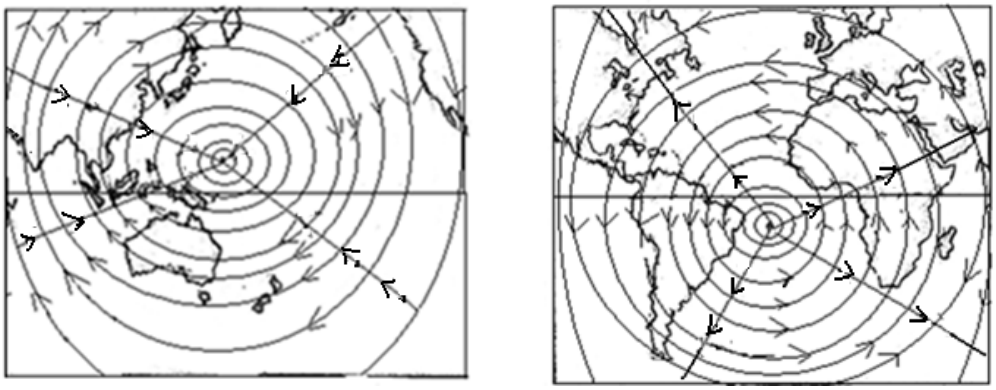

Figure 15-10-1

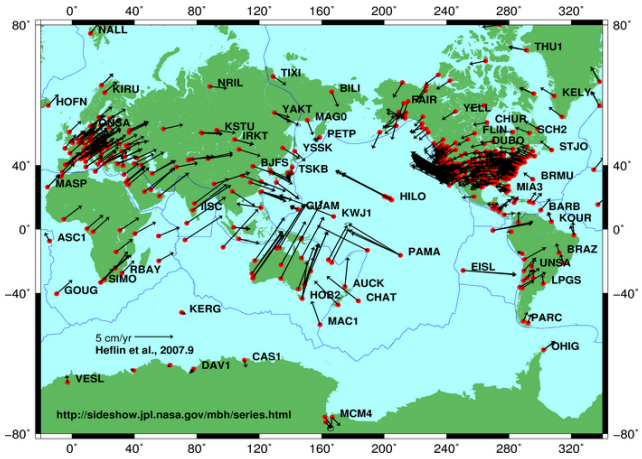

Global plate tectonic movement

Figure 15-10-2

The magnetic field caused by this inertial force is expressed on the map of Figure 15-8-50. The magnetic field by this inertial force on the opposite side of the map is expressed in Figure 15-8-51.

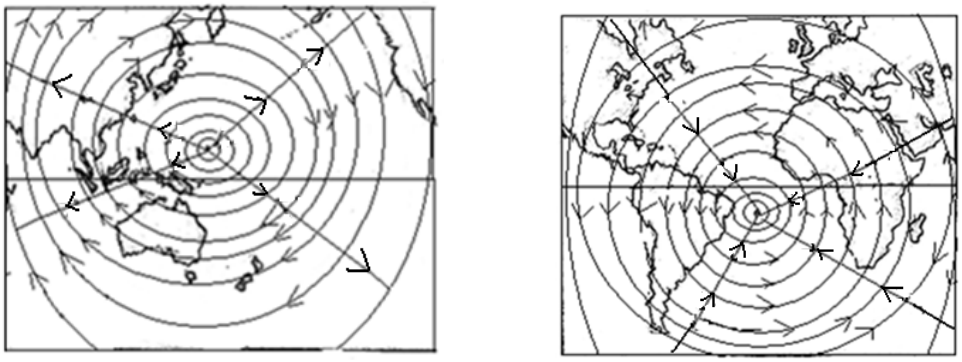

Figure 15-10-3

Currently, the magnetic field of Brazil is decreased and that of Siberia is increased, because of the interaction between the magnetic field from Earth's rotation and inertial force. Such interactions with vector lines are expressed on the maps of Figures 15-8-52 through 15-8-54.

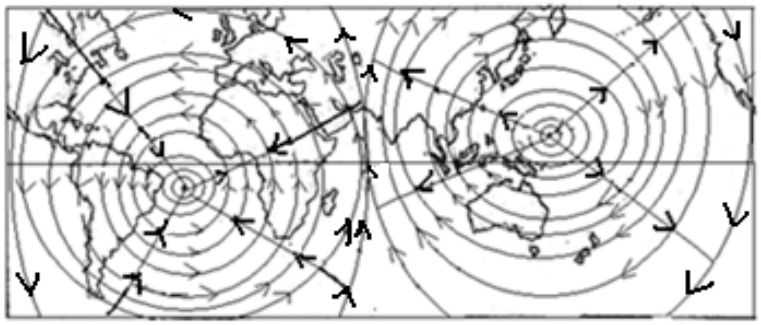

Figure 15-10-4

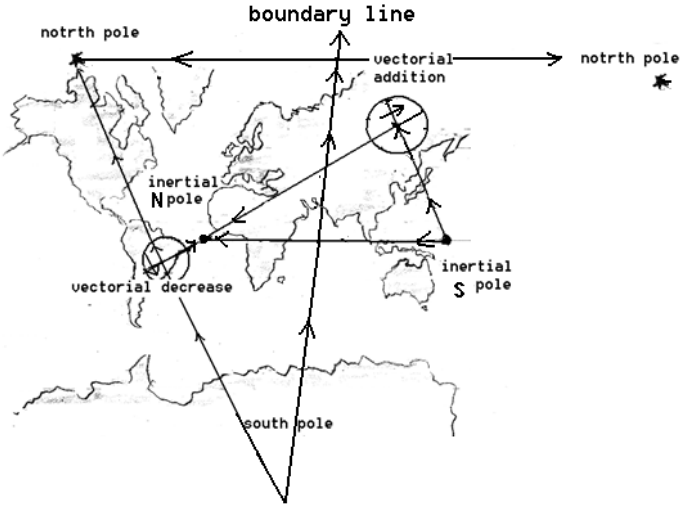

Figure 15-10-5

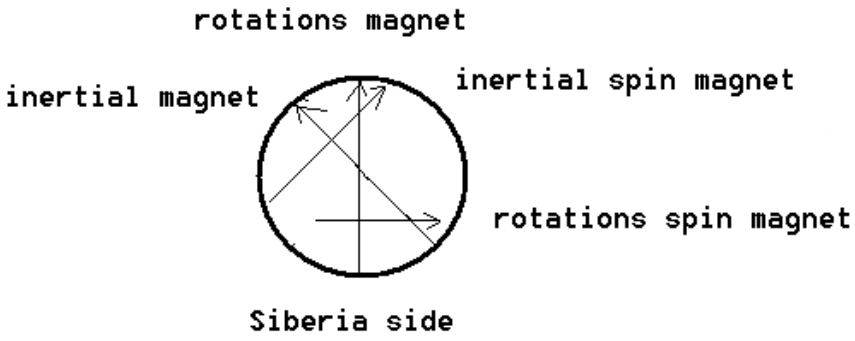

Figure 15-10-6

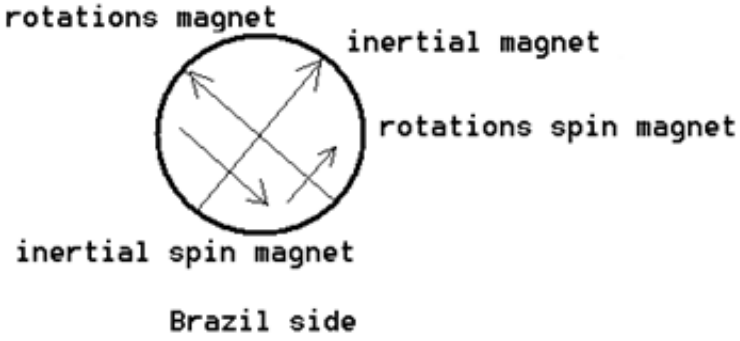

Figure 15-10-7

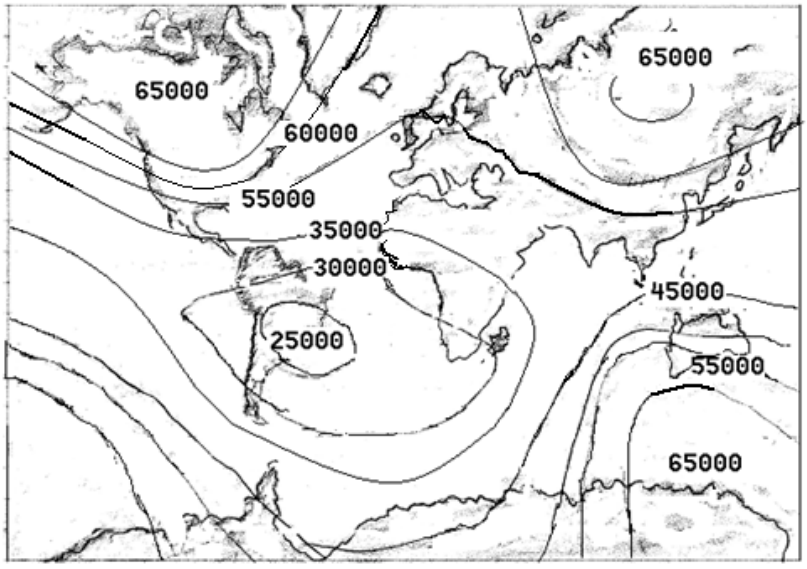

Figure 15-10-8

The rotations magnetic field and rotations spin magnetic field over Brazil are offset by the inertial magnetic field. In contrast, those same fields over Siberia are intensified by the inertial magnetic field and inertial spin magnetic field. Because Earth's present magnetic field from Earth's rotation is getting weaker, the inertial magnetic field should someday offset the main Earth magnetic field. Then Brazil will be bombarded directly by cosmic rays. Because of this interaction between the two magnetic fields, the radiation strength in the sky over Brazil is already 0.69 mGy. This strength is 10,000 times stronger than on Earth's surface. The present mirror height of Earth is a few hundred kilometers, but Brazil's mirror height is only less than 100 km, because of the interaction between Earth's main magnetic field and the inertial magnetic field. Therefore, in the sky over Brazil, the electronics of satellites have already been known to fail because of the direct strong cosmic rays.

Glacier decrease, sea-level rise, and magnetic field decrease are three clear unavoidable evidences of phenomena that threaten the future of Earth. Glacier decrease has already been observed in the Arctic Ocean. Sea-level rising was observed at Tuvalu Island in the South Pacific Ocean. Magnetic field decrease has been observed in the sky over Brazil. Therefore, it is incumbent in this chapter to provide theoretical and observational evidence to warn of such dangers. The important point to note is that such dangerous phenomena are not temporary. These phenomena will be continued for more than 2000 years. Furthermore, during this time interval, the strength of such phenomena should be expected to increase. This fact is the most important point of discomfort and concern for humankind.

Known dynamics of the subduction zone by modern seismology is principally simple. The subducting oceanic tectonic plate is currently stuck against the overriding crust of continental plate along the locked zone. This has caused the edge of the continental plate to wrap and elevate the land (strain). When the pressure finally causes the fault to rupture, the continental plate will flex and drop, producing a major earth quake and tsunami.

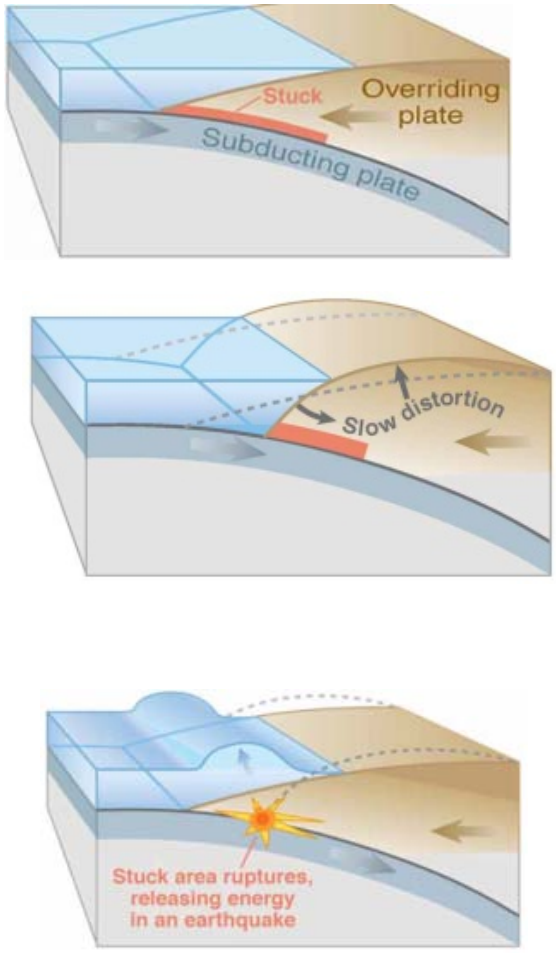

Figure 15-10-9

When the continental plate of subduction zone ruptures, it causes part of the seafloor to move abruptly upwards. This displaces the column of water above the ruptures, and result is a destructive huge powerful tsunami.

Table 15-10-1

Shaanxi	Jan 23,1556	China	Fatal 82,000	M 8.0
Haiti	Jan12, 2010	Haiti	Fatal316,000	M 7.0

Table 15-10-2

San Francisco	1906	USA	$ 9.5 billion	M 7.9
Tohoku	2011	Japan	$235 billion	M 9.0

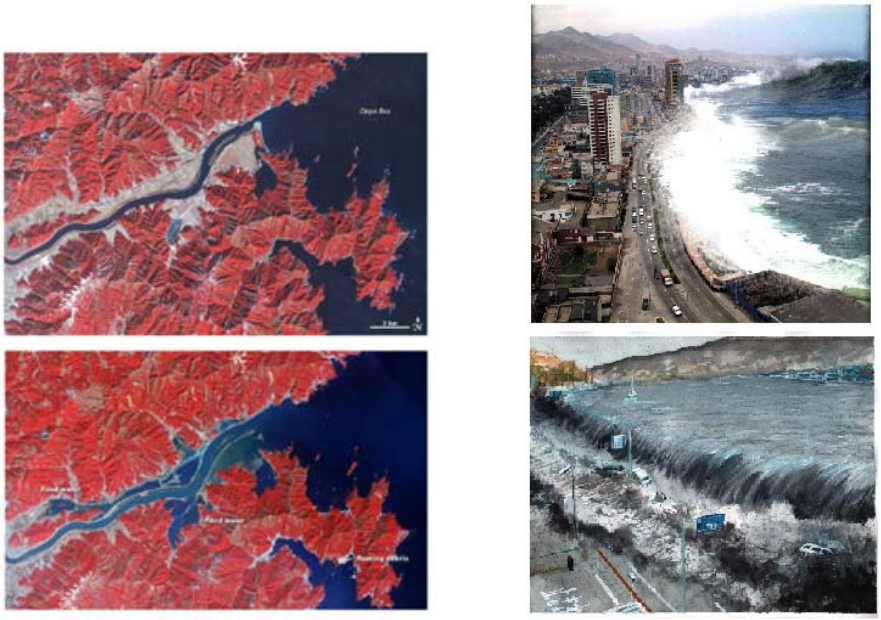

Left two photos showing before and after NASA satellite images of flooding the Kitakami River in Myagi Prefecture

Figure 15-10-10

Figure 15-10-11

Last century over 1 million people die only by earthquakes.

In 2011 occur 2494 earth quakes between M5.0~ M 9.9 and each year occur 1300~ 2500 earth quakes.

However, modern physics cannot know exactly about periodicity of earthquakes.

On 31 December 1703, a remarkably strong earthquake named Genroku 16 shook Edo (the old name of Tokyo), and on 1707 three earthquakes occurred at the same time in the east sea, south east sea, and the south sea, with a great eruption of the Fuji volcano. After 151 years, on 24 December 1854, another remarkably strong earthquake named Ansei Tokai, registering 8.4 M on the Richter scale, hit Suruga Bay (200 km south-west from Tokyo) with an accompanying tsunami. After 157 years, on 11 March 2011, the strongest earthquake (magnitude 9.0) in the history of Japan's national disasters occurred in the north-east sea, 373 km from Tokyo (38.322°N, 142.369°E) near the east coast of Honshu Sendai, with an accompanying destructive tsunami.

These and other remarkable earthquakes in Japan that are well known by historical documents and earthquake archeology are, in sequence of dates only at Nankai area. However, Earth quake of Tonankai in 1944 is except from Nankai earth quarkes, because Tonankai earth quake is same Nankai quake of 1946. Earth quakes in 1096 is except because same quake of 1099. Earth quake of 1360 is except from Nankai earth quakes, because of uncertain.

T_e= 1946−1854−1707−1605−1498−1361−1099−887−684 15-10-11

$$P_t = \frac{92+147+102+107+137+262+212+203}{8}$$

$$= \frac{1262}{8} = 157.7\text{years} \qquad 15\text{-}10\text{-}12$$

Earthquake prediction may be intrinsically impossible. It has been argued that the Earth is in a state of self-organized criticality" where any small earthquake has some probability of cascading into a large event". It has also been argued decision-theoretic grounds that prediction of major earthquakes is impossible.

That earthquake prediction might be intrinsically impossible has been disputed.

Earthquake prediction is an immature science—it has not yet lead to a successful prediction of an earthquake from first physical principles. Therefore, some research focuses on empirical analysis, either identifying distinctive precursors to earthquakes, or identifying some kind of geophysical trend or pattern in seismicity that might precede a large earthquake.

Scientists want predict for life to save and property damage to minimize. However, scientists cannot predict, because modern physics abandons the real gravitational force line and its force line element by general relativity, modern physics cannot even try to explain such phenomena.

Seismologists, they cannot predict and cannot smile and cannot easy sleep, because too much frequently too much people are dying and too much property are damaging with huge scale. However, it is not responsibility of seismologists. Responsibility is curved space time theory of general relativity that obstructs to make unified field theory.

However, now CFLE theory can explain about energy source and periodicity of earth quakes by inertial interacting of Earth with sun and moon.

According to inertial state from A to F radius of Earth is changed from long to short.

We can apply results of inertial interaction of the Earth as Figure 15-10-12 to the periodicity of earthquakes on any given observed area of Earth's surface, such as Japan.

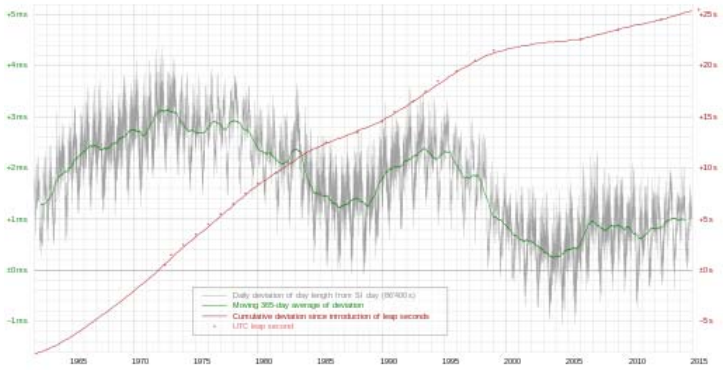

Deviation of day length from SI based day, 1962–2010

Figure 15-10-12

Because period of inertial interaction of the Earth is p= 64.029 days (15-10-3), Carrington period of the Sun is p = 27.2753 days (15-9-10) and the orbital period of the Moon is p=27.322 days, related common period of the 3 astronomical objects is

P_t =(64.029)(27.275)(27.322)(1.202)

= 57,353 days

= 157.03 yrs 15-10-13

Exact formula should be

$P_t = K(1 + r_l)$

$P_t = KW$, W=1+r_l

where K is pure value of P_t, r_l is local resistance by seabed topography.

This predicted value by CFLE theory agrees quite well with observed average value of 157.7 years of Japan. Expected local resistance of Tohoku 2011 should be

$$r_l = (\frac{157.7}{157.03} - 1) = 0.0043$$

Average W of Japan's oceanic plate was

W=1.0043

Average main earth quake period of Japan is

P_t =(157.03 yrs)(1.0043)=157.7 years

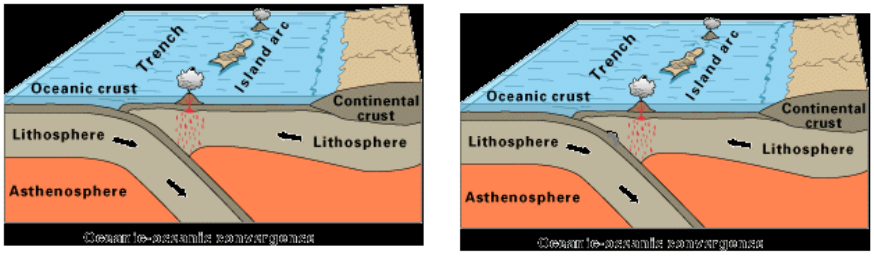

r_l =0 r_l =0.0043

Figure 15-10-13

However, CFLE theory gives us more important answer about cause of asperity of mega quakes. Given answer by CFLE theory is radius shortening by inertial interaction as Figure 15-10-13

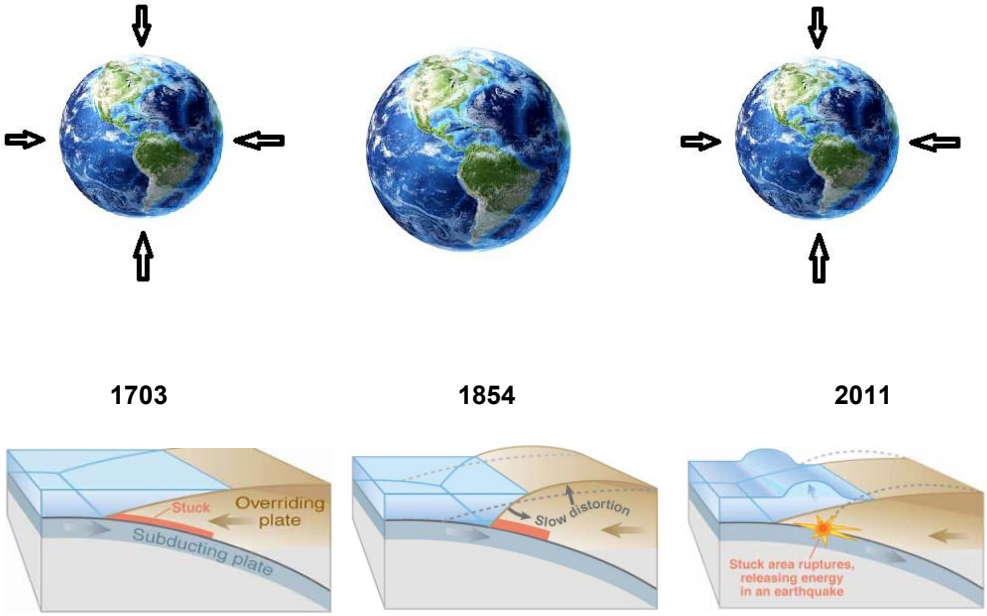

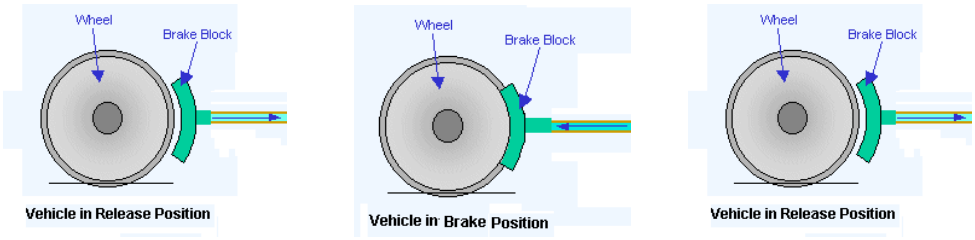

Figure 15-10-14

Maximum inertial lock by radius shortening becomes cause of major mega quake. This means that maximum inertial lock becomes asperity.

By different local variable$X_{(d_{C,M})}$ of sublocal seismological systems $SS_1, SS_{2,}SS_{3,}SS_{4,}SS_5$ of local seismological system, $SS_{2,} = S_{Nankai}$ are reacted differently and are appeared different results as Figure 15-10-14 (Different local asperity of different oceanic plate, continental crust and different pressure of local mantel). Observed values from $SS_1 \rightarrow$ $SS2 \rightarrow SS3 \rightarrow ...$ should be took 3~4 years.

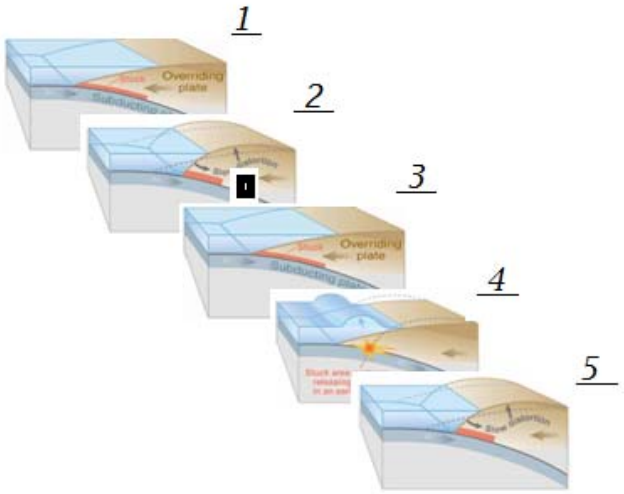

Figure 15-10-15

However, nevertheless almost same subducting speed of oceanic plate of Juan de Fuca plate at Cascadian subduction's zone and Philippine sea plate at Nankai trough of Japan is gravitational effect is very different.

Because two subducting plate move to different place under different continental crust that has different mass, gravitational effect by inertial interaction is appeared differently. Figure 15-10-15 show moving direction of Juan de Fuca plate and mass of north American continental plate where placed heavy Cascade Range(1,100 km long width 130km !!!).

Because relative strong seismological power is used for only one heavy Cascadian Mountains (Length: 1100km, Width: 130km) to distort, period of major quake becomes 3 times longer than Nankai major quake (3 continental crust at Nankai trough: Kyushu, Shikoku, Honshu) and slow quakes.

Average of observed value of factor 3 by core investigation of sediment from seabed during 10,000 years by 23 earthquakes is

$$p_t = \frac{10{,}000\ years}{23} = 434.78\text{years.}$$

$$f_3 = \frac{434.78\ years}{157.03\ years}$$

$$= 2.7688 \approx 3 \qquad 15\text{-}10\text{-}14$$

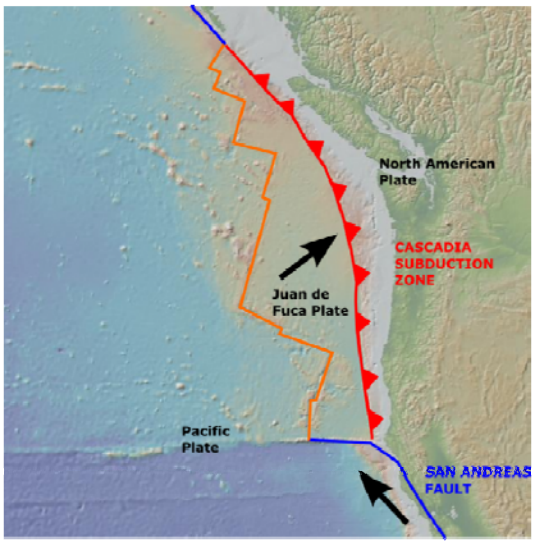

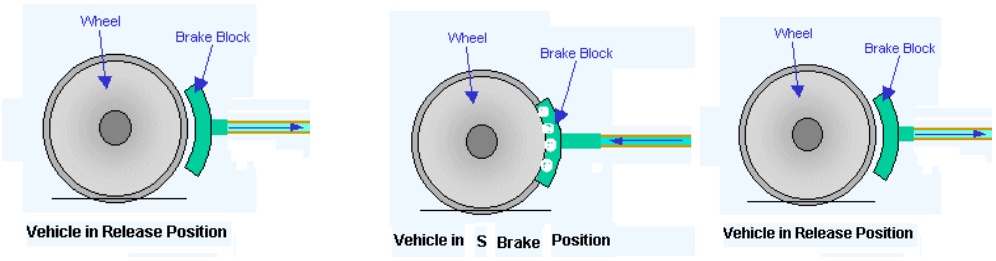

Figure 15-10-16

Usual inertial lock (annual inertial interaction) becomes slow quake as Figure 15-10-16

Therefore, predicted Earth quake period at Cascadian subductions zone by CFLE theory is

$$P_t = (157.03 \text{ yrs})(3)$$

$$=471.09 \text{ years}$$

$$\approx 500\ years \qquad 15\text{-}10\text{-}15$$

Observed and recorded values by earthquake archeology at Cascadian subductions zone is

$$T_e = 1700\text{-}(780\sim1190)\text{-}(690\sim730)\text{-}(350\sim420)\text{-}(660\sim440\text{BCE})\text{-}(980\sim890) \qquad 15\text{-}10\text{-}16$$

$$P_t = \frac{780+210+330+910+400+250}{6} = \frac{2880}{6}$$

$$= 480 \text{ yrs}$$

$$\approx 500 \text{ yrs} \qquad 15\text{-}10\text{-}17$$

Because continental crust is distorted by subduction and by this distortion continental crust is sinking and rising as Figure 15-10-17, we can solve origin mystery of New Madrid faults zone as why New Madrid becomes seismological source area.

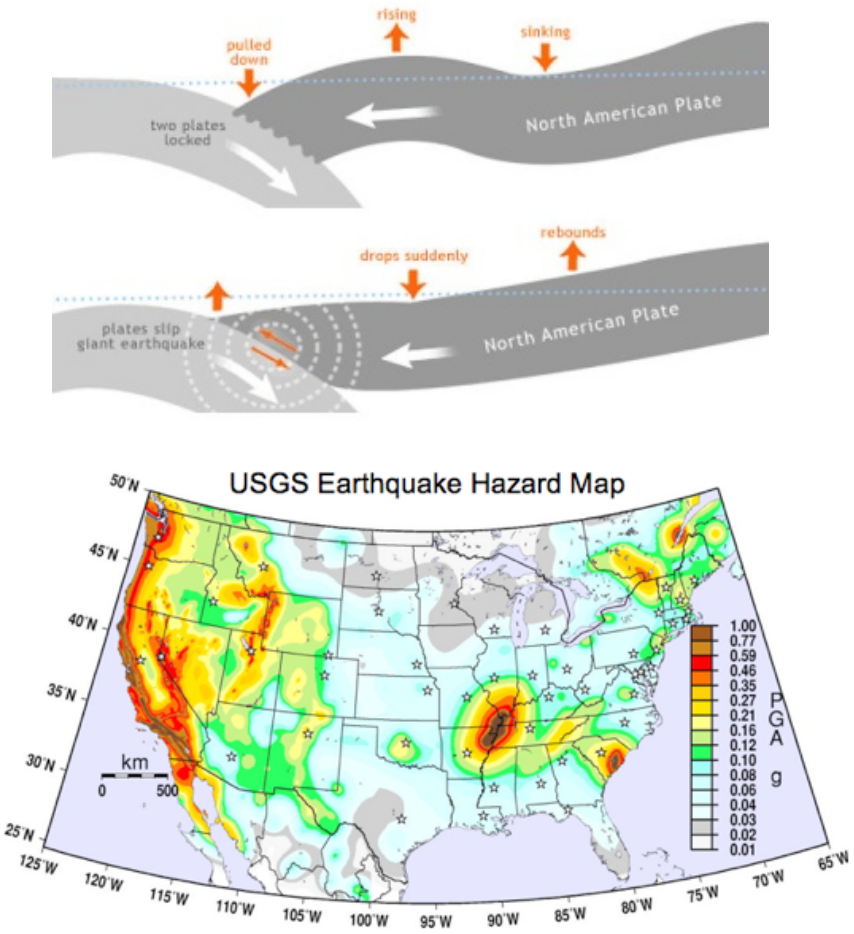

Figure 15-10-17

Distortion and restoration pattern should be repeated and reached to New Madrid in North America as typical inland quakes zone (example 2011 Tohoku earth quake in Japan reached and influenced to Norway), because North America is connected as continuous one continental crust with two subduction zones (Juan de Fuca plate and Rivera plate at Cocos plate from Farallon plate) as Figure 15-10-18. Distorting of continental crust by subducting from different two plate interfere one place. That is none other than New Madrid fault zone.

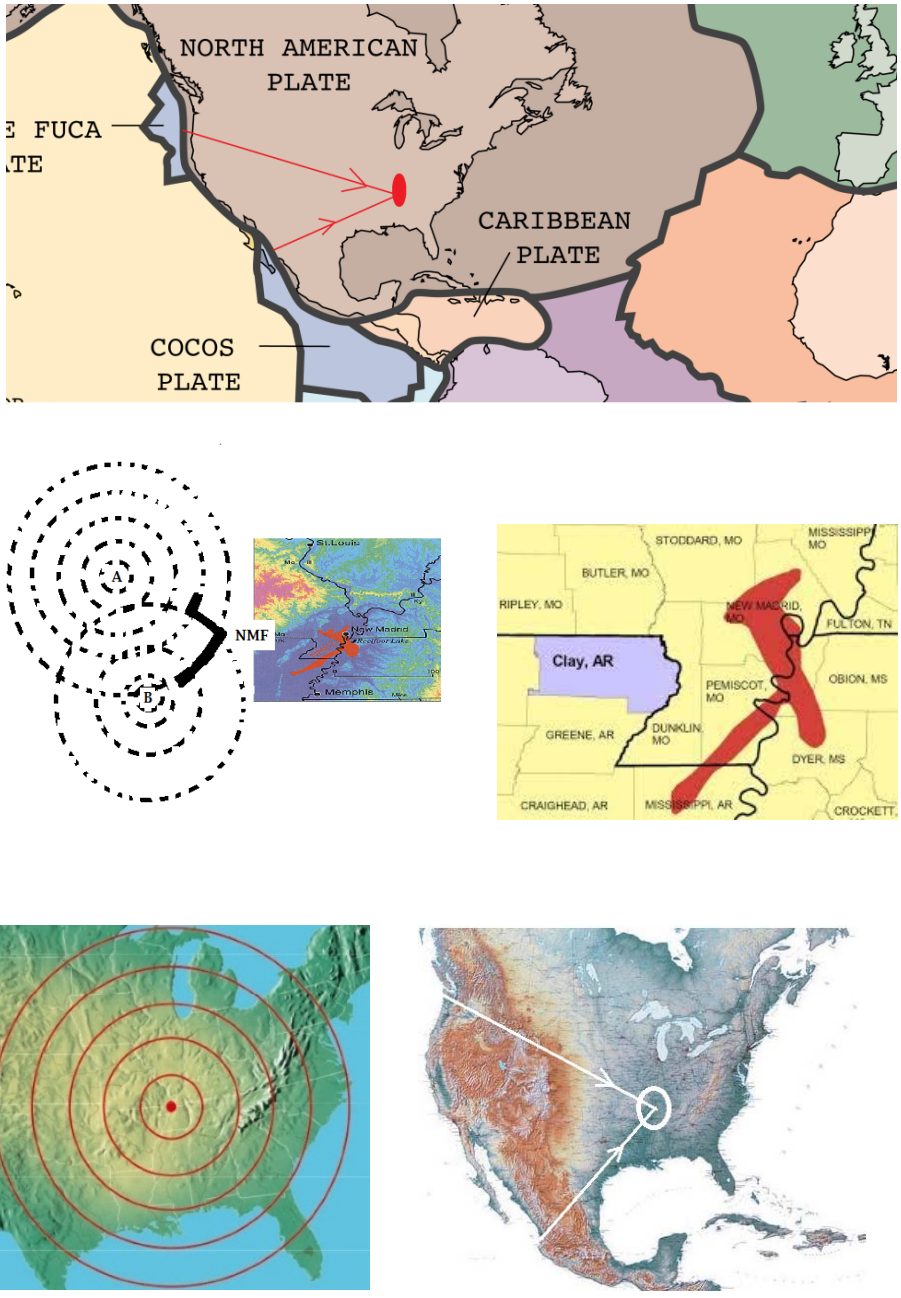

Figure 15-10-18

Between mountains range of pacific coast and the Appalachians is placed New Madrid fault line, because there is geologically weaker and softer than other region in the USA for seismological reaction from two different seismological sources to meet in one place together.

Therefore, nevertheless Tennessee earthquake fault zone is far from Cascade subduction zone and Cocos subduction zone, but major earthquake period of Tennessee should be 471.09 years theoretically.

$$f_3 = \frac{480}{157.03} = 3.056 \approx 3 \qquad 15\text{-}10\text{-}18$$

Observed value and recorded value by earth quakes archeology is

$$P_t \approx 500 \text{ yrs} \qquad 15\text{-}10\text{-}19$$

Such close relation between Cascadian subductions zone and New Madrid fault zone we can find clearly history of earth quakes in USA.

Earth quake of 1699. Dec. 25 that the first known written record of an earthquake felt in the New Madrid fault zone, was from a French missionary traveling up the Mississippi with a party of explorers. At 1 p.m., on Christmas Day 1699, at a site near the present-day location of Memphis, the party was startled by a short period of ground shaking.

One month after occurred along the Cascadia subduction zone on January 26 with an estimated moment magnitude of 8.7–9.2. This means that New Madrid earth quake occurred as last distortions earth quake by power from Cascadian subductions zone. Because Limit of distortion in New Madrid fault zone is broken, Juan de Fuca plate can move freely. This free moving of oceanic plate of Juan de Fuca was appeared as mega quake of 1700 at Cascadian subductions zone.

However, earthquake mechanism of San Andreas Fault zone is very different.

The San Andreas Fault is a continental transform fault that extends roughly 1300km through California. It forms the tectonic boundary between the Pacific Plate and the North American Plate, and its motion is right-lateral strike-slip (horizontal). The fault divides into three segments, each with different characteristics and a different degree of earthquake risk, the most significant being the southern segment, which passes within about 35 miles of Los Angeles. Therefore, earthquake-recurrence interval should be follow 157.03 years, because this transform fault doesn't need huge energy to heavy crust to lift up and bent.

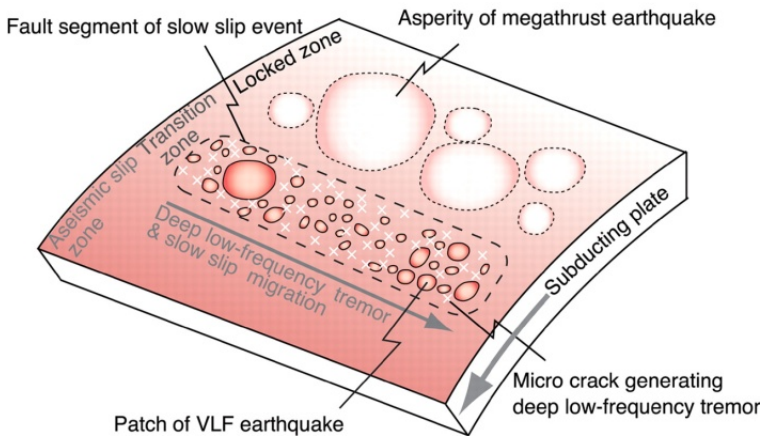

Figure 15-10-19

Slow earthquakes are occurred between oceanic plate and mantle. Therefore, for this mechanism is needed soft inertial change.

Figure 15-10-19 and Figure 15-10-20 well shows mechanism of slow quakes.

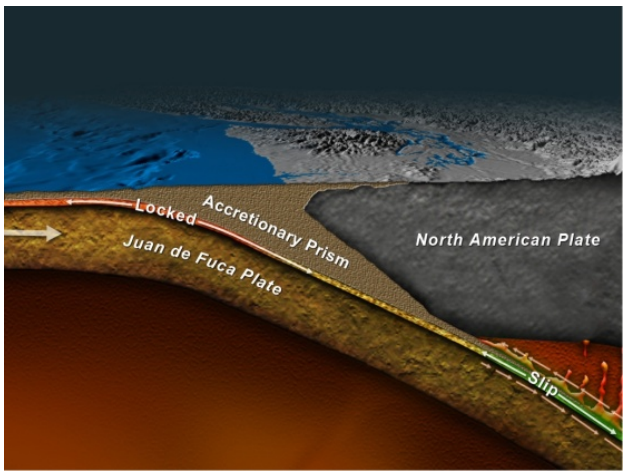

Figure 15-10-20

That is occurred by inertial change of annual inertial interaction.

Figure 15-10-21 shows potential change by earth orbit.

Therefore, period of slow quake should be more 1 years.

Because inertial interaction period of Earth is p= 64.029 days, minimum period should be

$P_{cascade}$ =6 times cycle = (6) (64.029 days) = 384.17days

= 54.9 weeks

= 13.7 months 15-10-20

Because slow earth quake occur between oceanic plate and mantle, period of slow earth quakes is influenced by different physical property of local oceanic plate.

Nankai trough is ~6 month, Cascadian subduction zone is ~14 month, Costa Rica subductions zone is ~15 month, and New Zealand is ~24 month. Because momentum (mass×speed) of oceanic plate of Nakai through is very big by thicker and heavier oceanic plate as much as Tohoku oceanic plate, for slow quake to occur is relatively more sensitive than other place of the Earth. Therefore, slow quake at Nankai trough can occur by relatively weak half annual inertial interaction change.

All of these different periods come from common factor of 64.5 days.

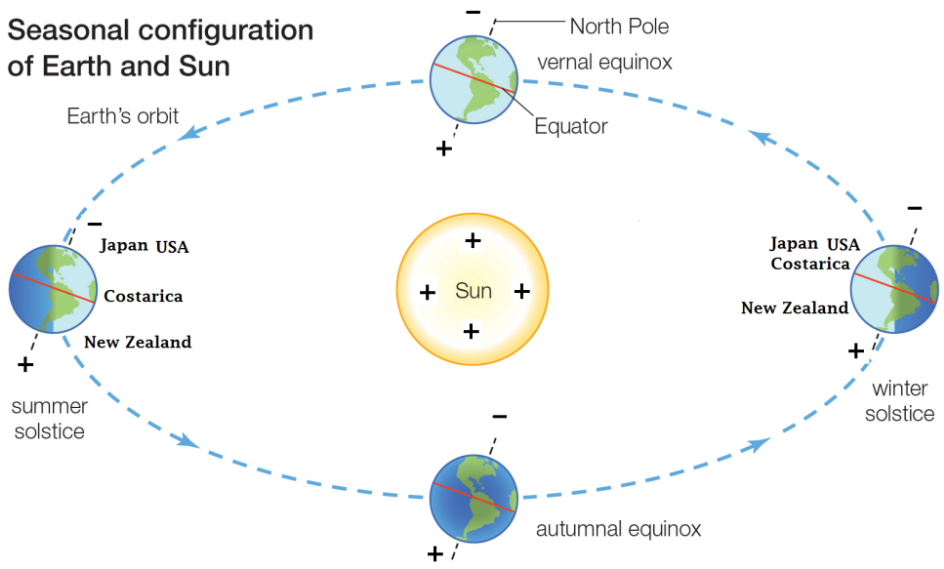

Figure 15-10-21

Figure 15-10-21 shows why such different period is established. Momentum of oceanic plate of Nankai trough should be relatively bigger than momentum of other oceanic plates of Costarica, Cascadia and New Zealand, therefore Shikoku area is relatively sensitive than other place.

Because seasonal configuration of gravitational property of the Sun and Earth is influenced differently at different place, period of slow quakes should be different as Figure 15-10-21.

Because, direction of movement of both oceanic plates is different as Figure 15-10-22, influence of inertial interaction should be different by different momentum.

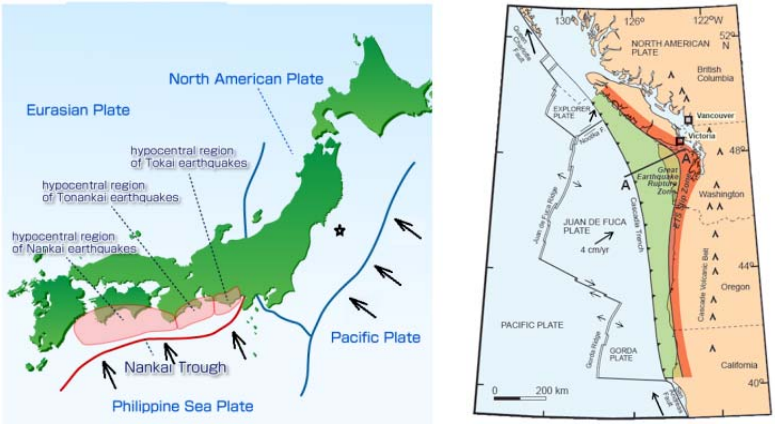

Figure 15-10-22

Observed value by G.Rogers et al in Geological Survey of Canada is

$$P_s = 13\sim16 \text{ months} \qquad 15\text{-}10\text{-}21$$

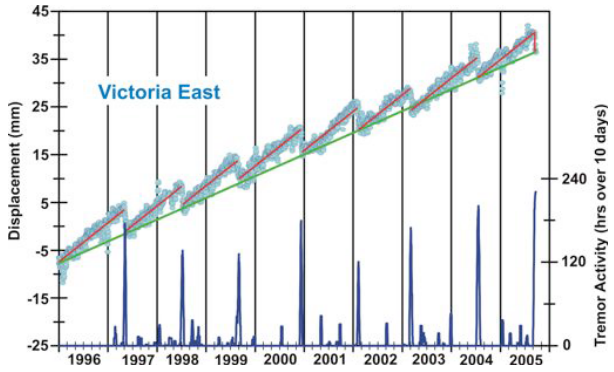

Continued Regularty of ETS in the Victoria Area by G.Rogers et al

Geological Survey of Canada Figure 15-10-23

This graph shows that inertial lock and release is repeated.

In other word, Earth is repeated expansion and contraction with periodicity.

Therefore, slow quakes period around 3 islands Kyushu, Shikoku, and Honshu is

$$P_{Nankai} = \frac{P_{cascade}}{2} = \frac{384.17\ days}{2} = 192.09\text{days}$$

$$= 27.4 \text{ weeks}$$

$$= 6.85 \text{ months} \qquad 15\text{-}10\text{-}22$$

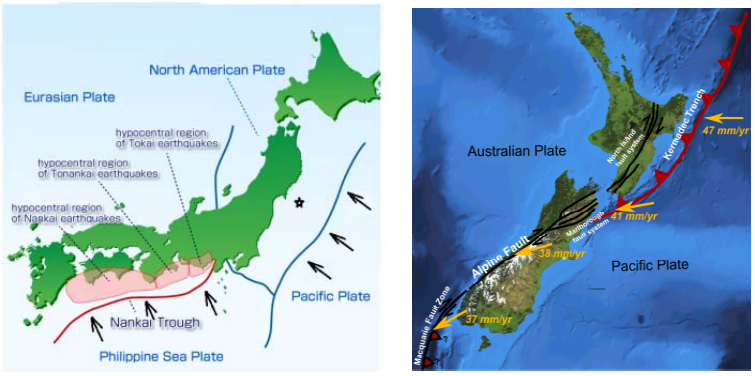

Figure 15-10-24

Because Earth's magnetic South Pole reacts as positive charge and Earth's magnetic North Pole react negative charge, total different between slow quakes periods of Japan and New Zealand should be

$$P_{Newzealand} = P_{Nankai} \times 4$$

$$= 109.6 \text{ weeks}$$

$$= 27.4 \text{ months} \qquad 15\text{-}10\text{-}23$$

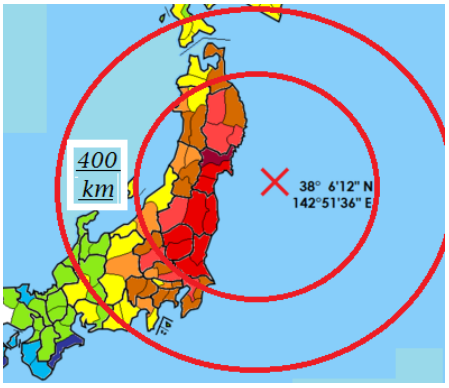

Distorted sinking area around 400km

from epicenter before Tohoku 2011

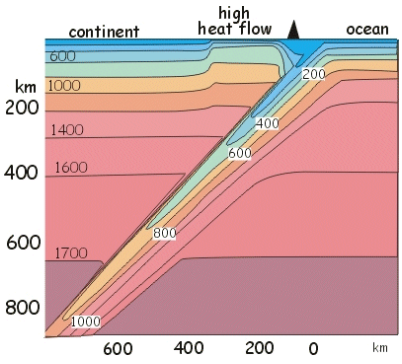

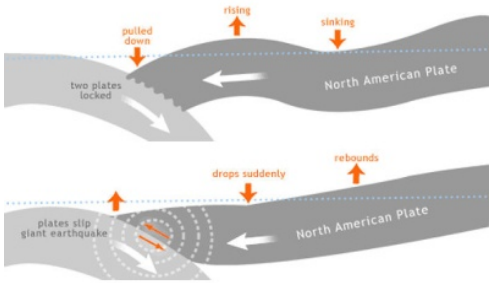

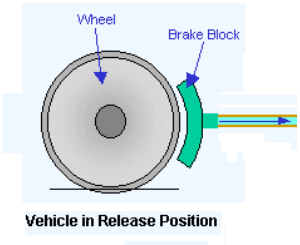

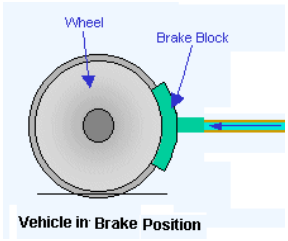

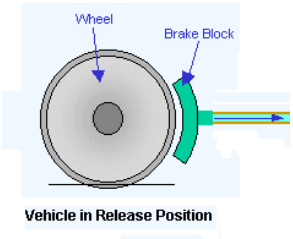

Figure 15-10-25

Different period of mega quake in Japan area is occurred by different local weight for asperity of continental crust of islands Kyushu, Shikoku, and Honshu. When asperity is established only just at Tokai, period of mega quake should be relative long term (over regular period of 157 years), because continental crust of Honshu is heavier than Shikoku and Kyushu. However, asperity is established only just at Kyushu, period of mega quake becomes relative short term (under regular period of 157 years), because continental crust of Shikoku is lighter than Honshu.

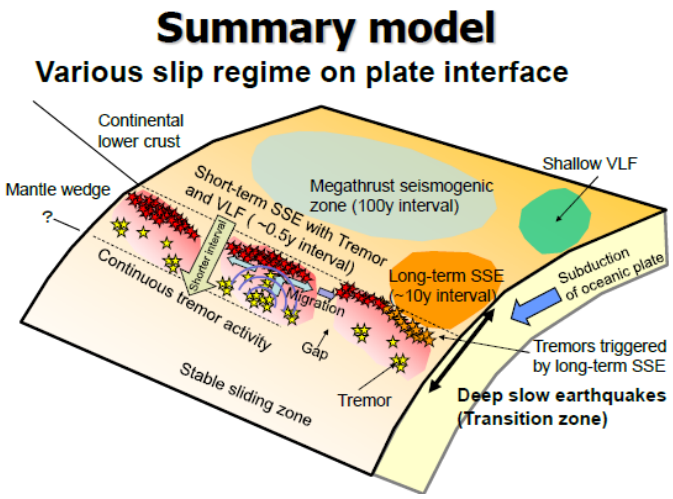

2010/10/10-14 Earthscope Workshop. Kazusige Obara, ERI, Univ. Tokyo

Figure 15-10-26

Figure 15-10-26 shows Obara's summary model of 20101010-14. This model can give first possibility to understand and to predict of earth quake (slow quakes and mega quakes) with CFLE theory why seismological locking and releasing between oceanic plate and continental crust occur.

Now, we can start to analyses about meaning of past earth quakes from AD 684 to 2011 in Japan. Before analyze we need to introduce new definition for earthquakes to classify. Figure 15-10-27 show 51 earth quakes from 1854 to 2011. Because from line of Sagami trench and central tectonic line of Honshu (is called central line) is started two different tectonic plates, each inland earths quakes and sea earth quakes should be distinguished as different earthquakes by different seismological sources. Because real seismological source of mega quake is only one asperity by inertial locking from inertial interaction, there should be only one main quake as mega quake. When asperity (black point of central line of west: left of Figure 15-10-27) is released at one seismological point, is started restoration. Because of this restoration is occurred earth quakes, these earthquakes are called restorative earthquakes (earth quakes of west of central line: left of Figure 15-10-27). These earth quakes are called transient earthquakes.

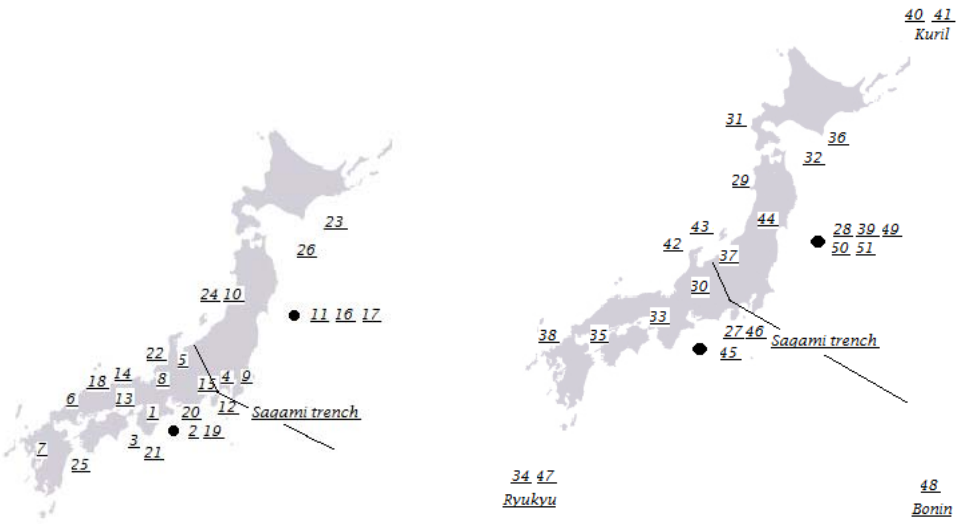

Figure 15-10-27

When restorative energy dissipates, is started real distortion. Right side of Figure 15-10-27 show distortive earthquakes.

Because by central line is separated two different seismological sources, all of earth quakes in Japan can be separated western earth quakes and eastern earth quakes.

Now, we can start analyze of historical recorded earth quakes from Table 15-10-3.

Figure 15-10-28 shows only distinguished earth quakes as main earth quakes.

Because earth quakes of AD 745-Minoh, 1361-Shohei, 1568-Tensho, 1605-Keicho,1611-Aizu,1611-keicho -Sanriku,1707-Hoei,1771-Yaeyama, 1792-Unzen, 1828-Echigo-Sanjo and 1847-Zenkoji are not main quakes, it was treated as distortive or restorative transient quakes.

Because epicenter of this necessary main earth quake AD ~ 1088 too far from Japan could be, it could not be observed.

AD~1088 quake is needed as main quake for periodicity to satisfy.

Therefore AD~1088 quake is put in the list.

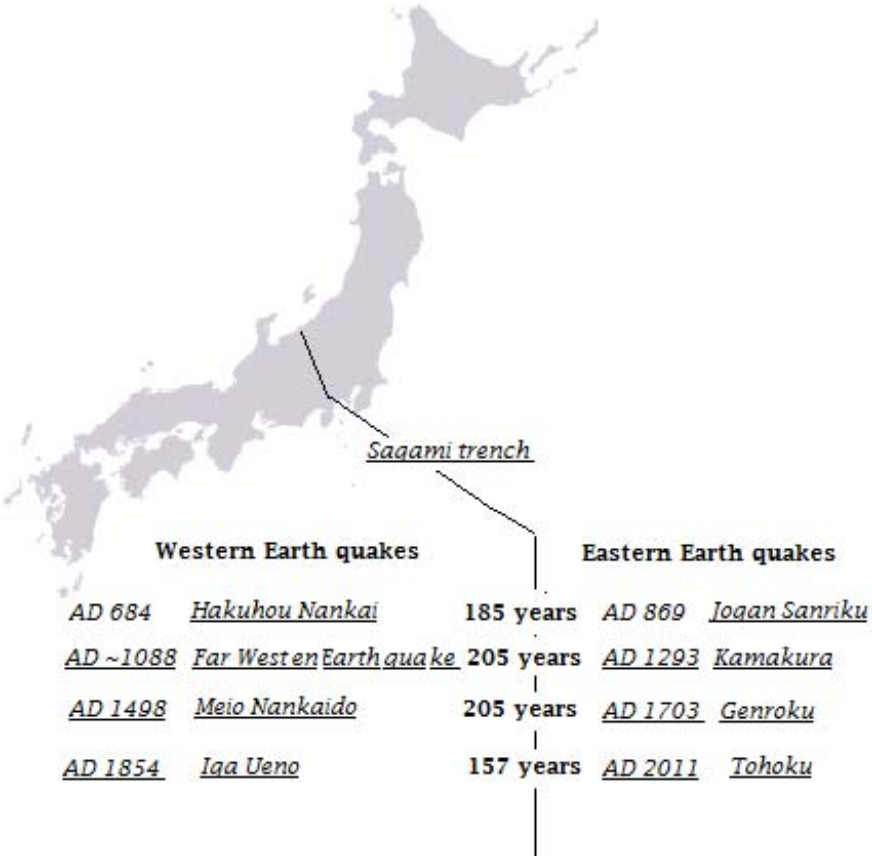

Figure 15-10-28

November 26, 684	Hakuhou Nankai	December 2, 1611	Keicho Sanriku
June 1, 745	Minoh	Dec 31, 1703	Genroku
July 9, 869	Jogan Sanriku	October 28, 1707	Hoei
May 20, 1293	Kamakura	April 24, 1771	Yaeyama
July 26, 1361	Shōhei	May 21, 1792	Unzen
Sep. 11, 1498	Meio Nankaido	Dec18, 1828	Echigo Sanjo
January 18, 1586	Tensho Ise Bay	May 8, 1847	Zenkoji
February 3, 1605	Keicho Nankaido	July 9, 1854	Iga Ueno
Sep 27, 1611	Aizu	March 11, 2011	Tohoku

Table 15-10-3

Next step of analyze is for number of transient earth quakes of sea by soft inertial interaction change according to half period of suns activity as Figure 15-10-29.

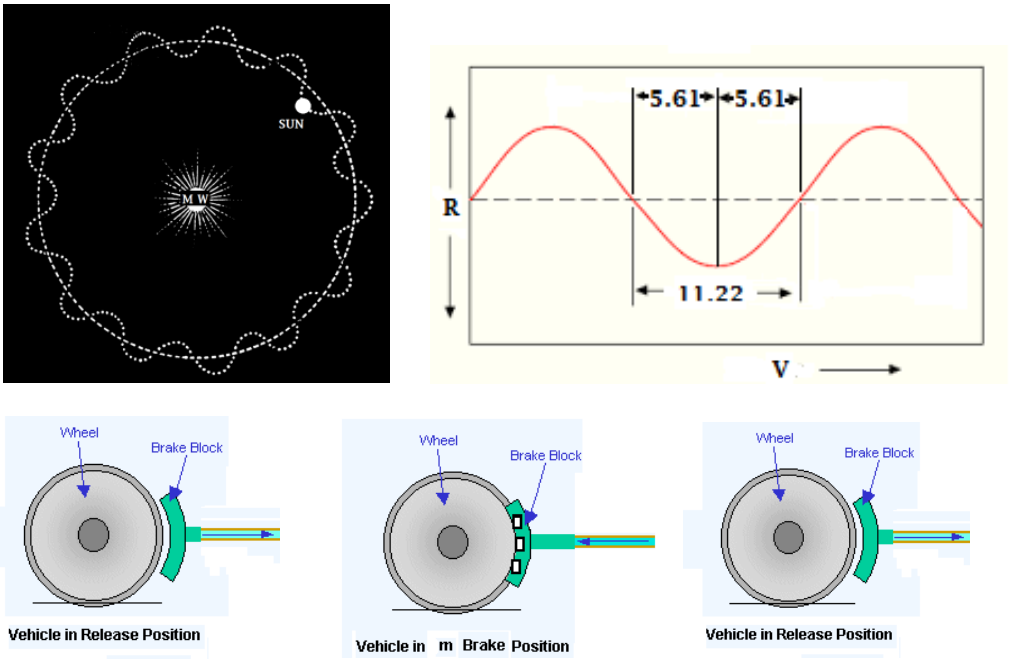

Figure 15-10-29

Because as leftover of Figure 15-10-29 sun move along galactic orbit, strength changes of inertial interaction occur periodically.

That is

P_t =(5.61 yrs)(1.035993) =5.812 yrs 5-10-24

where $x_{eff} = 1.035993$ is changed gravitational permittivity of earth

$x_{Earth} = 1.073176$

by ratio

$R_D = \frac{2.7 g.cm^{-3}}{5.5 g.cm^{-3}}$ of density between earth's average density and continental crust.

Therefore sea earth quakes can occur

$N_{sea} = \frac{157.03 yrs}{5.812 yrs}$=27.02 times 5-10-25

Observed value of sea (oceanic crust) earth quakes in Japan are

N_{sea} = 27 times 15-10-26

Essence of inland quakes and other sea quakes are distortive or restorative faults quakes by Asperity at subduction zone by inertial interaction as Figure 15-10-30.

Because energy for inland quakes are changed

by density difference between oceanic plate and continental crust,

$$R_{density} = \frac{3.3gcm^{-3}}{2.7g.cm^{-3}} = 1.222 \qquad 15\text{-}10\text{-}27$$

by gravitational permittivity difference of seawater,

$$x_{seawater} = 1.010588 \qquad 15\text{-}10\text{-}28$$

and by effective gravitational permittivity difference,

$$x_{eff} = 1.035993$$

number of inland quakes is changed as much as

$$f_n = 1.222 \times 1.036588 \times 1.010611$$

$$= 1.280152 \qquad 15\text{-}10\text{-}29$$

Therefore, possible total number of inland quakes in Japan is

$$N_{Inland} = \frac{27.06\ times}{1.280152} = 21.14 \text{ Times} \qquad 15\text{-}10\text{-}30$$

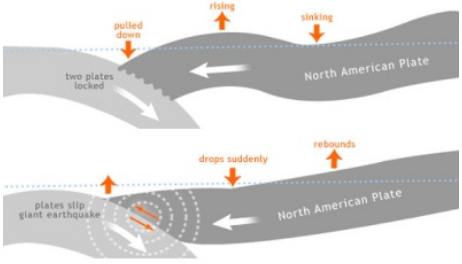

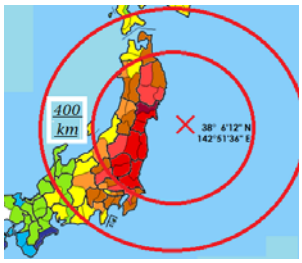

Restorative rising area around 400km from epicenter after Tohoku 2011

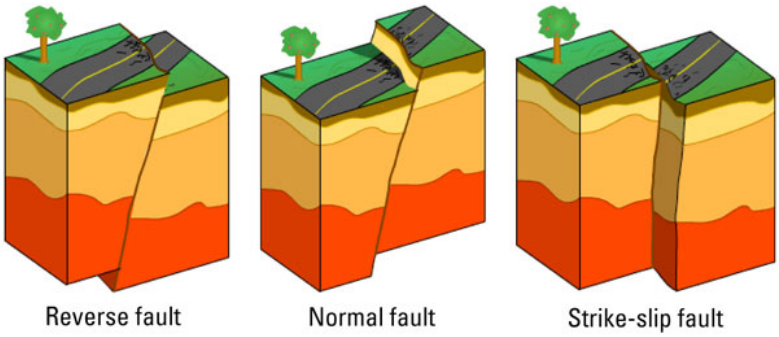

Figure 15-10-30

Historical observed list of earthquakes from 1854 before 2011 is

Table 15-10-4

1. 1854 Iga Ueno earthquake@.	25. 1968 Hyūga-nada earthquake
2. 1854 Ansei-Tōkai earthquake.	26. 1968 Tokachi earthquake
3. 1854 Ansei-Nankai earthquake.	27. 1974 Izu earthquake@.
4. 1855 Ansei Edo earthquake@.	28.1978 Miyagi earthquake
5. 1858 Hietsu earthquake@.	29. 1983 Japan Sea earthquake
6. 1872 Hamada earthquake@.	30. 1984 Otaki earthquake@.
7. 1889 Kumamoto earthquake@.	31. 1993 Hokkaidō earthquake
8. 1891 Mino-Owari earthquake@.	32. 1994 Sanriku earthquake
9.1894 Meiji Tokyo earthquake@.	33. Hanshin earthquake@.
10. 1894 Shōkai earthquake@.	34. 1998 Ryukyu earthquake
11.1896 Meiji-Sanriku earthquake.	35. 2001 Geiyo earthquake
12. 1923 Great Kantō earthquake@.	36. 2003 Hokkaidō earthquake
13. 1925 Kita Tajima earthquake@.	37. 2004 Chūetsu earthquake@.
14. 1927 Kita Tango earthquake@.	38. 2005 Fukuoka earthquake
15. 1930 North Izu earthquake@.	39. 2005 Miyagi earthquake

16. 1933 Sanriku earthquake.	40. 2006 Kuril earthquake
17. 1936 Miyagi earthquake.	41. 2007 Kuril earthquake
18. 1943 Tottori earthquake.	42. 2007 Noto earthquake@.
19. 1944 Tōnankai earthquake.	43. 2007 Chūetsu earthquake
20. 1945 Mikawa earthquake	44. 2008 Iwate earthquake@.
21. 1946 Nankaidō earthquake.	45. 2009 Izu earthquake
22. 1948 Fukui earthquake@.	46.2009 Tokai earthquake
23. 1952 Hokkaido earthquake.	47. Ryūkyū earthquake.
24. 1964 Niigata earthquake@.	48. 2010 Bonin earthquake

Total observed number of Inland (continental crust) earthquakes is

$$N_{@IN} = \frac{27.06}{1.280152} = 21 \text{ times} \qquad 15\text{-}10\text{-}31$$

From Table 15-10-4 we can list 21 transient inland quakes as

$$N_{@IN} = 21$$

$$= \{1_1 4_{2P} 5_3 6_4 7_5 8_6 9_7 10_8 12_{9P} 13_{10} 14_{11} 15_{12} 18_{13} 22_{14}$$

$$24_{15P} 27_{16} 30_{17} 33_{18} 42_{20P} 44_{21P}\} \qquad 15\text{-}10\text{-}32$$

From 21 inland quakes number of eastern inland quakes is

$$N_{@INeast} = 6$$

$$= \{4_{2P} 12_{9P} 24_{15P}\ 37_{19P} 42_{20P} 44_{21P}\} \qquad 15\text{-}10\text{-}33$$

In Figure 15-10-31 we can find only 6 eastern inland quakes and same sea quakes of western and eastern. This means that eastern inland mass (eastern Honshu from central line) is ~ 3 times bigger than western inland mass (western Honshu, Shikoku, and Kyushu).

Ratio of inland quake number between total inland and eastern quakes is

$$R_{IN} = \frac{6}{21} \approx \frac{1}{3} \qquad 15\text{-}10\text{-}34$$

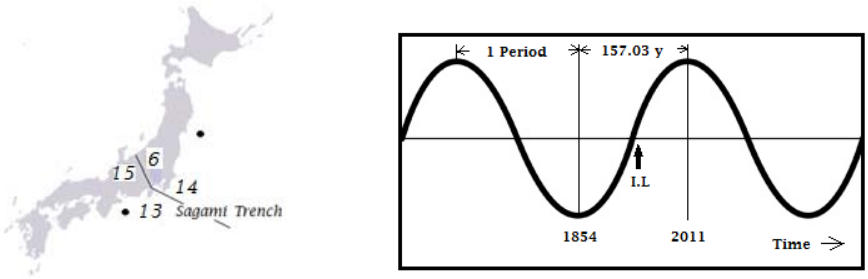

Figure 15-10-31

Now we can calculate when inertial locking by inertial interaction was started for Tohoku mega quake of 2011.

Because 1 period is 157.03 years, inertial locking should be started

$$T_{IL} = \frac{157.03yrs}{2} = 78.52\ yrs \qquad 15\text{-}10\text{-}35$$

Because Iga-Ueno earth quake occurred in July.9.1854, this is 1854.51 by Calendar of 1854.

That is

d_{tot} =Jan: 31+Feb: 28+Mar: 31+ Apr: 30+May: 31+Jun: 30+Jul: 7

=188days = 0.51 year 15-10-36

Therefore, expected locking date was

T_{expect} =1854.51+78.52=1933.03

0.03 year is 11days by calendar of 1854

1933.03 year means January 11.1933.

Historically, 8.4M_wSanriku earth quake at 02:31 AM local time on Friday March 3.1933 (Thursday at 17:31 March 2, 1933 UTC) located offshore, 290 km east of the city of Kamaishi, Iwate (Epicenter$39^o 7.7' N 144^o 7' E$) occurred really two month after theoretical inertial locking date of Jan.11.1933.

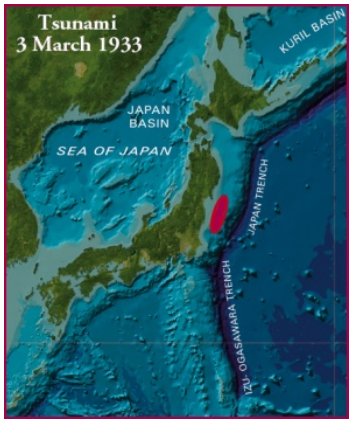

1933 Sanriku earthquake

Plate	Absolute Velocity (cm/yr)*
Antarctic	~2.05
African	~2.15
Arabian	~4.65
Caribbean	~2.45
Cocos	~8.55
Eurasian	~0.95
Indian	~6.00
Nazca	~7.55
North American	~1.15
Pacific	~8.10
Philippine	~6.35
South American	~1.45

Form the Physics Fact book

Edited by Glenn Elert

Figure 15-10-32

Therefore, we can calculate how long distorted continental crust from the inertial locking point at Tohoku sea area of 2011 by subducting pacific plate.

Because average annual subducting speed of pacific plate according to Glenn Elert(right side of Figure 15-10-32) is

$$v_{pacific} = 8.10 cm/yr \qquad 15\text{-}10\text{-}37$$

Therefore, total distant of distorted continental crust at Tohoku is

$$d_{distorted} = \left(\frac{8.10cm}{yr}\right)\left(\frac{157.03yrs}{2}\right)$$

$$= 636cm \qquad 15\text{-}10\text{-}38$$

Figure 15-10-33 show observed total restorative movement of continental crust after March11, 2011 Tohoku earth quake.

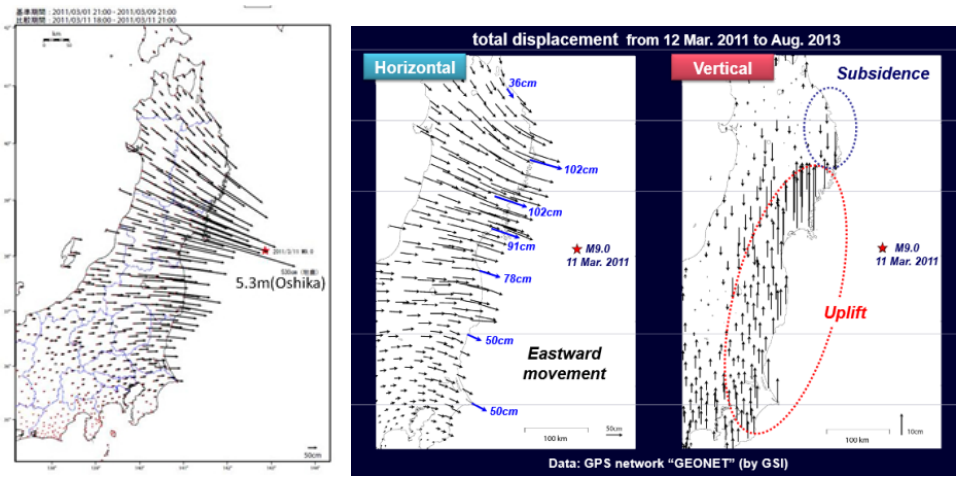

Figure 15-10-33

Observed maximum value of GEONET by GSI in Japan is

$$d_{crust} = 530\text{cm} + 102cm$$

$$=632\text{cm} \qquad 15\text{-}10\text{-}39$$

Expected average speed of pacific plate in Tohoku area should be

$$v_{everage} = \frac{632cm}{78.52yr}$$

$$= 8.05cm/yr \qquad 15\text{-}10\text{-}40$$

Observed value by G.Elert is

$$v_{everage} = 8.10cm/yr \qquad 15\text{-}10\text{-}41$$

Strongest inertial interaction as 2011 Tohoku earth quake that is cause of strongest mega quake occur by gravitational configuration of galaxy and sun and moon as Figure 15-10-34

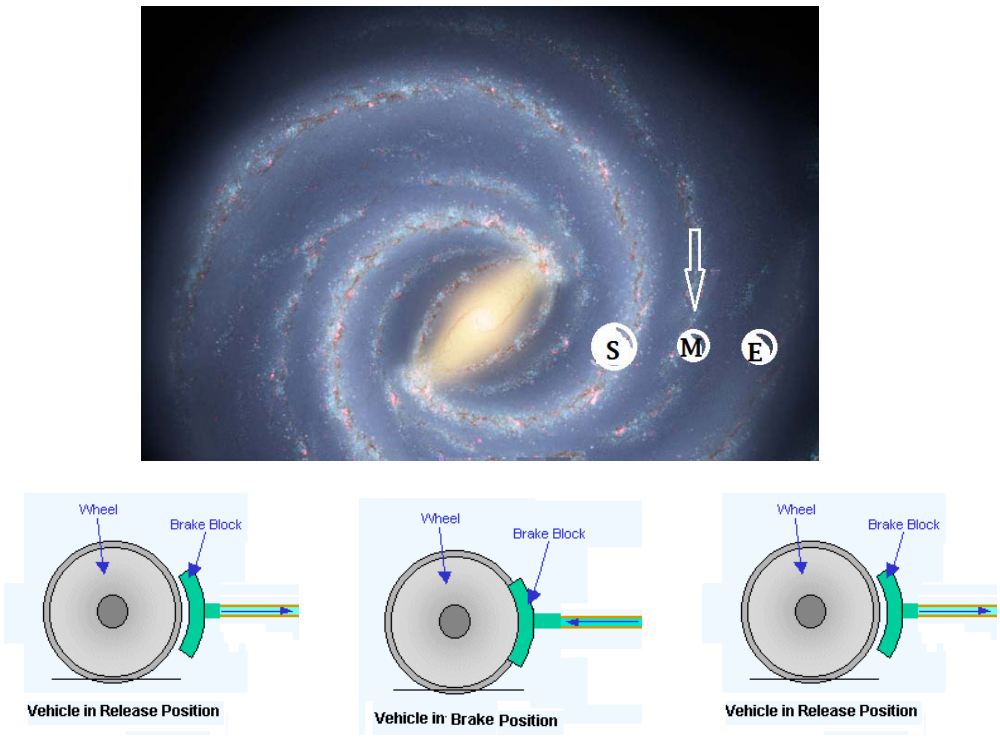

Figure 15-10-34

Observed value after 2011 Tohoku observed value of speed of plate of Nankai trough 2012~ 2015 is

$$v_{everage} \approx 6cm/yr \qquad 15\text{-}10\text{-}42$$

This speed is normal speed before inertial locking, but not unusual fast speed.

Figure 15-10-35 show Pre-and post seismic slow slip surrounding the 2011Tohoku-oki earthquake rupture by Naoki Uchida n, Toru Matsuzaw from journal of Earth and Planetary Science Letters (Journal homepage: www.elsevier.com/locate/epsl.Article history is that Received 27 October 2012, Received in revised form 9 May 2013, Accepted 12 May 2013. Editor: P. Shearer. Available is online 14 June 2013). Important point of this figure is that we can predict next point of asperity. Because CFLE theory can calculate next inertial locking date and release date as same date of mega quake as Tohoku 2011, such observation is needed absolutely.

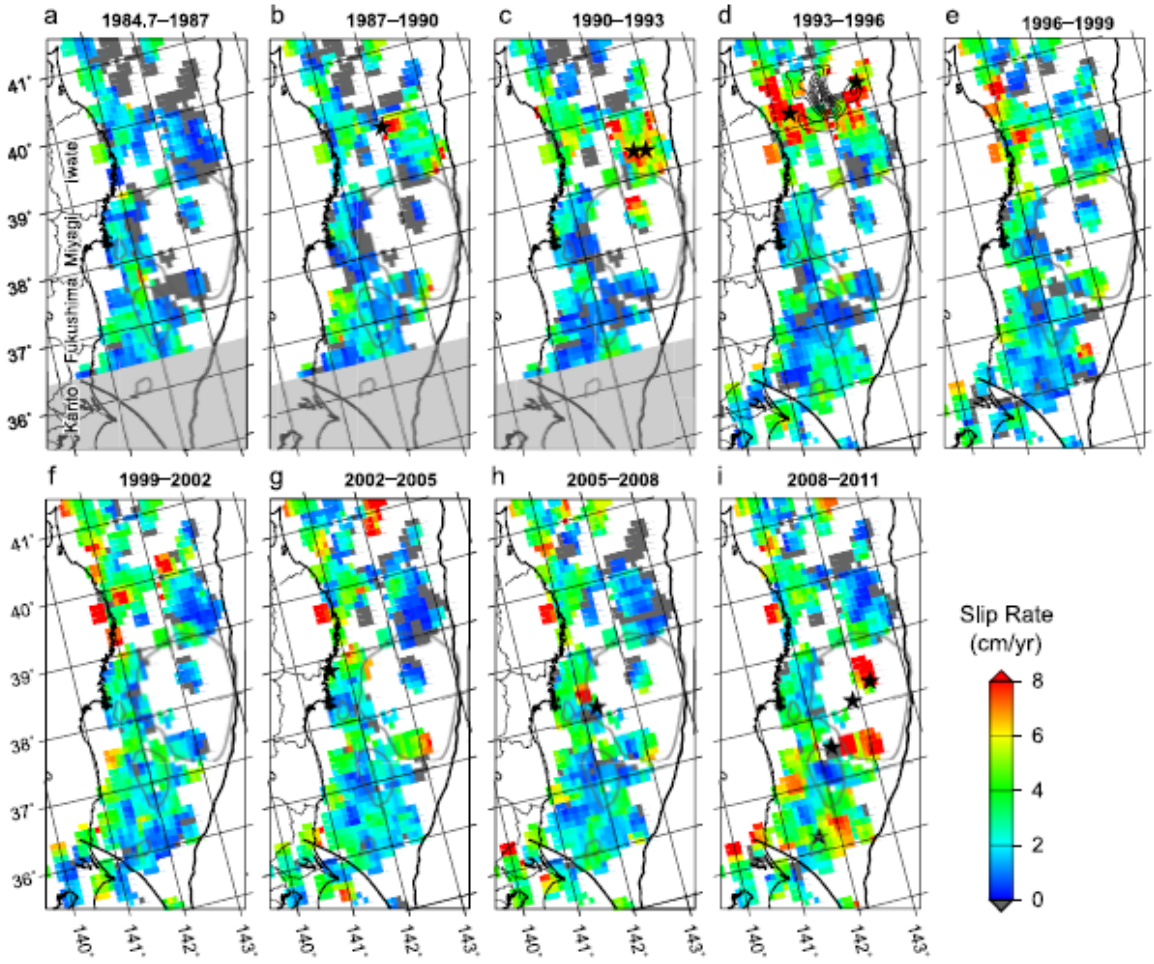

Inter plate slip rate distribution in each3- yr interval (colour).

The slip amounts estimated from repeaters are averaged in 0.31_0.31 windows shifted in0.11 increments. The windows (regions) with two or less repeating earthquake groups are shown in white. Grey windows indicate zero a seismic slip (no repeater activity) during the period.

Black stars show earthquakes of M6.9 or larger and shallower than 70km depth. Grey lines show 10m co seismic contour of the Tohoku-oki earth quake (linuma et al., 2012). The black line marks the north eastern limit of the Philippine Sea plate. Note that relatively high slip rates were observed in the co seismic slip area of the Tohoku- oki earth quake for the period just before the Tohoku-oki earth quake. Light grey are as before1993 show no estimation because of data limit at ion in that period. Relatively high and stable slip rates are seen in the deeper (western) portion of the plate boundary. The high slip rate in the northern part in1993–1996(d) is related to the Sanriku- haruka-oki earth quake in 1994(M7.6) whose slip distribution is shown by contours (Uchida etal. 2004; Yamanaka and Kikuchi, 2004). (For interpretation of the references to colour in this figure legend, the reader is referred to the web version of this article.)

Figure 15-10-35

By Figure 15-10-36 we can find and fix next date of inertial locking, asperity and main mega quake after 157.03 years in Nankai trough when solar cycle is normal.

2011 2168

Figure 15-10-36

Prediction for next Inertial Locking date by CFLE theory is below.
Date of March, 11.2011 is calculated 2011.19 by Calendar of 2011

Jan: 31+Feb: 28+Mar 11=70days=0.19 years

Therefore, next inertial locking could be started at

$T_{I.N}$= 2011.19 + $\frac{157.03}{2}$ = 2089.71 15-10-43

Date of 2089.71 is October, 17. 2089 by calendar of 2089.
That is
0.71year = 259.3 days →
Jan: 31+Feb:28+Mar:31+Apr:30+May31+June30+July31+
Aug:31+Sep: 30+Oct: 17.3 days 15-10-44

Expected location should be Nankai trough around south sea of Izu peninsula or east sea of Iga as figure 15-10-36.
Expected Magnitude could be

$M_w \approx 8.4$ 15-10-45

Date Prediction for next main quake as mega quake by CFLE theory should be

$T_{M.M} = 2089.84+78.515=2168.36$ 15-10-46

Date of 2168.36 is May, 11.2168 by calendar of 2168.
That is
0.36year=131.49 days→
Jan: 31+ Feb: 29+Mar: 31+Apr: 30+May: 10.9 days 15-10-47
Expected location should be Nankai trough around south sea of Izu peninsula or east sea of Iga as figure 15-10-36.
Expected magnitude should be
$M_w \leq 9.0$ 15-10-48

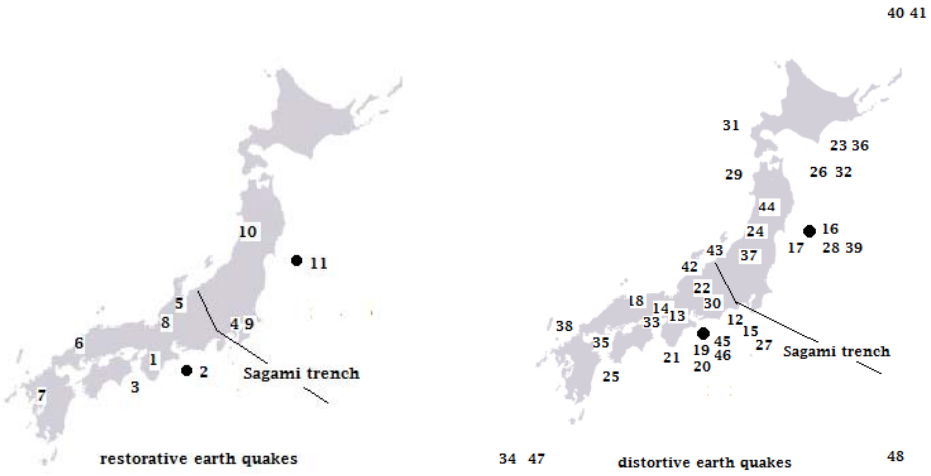

Figure 15-10-37

Because of emancipation of distorted energy of Figure 15-10-37 should be expected that distortive earth quakes is changed to restorative earth quakes and restorative earth quakes is changed to distortive earthquakes.

Because central Honshu is heaviest land of all of Japan is expected lot of restorative earth quakes from Tohoku event of March, 11.2011. Observed earth quakes in Japan from 2011 to 2015(30 events of 2011and 13 events of 2012 is expressed in Figure 15-10-38) are

Table 15-10-5

1.2011-Tōhoku foreshock	14.2013- 326km E of Namie
2. 2011-Tōhoku main	15. 2014-110km NW of Nago
3. 2011-Tōhoku aftershock	16. 2014-15kmNNE Kunisaki
4. 2011-Miyagi aftershock	17. 2014-23kmESE Ito
5. 2011-Fukushima aftershock	18. 2014-134km ES Iwo jima
6. 2011-Fukushima aftershock	19. 2014-Bonin island
7. 2012 -Izu Islands	20.2014- 135 ESE Namie
8. 2012-Kamaishi among 13	21.2014-81km E Mutsu
9.2013- 15km SW Obihiro	22.2014-154ENE Hachinohe
10.2013- 107km E Miyako	23.2014-16km N Omachi
11.2013-Izu island	24.2015-83km ENE Miyako
12.2013- 50 km Namie	25.2015-140km E Miyako
13.2013- Izu island	26.2015-130km E Miyako

Distribution of these events is

Where square means same area quakes of Honshu

Figure 15-10-38

These distributions of restorative earth quakes in Figure 15-10-37 are very similar with distribution of distortive earth quakes by main Tohoku 2011 in Figure 15-10-38.

Therefore, expected total quakes number from 2011 to 2168 should be

$$N_{total} = 48 \qquad 15\text{-}10\text{-}49$$

Expected total inland quakes should be

$$N_{inland} = 21 \qquad 15\text{-}10\text{-}50$$

Expected eastern inland quakes should be

$$N_{eastern} = 6 \qquad 15\text{-}10\text{-}51$$

Expected sea quakes should be

$$N_{sea} = 27 \qquad 15\text{-}10\text{-}52$$

Figure 15-10-38 shows change of sunspot number from Solar cycle 23 (2000-2008) to Solar cycle 24(2008-2015).

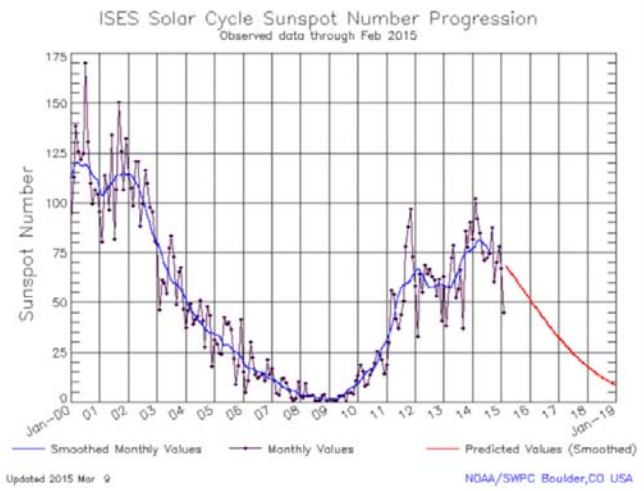

Figure 15-10-39

Because between mass and mass magnet is there different as much as

$$\frac{1.463}{8} = 0.183 \qquad 5\text{-}3\text{-}8\text{-}7$$

Correspondence factor is

$C_c = 1.5$

and period of sun's magnetic change is

$P_t = 11.22$ years 15-9-12

Retarded interval from gravito magnetic interaction to gravitational inertial interaction should be

$I_{re} =$ (11.22 years)(0.183)(1.5)

=3.080 years 15-10-53

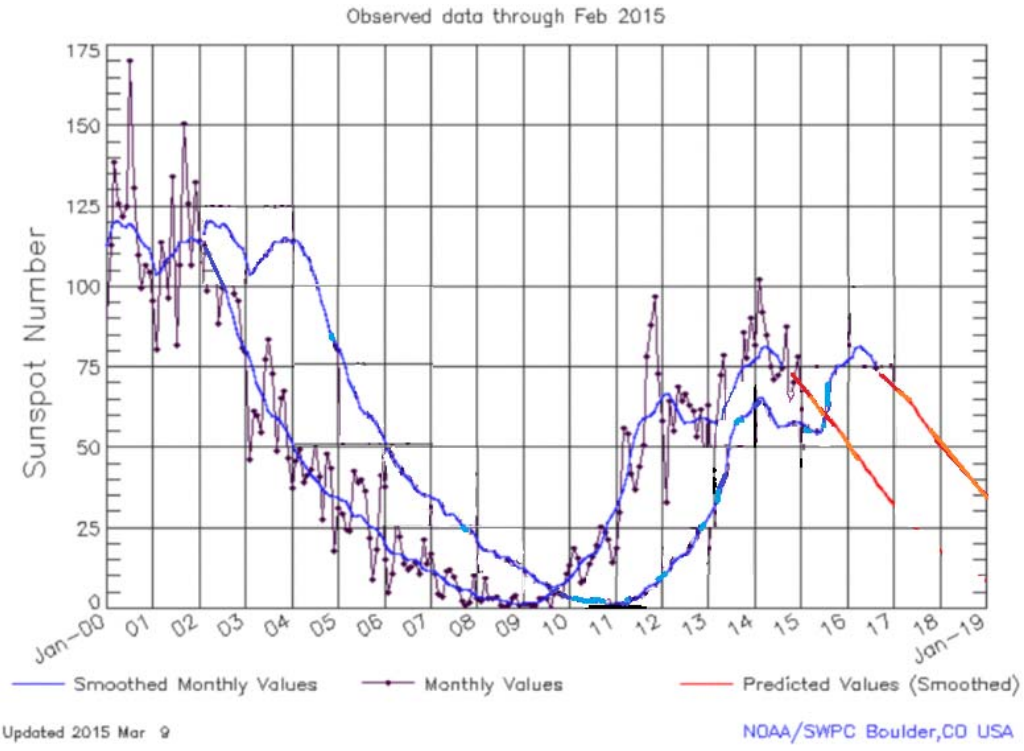

2002	2003	2004	2005	2006	2007	2008	2009	2010	2011	2012
1341	1358	1672	1844	1865	2270	1948	2057	2136	2494	1558

Figure 15-10-40

Gravitational minimum date is March, 11. 2011 of Tohoku event.

Start date of new sunspot period should be

T_{in} = 2011.19 years – 3.080years

= 2008.11years 15-10-54

2008.11year is Feb, 10 2008 by calendar of 2008

That is

0.11 year= 40.18 days→ Jan: 30 +Feb: 10.18

→Feb.10. 2008 15-10-55

Observed value is

T_d =January, 24.2008 15-10-56

Top of figure 15-10-40 shows change of sunspot number and gravitational retarding from Feb, 10.2008 to Mar, 11.2011. Middle of figure 15-10-40 shows increasing number of earthquakes.

This increasing is peaked 2011.

Here, we can find exact close relation between sun's position (sunspot number) and earth quakes number.

Therefore, we can determine about meaning of solar cycles from

Solar cycle 9 (1843-1855) to Solar cycle 24(2008-) as figure 15-10-41

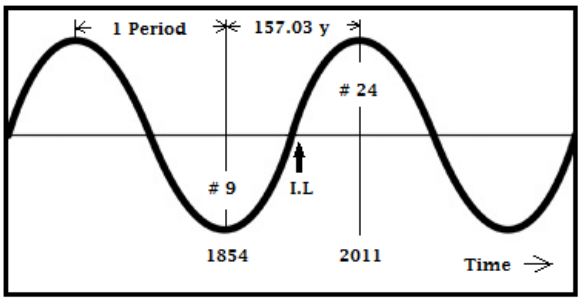

Figure 15-10-41

Figure 15-10-41 shows galactic orbital radius change of the Sun.

In 1854 (Ueno-Iga earth quake) of Solar cycle 9 Sun was nearest position from center of Milky Way and in 2011(Tohoku earth quake) of Solar cycle 23 Sun was fares position from the center of Milky Way.

Now, by CFLE theory we can predict strongest destructive main earth quakes that give us global economical damage only by one time. Problems of other transient earth quakes are only problems that resolution is not only prediction of each transient earth quake, but also perfect architectural engineering for building, residence, bridge, effective defense system against transient earth quakes and mega tsunami by new defensive city design.

A sinkhole, also known as a cenote, sink, sink-hole, shakehole, swallet, swallow hole, or doline (the different terms for sinkholes are often used interchangeably), is a depression or hole in the ground caused by some form of collapse of the surface layer. Some are caused by karst processes—for example, the chemical dissolution of carbonate rocks or suffosion processes.

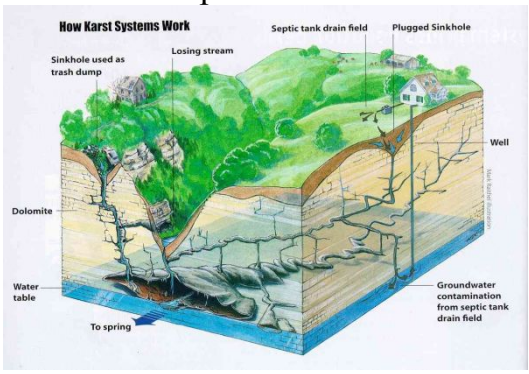

Figure 15-10-42

Formation of sinkholes is a well known phenomenon, occurring in many parts of the world (Spain, United States, Italy, Thailand, and more).

The mechanism that is responsible for the appearance of sinkholes is dissolution of soluble rocks and creation of subsurface cavities.

Sinkholes may vary in size from 1 to 600 m both in diameter and depth, and vary in form from soil-lined bowls to bedrock-edged chasms. Sinkholes may be formed gradually or suddenly, and are found worldwide.

Figure 15-10-43

Sinkholes are common where the rock below the land surface is limestone or other carbonate rock, salt beds, or in other rocks, such as gypsum, that can be dissolved naturally by circulating ground water. Sinkholes also occur in sandstone and quartzite terrains.

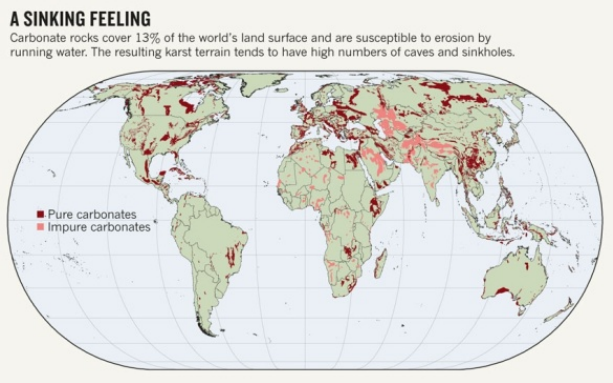

Figure 15-10-44

Sinkholes also form from human activity, such as the rare collapse of abandoned mines and salt cavern storage in salt domes in places like Louisiana, Mississippi and Texas. More commonly, sinkholes occur in urban areas due to water main breaks or sewer collapses when old pipes give way. They can also occur from the over pumping and extraction of groundwater and subsurface fluids.

However, in CFLE theory sinkhole is called sink quake or spot quake. Because, last reason is inertial interaction as figure 15-10-45.

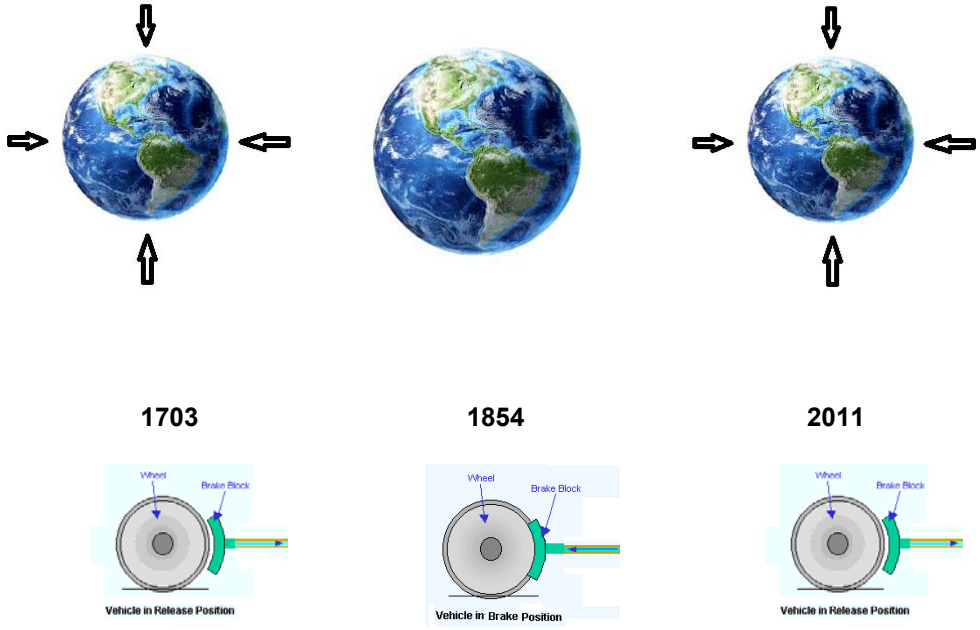

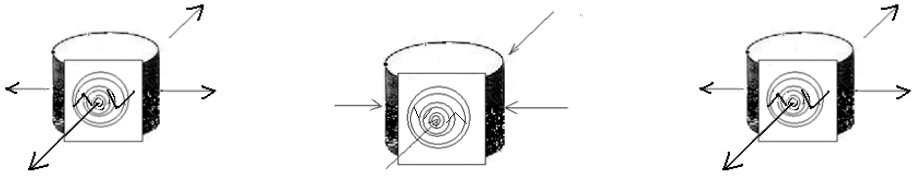

Figure 15-10-45

By inertial interaction is changed relative volume of the Earth.

Earth volume of 1854 is bigger than 2011.

This means that possible volume of 2011 for sink hole is bigger than 1854.

Therefore, expected sink holes number of 2011 should be more than 1854 world widely.

Map of source IPs connecting to a two-week sinkhole of 100 no-ip.org domains from at ARBOR NETWORKS DDos & Security Report.

By: Dennis Schwarz - 02/04/2013

Figure 15-10-46

Figure 15-10-48 shows how many events of sink hole occur during two week globally.

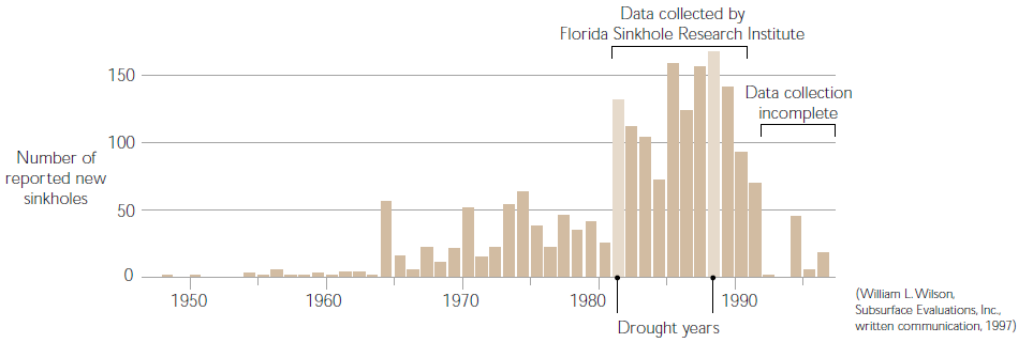

Figure 15-10-47

Figure 15-10-49 shows increase tendency of Florida sink hole, nevertheless collected data is incomplete by Florida Sink hole Research Institute. Sinkholes are a natural component of Florida's landscape. In Florida sinkholes form in carbonate bed lock, principally limestone and dolostone.

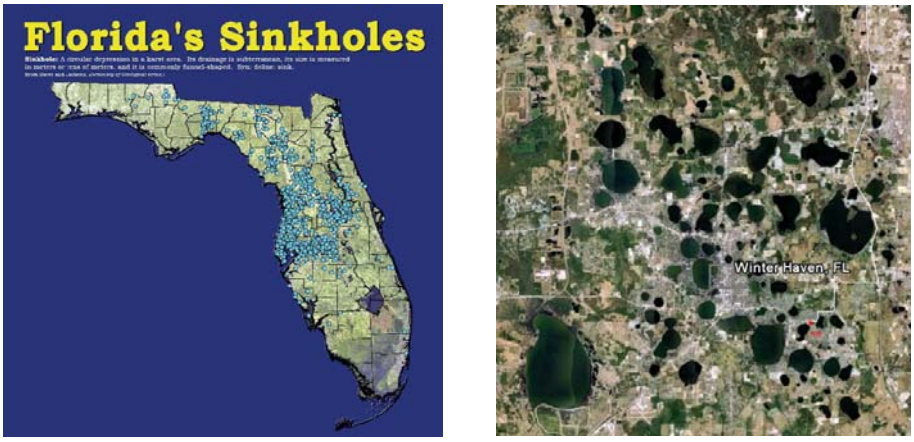

Figure 15-10-48

Figure 15-10-50 shows distribution of sinkhole in Florida by Florida Geological Survey 2004.

The natural sinkhole growing tendency, however, we can clearly confirm Dead Sea sinkholes.

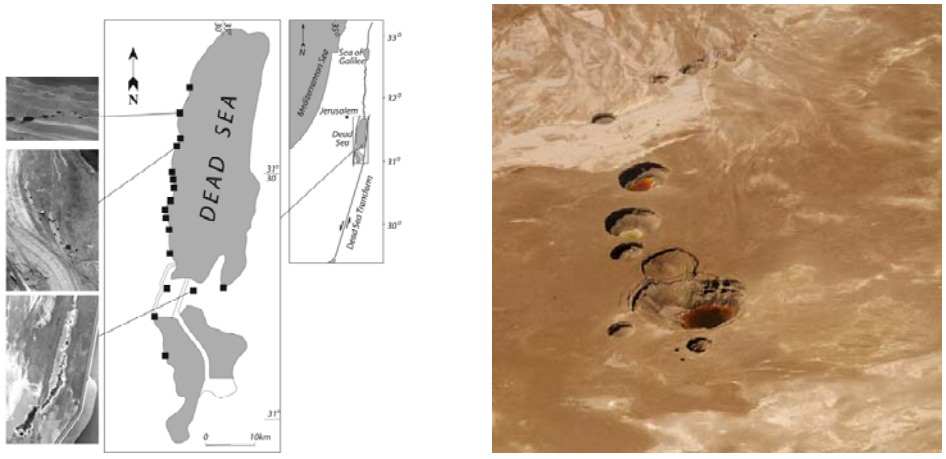

Figure 15-10-49

The formation of sinkholes at the Dead Sea area reflects subsurface cavities formed by salt dissolution. This dissolution is related to the recession of the Dead Sea; the groundwater level and the fresh/saline water interface along the shore decline at a similar rate to the rate of the Dead Sea recession, and brines that used to occupy layers below this interface are flushed out by freshwater.

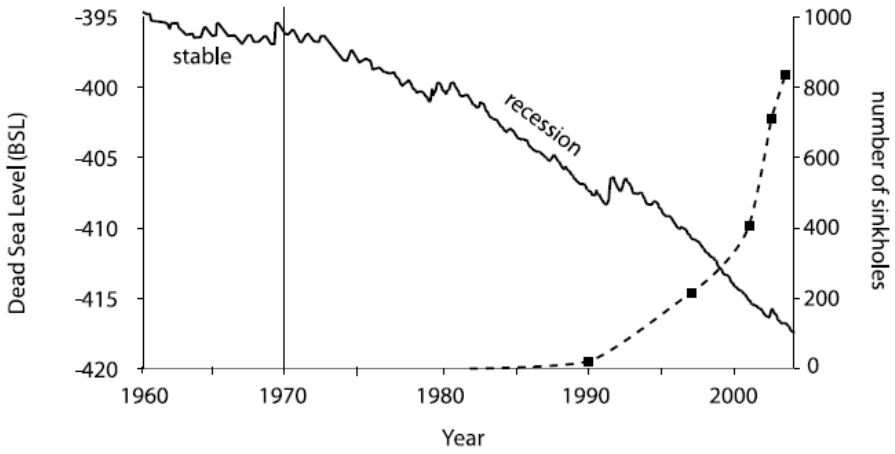

Figure 15-10-50

Figure 15-10-50 shows that Dead Sea level (solid line) and number of sinkholes at the western shore of the Dead Sea (dashed line).

Reasonable combination of various model parameter including flux, hydraulic head change, porosity-permeability relation, and salt layer

thickness can reproduce the observed rate and pattern of sinkhole formation. This strongly supports the mechanism of salt dissolution as a major process that controls sinkhole formation. Dissolution of a salt layer as a result of water level recession is shown to be a plausible mechanism to explain the fast creation of sinkholes at the western shore of the Dead Sea over the past 30 years. The recession of the Dead Sea level causes a recession in the groundwater level and in the fresh/saline water interface.

However, according to CFLR theory, major cause of the recession of the Dead Sea level is inertial interaction of the Earth.

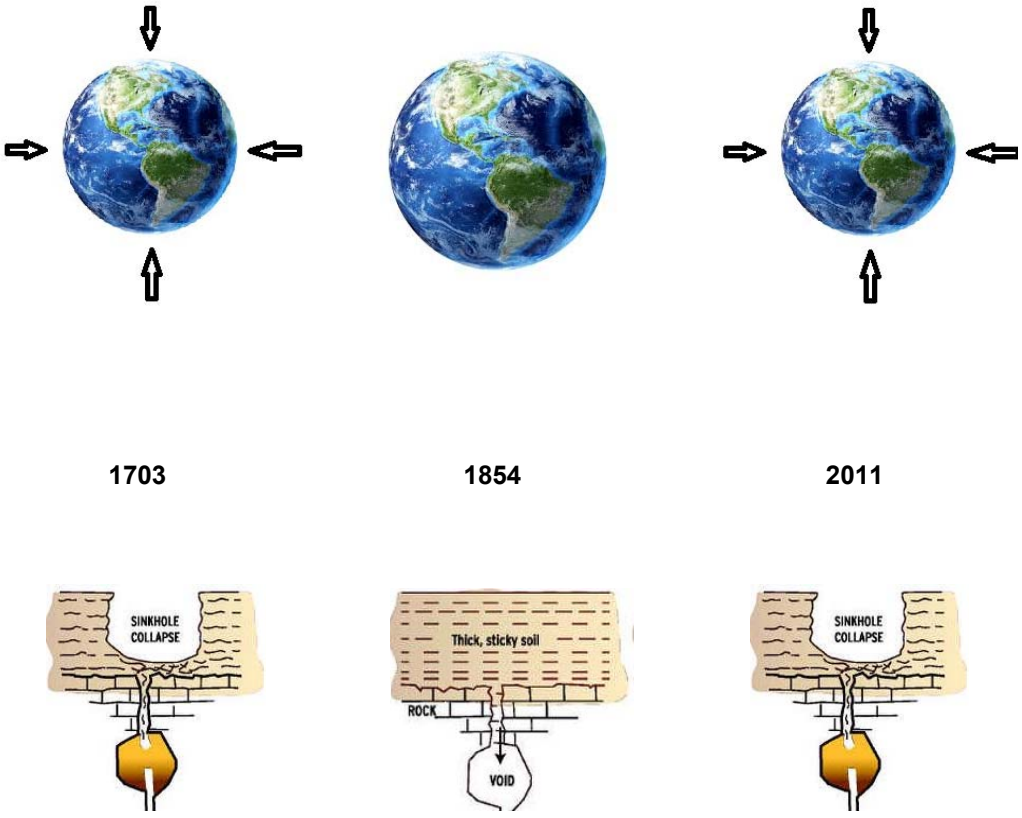

Figure 15-10-51

Figure 15-10-51 shows clearly that important cause of the recession of the Dead Sea level. Such water level change is not strange phenomenon, but also well known related phenomenon of earth quakes

in Japan. Here, important point is that the recession of the Dead Sea level is associated global swelling and collapsing of the Earth. Because Earth of 2011 is collapsing down than Earth of 1854, is changed water level of the Dead Sea. Therefore, major cause of sink holes should be collapsing Earth by periodical inertial interaction. Therefore, sink hole can be called sink quake.

During swelling and collapsing of the earth, earth's atmosphere is swelled and collaped too. Because of this volume change is changed globally heat energy density of the air and water density of the soil periodically like Dead Sea level. Therefore, global drought is occurred periodically.

That is

$$\boldsymbol{P_{drought}} = \frac{\mathbf{157.03}\boldsymbol{yrs}}{\mathbf{1.2655}}$$

$$= 124.09 \text{ yrs}$$

$$\approx 124 \text{ yrs} \qquad \text{15-10-57}$$

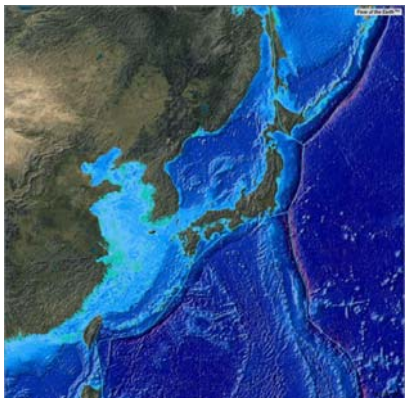

Japan and Korea

Figure 15-10-52

where 1.2655 that is needed for net influence at air from inertial energy to calculate, is constituted

1.2655= (1.202) (1.010892) (1.033548) (1.007068) (1.000589)

15-10-58

1.202 is keplerian missing factor from Earth's force line curve. x_g = 1.010892 is the gravitational permittivity of seawater for seawater evaporation. $x_{gair} = 1.033548$ is gravitational permittivity of air at $g = 2$. x_{eair} = 1.007068 is electrical permittivity difference of air at $g = 8 \times 1.5$. $x_{eair} = 1.000589$ is electrical permittivity of air at $g = 1$.This result means that this maximum average period can be used to analyze the periodicity of drought for a given observed area. Such periodicity of drought and related bad harvests can be calculated and proven in South Korea, which has an over 2000-years-long national historical document about drought and bad harvest.Calculated value of extreme drought period by historical record in Korea by H.R Byun is

$P_{drought} \approx 124$ yrs 15-10-59

H.R .Byun who is professor of atmospheric environmental research institute in Pukyong national university in South korea and pre president of Korean meteological society, report in "Study on the periodicities of Drought in Korea" as that Five kinds of drought periodicities in Korea were found. The extreme droughts with 124 years interval, severe droughts with 38 years interval, disappear of Changma with 12 years interval, Normal droughts in somewhere in Korea with 6 years interval, and abrupt occurrence of droughts were found in this study.The extreme droughts in 1901 were found to have relations with the decay of Chosun dynasty. The severe droughts shown two waves; the second one comes 5 years after first one. These three waves were found to come together to Korea after 2012.Summer droughts in Korea were found to occur after heavy precipitation over Tailand at January. With this tele-connection, summer droughts became to be possible to predict.Along the fact that there have been no droughts in Europe where they have many ice caves, the science of ice were investigated, and finally the method suppressing evaporation over water body were designed and patented. By S.O.Youn and S.I. Hwang in " Drought Study in Records of Samguk saki" on natural

hazards such as droughts, floods, smallpox and attacks of grasshoppers are analyzed during the Ancient Times(BC 57~AD 935), they report as that Records on natural hazards such as droughts, floods, smallpox and attacks of grasshoppers are classified and analyzed during the Ancient Times(BC 57~AD 935) based on the Historical Records of the Three Kingdoms Age(Samguksaki main record), and influences on human activities and relationships of each natural hazard are studied. The strongest influences on the agricultural productivity were the drought and the influences of floods were weak. The most floods were not destructive hazards because the cultivated lands were distributed in the valley plains and the towns and villages were constructed in the area free from the floods during the Ancient Times. The attacks of grasshoppers have the high frequencies with the droughts. The smallpox of the Ancient Times has no relationships with the dearth, floods and droughts. This means that the waterborne infections happened periodically and after the unification, the infectious diseases happened continuously due to the urbanization leading the concentration of population on the capital. Two cycles of droughts are recognized, and they happened with the time intervals of approximately 500 years during approximately 1000 years in Shilla dynasty. And their another research in “Drought Study of Korean Medieval Times”, they report as that the natural hazards such as droughts, floods and frost injuries, and their relationships with the social unrest phenomena such as years of famine, smallpox and revolutions during the Medieval times (AD 936~1391) in Korea are compared and analyzed based on the History of Goryeo containing astronomical weather and climate events during the Goryeo Dynasty. Among the natural hazards during the Goryeo Dynasty, the droughts with a period of 4~5 years on average are recorded most frequently. By time series analysis, the most frequency of droughts can be found in AD 286~335, AD 786~835 and AD 1261~1320 during the Ancient and Medieval times. It is suggested that three cycles of the droughts during approximately 1,500 years of the Ancient and Medieval times are recognized and they had happened with the time intervals of approximately 500 years. The frequency of droughts increased in the late Goryeo Dynasty is consistent with those of the social chaos factors such as years of famines, smallpox and revolutions. These records suggest that the natural hazard such as years of famines was one of the most important factors influencing on the collapse of the Goryeo Dynasty, agrarian country.

5.11 Solving Origin of Pulsars Emission, Jet and Glitch from Neutron Stars by CFLE theory

Everybody can say that A pulsar (short for *pulsating radio star*) is a highly magnetized, rotating neutron star that emits a beam of electromagnetic radiation. This radiation can only be observed when the beam of emission is pointing toward the Earth, much the way a lighthouse can only be seen when the light is pointed in the direction of an observer, and is responsible for the pulsed appearance of emission.

However, as "The theory of how pulsars emit their radiation is still in its infancy, even after nearly forty years of work" said Werner Becker (the Max Planck Institute for Extraterrestrial Physics, Garching, and Germany) in 2006, there are many models about pulsar emission but no generally accepted theory.

However, CFLE theory can explain about emission of Pulsars.

Answer by CFLE theory is that physical essence of pulsar emission is same physical essence of coronal mass ejection of the Sun.

Because of strong gravity and its gravito magnet field of Neutron star jet or beam can be radiated only $\pm z$ direction (South and North magnetic main poles) by inertial pole jumping as figure 15-11-1.

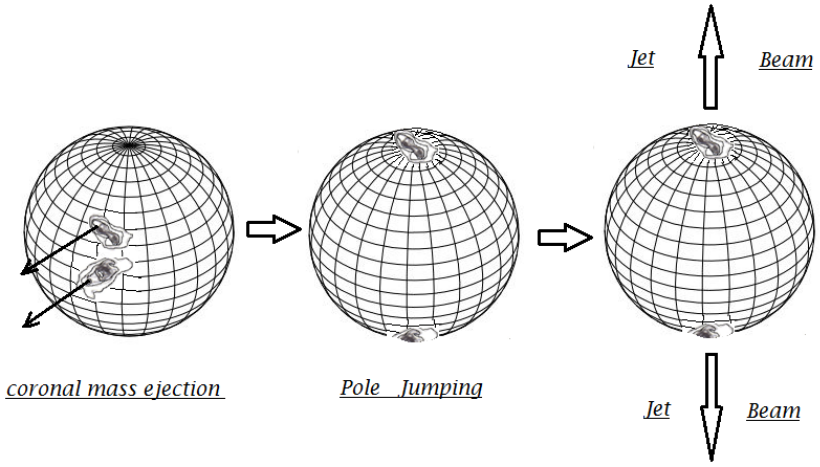

Figure 15-11-1

Such physical essence can apply to active galaxy as figure 15-11-2

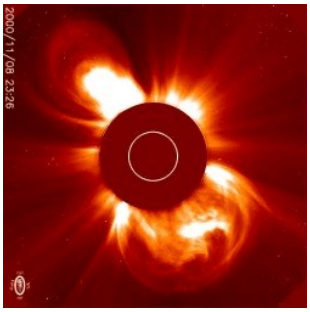

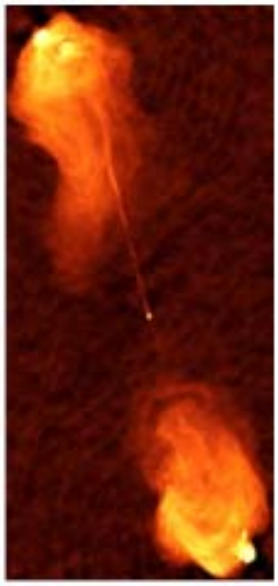

Solar mass ejection

2000.11.08.23:26

Active nulcleus of 3C405

AUI Perley et al 1984

Figure 15-11-2

Nevertheless coronal loops of the sun have magnetic polarity, they didn't move to magnetic main poles, because sun's magnetic field is weak.

However, coronal loops of the pulsar, they have to move to magnetic main poles by strong gravity and its gravito magnetic field.

Equatorial coronal mass ejection of pulsar is hold down by strong gravity of pulsar. Same time polarities of main poles attract magnetic coronal loops of pulsar.

Therefore, coronal mass ejection of pulsar becomes jet and beam of pulsar that is ejected $\pm$ z direction or SN magnetic main poles as figure 15-11-3.

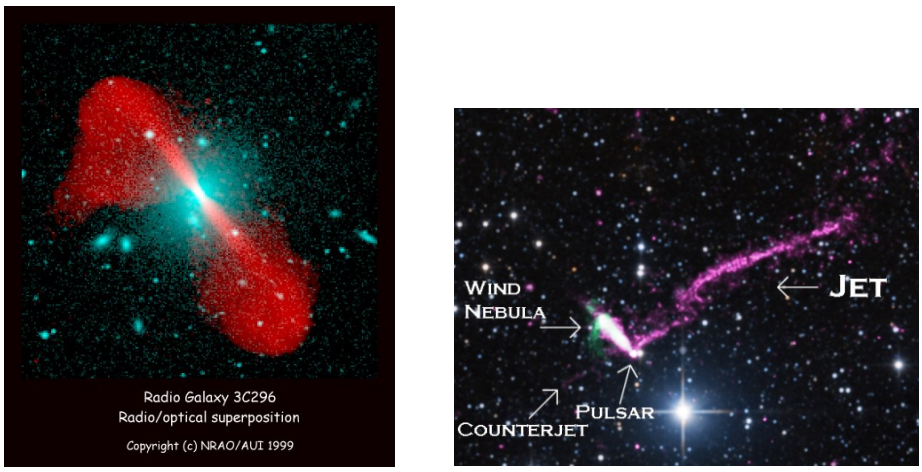

Figure 15-11-3

Pulse and Glitch analyze give us certain confirmation that jet or beam of the pulsar is same phenomenon of coronal mass ejection of the Sun.

For some pulsars, including the Crab Nebula's, astronomers can detect a main pulse and an inter pulse. By by J.A. Eilek & T.H. Hamkins at New Mexico Tech, Socorro NM,USA are founded that in the Crab Nebula pulsar, the main pulse is characterized by extremely short, powerful bursts, whereas the inter pulse is broad and smooth.

The main pulse can last just four-tenths of a nano second. These so-called nano shots are believed to be produced by small plasma clouds in the pulsar's atmosphere that are only 5 inches (12 centimeters) wide.

The inter pulse, meanwhile, makes radio emissions unlike any that have been detected before from a pulsar.

This irregularity, as well as the difference between the main pulse and inter pulse, cannot be explained by existing pulsar models.

Astronomers said “The inter pulse's emission is one of the weirdest things. There's definitely something extremely odd happening with the Crab pulsar."

According to T.H. Hankins, an additional polar element could be causing the unusual emission. This is a very violent explosion, and these extra poles could be remnants from when the pulsar was actually formed a thousand years ago.

So how could an additional set of poles have formed?

Answer by CFLE theory is Pole Jumping by strong gravito magnetic SN main pole of pulsar as figure 15-11-1.

Because magnetic strength of pulsar pole is stronger than magnetic strength of suns pole, pulsar pole can attract strong magnetic pulsar spots as figure 15-11-4.

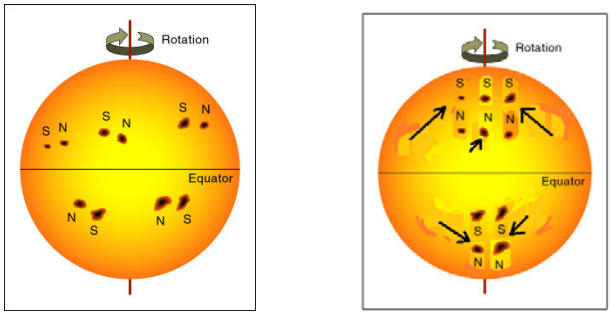

Sun spots **Pulsar spots**

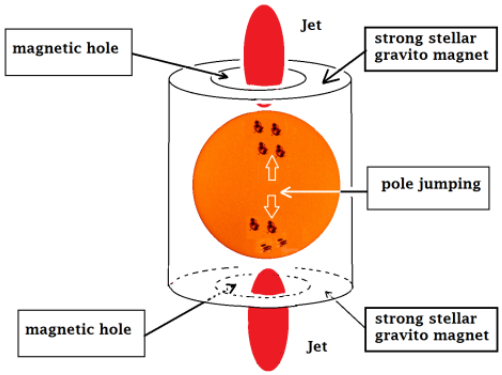

Figure 15-11-4

Because, pulsar is surrounded strong stellar gravito magnet, jets can be emitted only pole areas where strong magnet neutralize by pole jumping and magnet strength become weakest on the pulsar.

By such physical base we can explain every characteristic properties of main pulse (MP) from inertial poles of pulsar spots and inter pulse (IP) from main poles of pulsar.

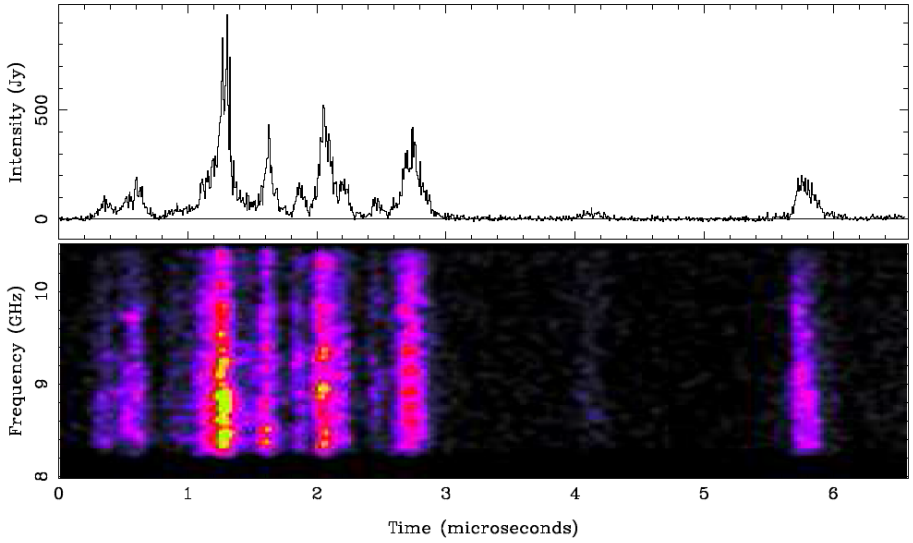

Figure 15-11-5

An occasional giant MP as figure 15-11-5, however, consists of many short-lived nano shots, which are well separated enough to individually resolved as figure 15-11-6

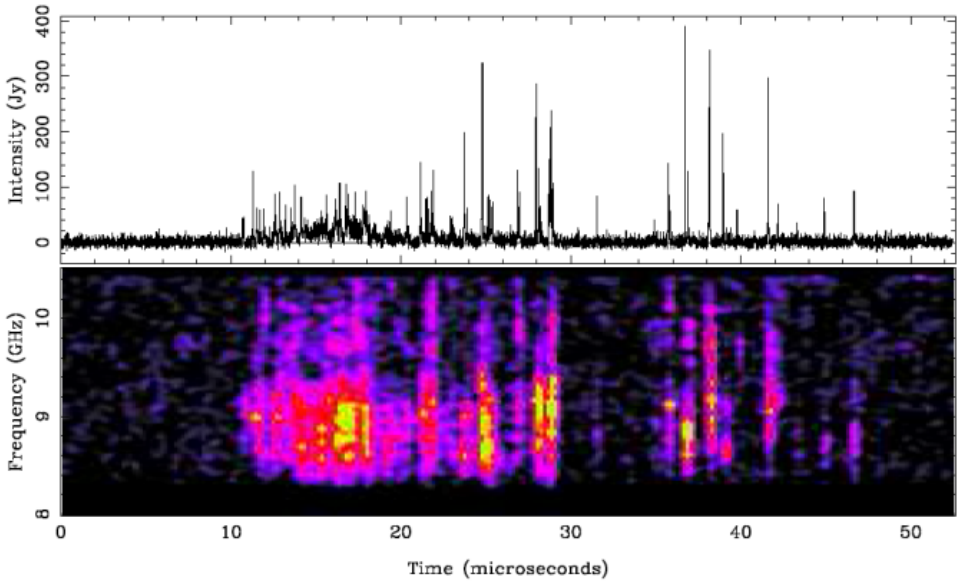

Figure 15-11-6

Most giant MPs consist of several micro bursts, as shown here. The total intensity is plotted with time resolution 6.4 ns. The dynamic spectrum is plotted with 19.5 MHz spectral resolution and 51 ns time resolution. This and all data shown were observed at Arecibo and

coherently dispersed. Several micro bursts of MP of pulsar corresponds several coronal mass ejections of the Sun

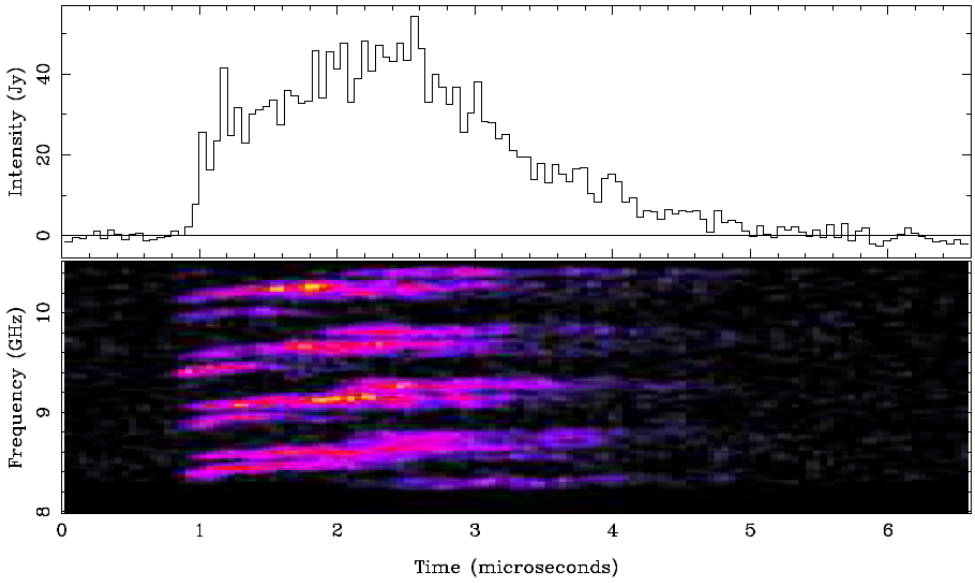

Figure 15-11-7

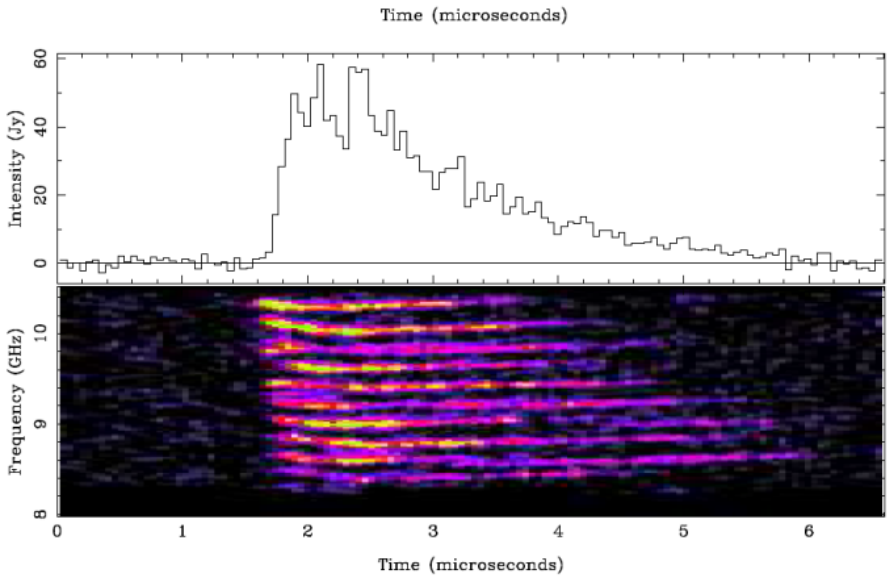

Figure 15-11-8

Figure 15-11-7 and 15-11-8 shows two typical giant IP. The dynamic spectrum of IP contains several sets of emission bands, each of which last a fewμs. These bands appear in every giant IP, but not in giant MPs observed at the same times. Time resolution is 6.4 ns. Dynamic spectral resolution is 19.5 MHz and 52 ns.

This emission is occurred by main poles of pulsar.

Inter pulse of pulsar corresponds solar usual emission (time independent and frequency unchanged).

Main pulse of pulsar corresponds solar flare and sun spots (time defendant .frequency changed).

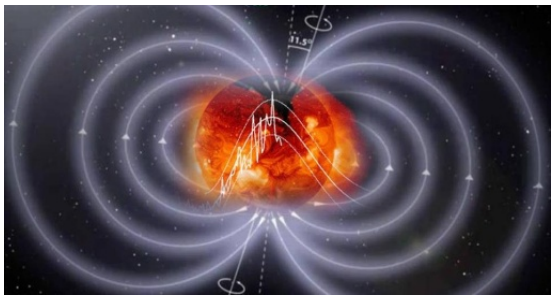

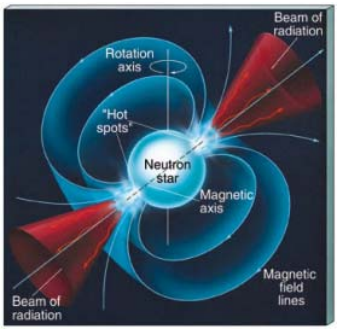

Inter pulse state: Sun **Pulsar**

Figure 15-11- 9

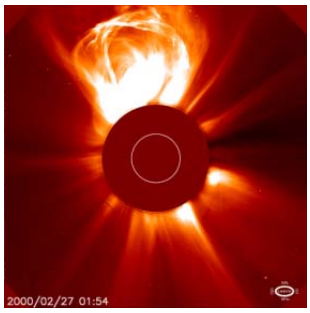

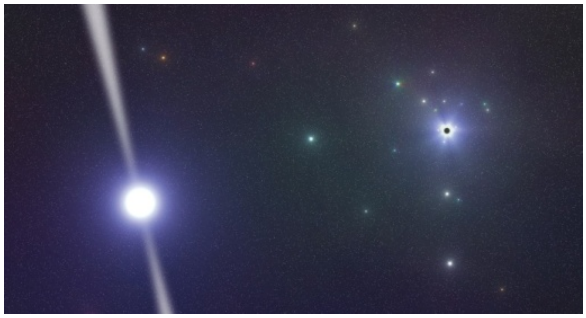

Main pulse state: Sun **Pulsar**

Figure 15-11-10

All of such phenomena of pulsar can be said simply that strong gravity and its gravito magnet of pulsar crush all of activity of emission. Only

permitted passage for radiation is $\pm z$ direction (SN main poles) where there gravity is weakest in the pulsar as figure 15-11-10 shows.

Finally speaking, pulse analyze give us certain confirmation that Jet or beam of the pulsar is same phenomenon of coronal mass ejection of the Sun.

A glitch is a sudden increase (up to 1 part in 10^6) in the rotational frequency of a rotation-powered pulsar, which usually decreases steadily due to braking provided by the emission of radiation and high-energy particles.

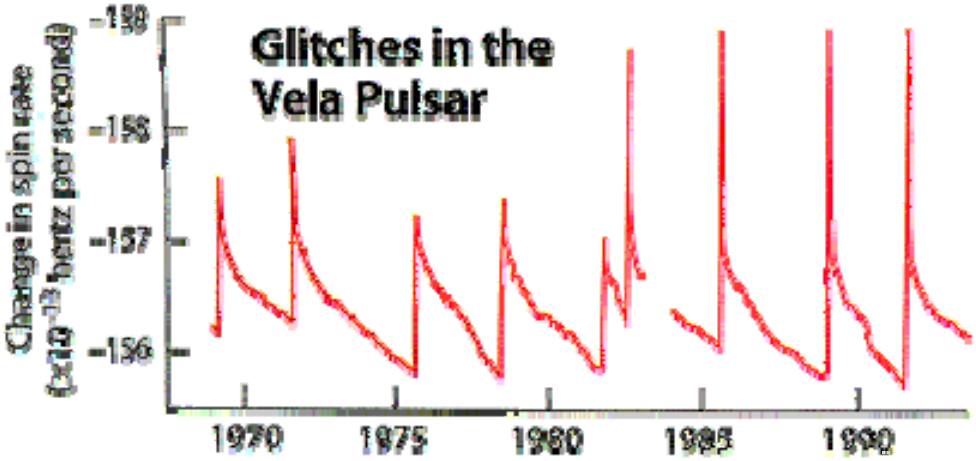

Courtesy Pulsar Astronomy by Andrew G. Lyne and Francis G. Smith

Figure 15-11-11

Following a glitch is a period of gradual recovery where the observed periodicity slows to a period close to that observed before the glitch. These gradual recovery periods have been observed to last from days to years. Currently, only multiple glitches of the Crab and Vela pulsars have been observed and studied extensively.

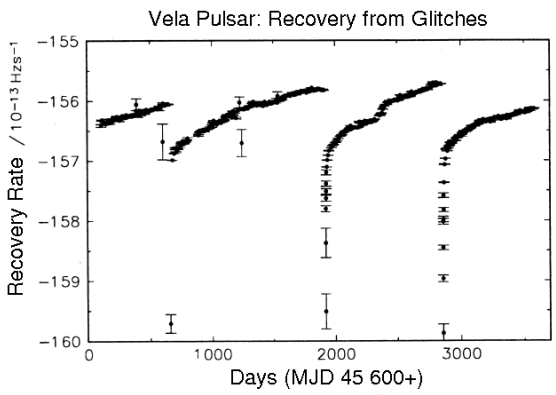

Image courtesy of Claire Flanagan by the HartRAO 26m Telescope

Figure 15-11-12

While the exact cause of glitches is unknown, they are thought to be caused by an internal process within the pulsar. This differs from the steady decrease in the star's rotational frequency which is caused by external processes. The details of the glitch process are unknown.

Astronomers have observed lots of glitches in pulsars, and they all behave in a similar way.

However, the Nature article presents an observation of an anti-glitch. In other words, researchers observed a rapid slowdown in particular magnetar. Scientists focused on the magnetar 1E 2259+586, located about 10,000 light-years from Earth in the constellation of Cassiopeia, using NASA's Swift observatory to watch it from July 2011 to mid-April 2012. Ordinarily, the magnetar completed a revolution every seven seconds, but the researchers discovered it had later slowed by 2.2 millionths of a second. They looked at the data and were shocked, because the neutron star had suddenly slowed down. The slowdown of this magnetar actually happened in two stages. There was an initial anti-glitch, and then a second shift that could be modeled as a glitch or a second anti-glitch.

Some existing models of neutron star glitches cannot explain some of the behavior astronomers have seen from them.

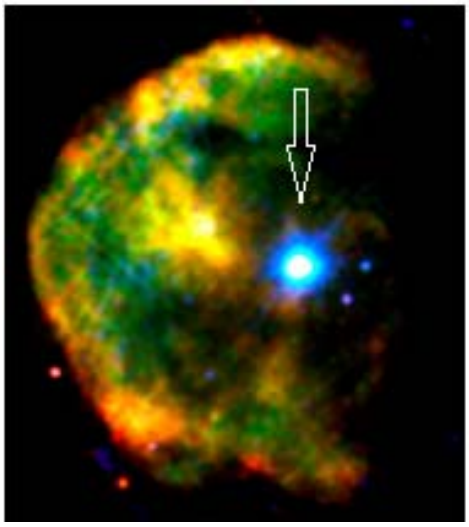

The magnetar 1E 2259+586 shines a brilliant blue-white in this false-color X-ray image of the CTB 109 supernova remnant, which lies about 10,000 light-years away toward the constellation Cassiopeia. by the European Space Agency's XMM-Newton satellite in 2002. Credit: ESA/XMM-Newton/M. Sasaki et al.

Figure 15-11-13

However, CFLE theory can explain glitch and anti glitch easily.

According to CFLE theory glitch is same phenomenon of inertial interaction between sun's orbital revolutional mass current and sun's rotational mass current. This is cause of sun's activity.

During active period sun's volume is changed like Earth as figure 15-10-12.

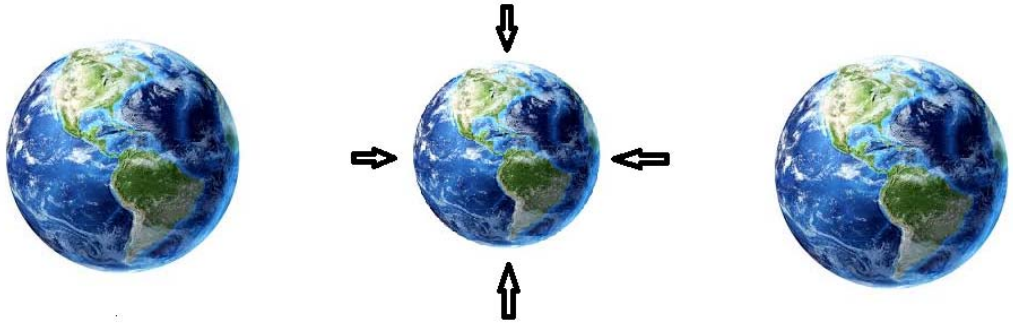

Figure 15-10-12

Because, glitch is same phenomenon of sun's activity according to CFLE theory, rotation speed should be faster than before according to conservation's low of angular momentum as figure 15-11-14.

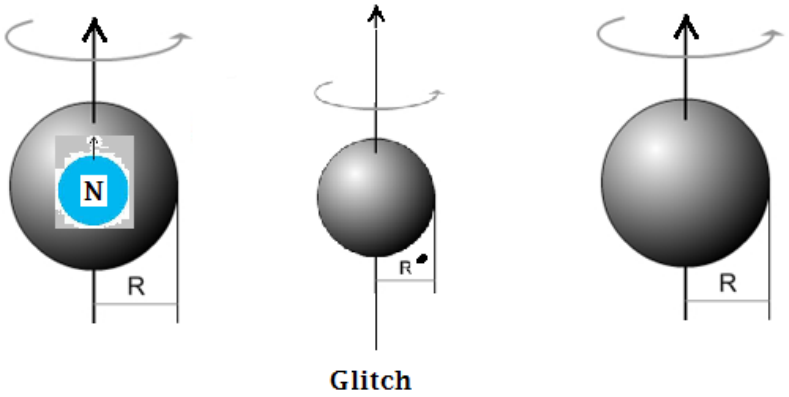

Figure 15-11-14

In this time rotation spin of pulsar $\uparrow_{pulsar}$(up-spin) and intrinsic spin of constituent neutron $\uparrow_{neutron}$(up-spin) is same as figure 15-114.

However, in case of anti glitch rotation spin of pulsar $\uparrow_{pulsar}$(up-spin) and intrinsic spin of constituent neutron $\downarrow_{neutron}$(down-spin) is different as figure 15-11-15

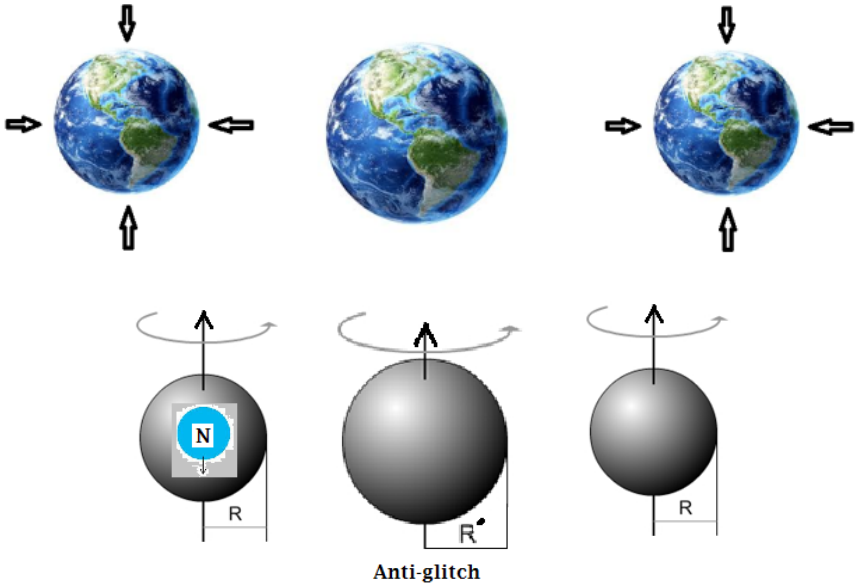

Figure 15-11-15

Because, down-spin of constituent neutron disturbs up-spin of pulsar rotation, volume of pulsar should be bigger than before as figure 15-11-15. Therefore, it is appeared sudden slow down of rotation speed according to conservation's law of angular momentum.

Because quantity of spin of constituent neutron is not constant according to Pauli's exclusions principle, glitch activity cycle is changed as figure 15-11-16.

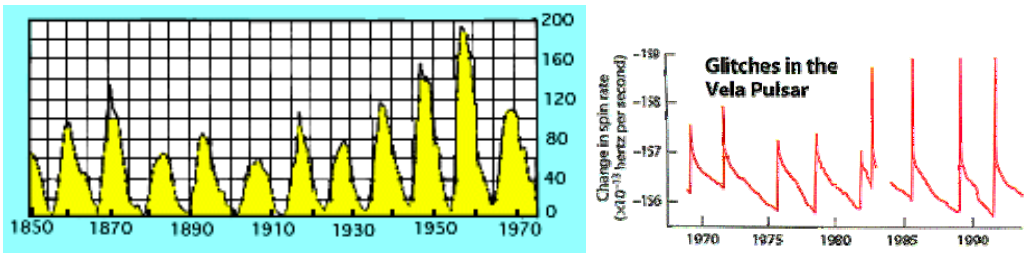

Sun's activity cycle **Glitch activity cycle**

Figure 15-11-16

When quantity of up-spin of constituent neutron is enough, rotation speed of pulsar should be faster and activity period should be shorter. When quantity of up-spin of constituent neutron is small, rotation speed of pulsar should be slower and activity period should be longer.

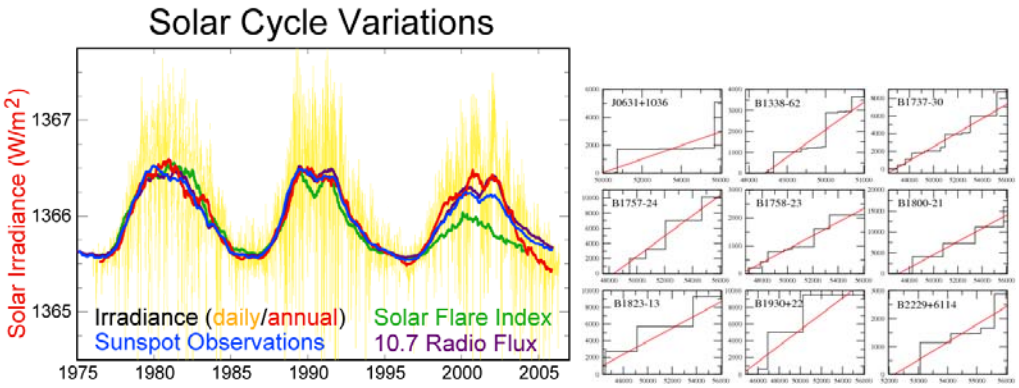

Solar and Glitch Cycle Variation

Figure 15-11-17

Sun's activity cycle is almost regular. But glitch cycle is not regular, because rotation speed of pulsar is very fast and quantity of up-spin of constituent neutron is changed very sensitively.

Finally speaking glitch analyze too give us certain confirmation that inertial interaction of the sun and inertial interaction of pulsar produce qualitatively same phenomena.

15.12 Supplementary Data Analysis of Gravity Probe B and its Meaning by CFLE Theory

As discussed in §1.1, Schiff's formula of classical relativity can be used to predict the geodetic effect and dragging effect:

$$\Omega = \frac{3}{2}\frac{G}{C^2R^3}\frac{M}{(R\times V)} + \frac{G}{C^2}\frac{I}{R^3}[(\omega R) - \omega] \qquad 15\text{-}12\text{-}1$$

where G is the Newtonian gravitations constant, I is the inertial moment, and ω is the angle speed. The first term is the geodetic effect, and the second term is the dragging effect. When the orbital distance is 642 km, the predicted value of the geodetic effect is

$E = -6{,}606.1$ marc-s/year 15-12-2

whereas the predicted value of the dragging effect is

$E = -39.2$ marc-s/year 15-12-3

After data analysis by C.W.F Everitt et al in 17, May.2011, the observed values taken with 4 gyroscopes were

concluded to be

$E = -6{,}601.8 \pm 18.3$ marc-s/year 15-12-4

whereas the observed value of the dragging effect is

$E = -37.2 \pm 7.2$ marc-s/year 15-12-5

Table 15-12-1

source	γNS(mas/yr)	γWE(mas/yr)
Gyroscope 1	-6,558.6±31.7	-41.3±24.6
Gyroscope 2	-6,707.0±64.1	-16.1±29.7
Gyroscope 3	-6,610.5±43.2	-25.0±12.1
Gyroscope 4	-6558.7±33.2	-49.3±11.4
Joint	**-6,601.8±18.3**	**-37.2±7.2**
GR prediction	**-6,606.1**	**-39.2**
Toatal Stat + Sys	18.3	7.2

These values are not wrong, but at the same time they are not accurate enough, because the accuracy of this experiment was designed as 0.5 marc-s/years.

However, the classical theory of relativity cannot explain this defective result.

But, CFLE theory can explain exactly what the reason of this difference is. Because the rotor of the gyroscope was coated with niobium and its magnetic field was measured, the electrical permittivity needs to be considered. That is

$$E = (-6{,}601.8 \quad \text{marc-s/year})(1.000589)$$

$$= -6{,}605.7 \quad \text{marc-s/year} \qquad 15\text{-}12\text{-}6$$

Now, difference between prediction and experiment is

$$d_E = \left(-6{,}606.1 \quad \text{marc}\frac{\text{s}}{\text{year}}\right) - (\ -6{,}605.7 \quad \text{marc-s/year})$$

$$= -\ 0.4 \quad \text{marc-s/year} \qquad 15\text{-}12\text{-}7$$

This value now agrees with that accuracy goal of this experiment

$0.4 < 0.5$ marc-s/years.

With this result we can agree as acceptable result from expensive, hard and long term experiment about geodetic drift rate.

However, because for frame-dragging drift rate to observe the experiment was performed in the orbit of Earth, there exists a difference of as much as the gravitational permittivity of air. Therefore, the final value is

E = (−37.2 marc-s/year)(1.050352)

= −39.07 marc-s/year 15-12-8

where factor of 1.050352 of gravitational permittivity of air at Earth surface is

$$Q_{ga} = 0.016774 \times 3.002 = 0.050352$$

$$x_g = 1.050352 \quad \text{15-12-9}$$

where factor of 3.002 is force line curve of air at earth surface $g = 2$ and correspondence number between gravity and electricity $c_c = 1.5$ and electrical permittivity of air at earth surface $x_e = 1.000589$

$$f_n = (2)(1.5)(1.000589) = 3.002 \quad \text{15-12-10}$$

Now, difference between prediction and experiment is

$$d_E = (-39.2 \ \text{marc} - \text{s/year}) - (-39.07 \ \text{marc-s/year})$$

$$= -0.13 \ \text{marc-s/year} \quad \text{15-12-11}$$

This value now agrees with that accuracy goal of this experiment

$0.13 < 0.5$ marc-s/years.

With this result we can satisfy as agreeable result from expensive, hard and long term experiment about frame-dragging drift rate.

Therefore, CFLE theory provides assurance that this experiment "Gravity Probe B," designed and operated for 50 years was successful as one experiment.

However, same time experiment of Gravity Probe B shows clearly that Einstein's general relativity is wrong, because predictions value and observations value of very important frame dragging effect too big.

Difference is

$$d_E = (-39.2 \ \text{marc} - \text{s/year}) - (\ -37.2 \ \text{marc-s/year})$$

$$= -2 \ \text{marc-s/year} \qquad \text{15-12-12}$$

This value is too big as much as factor of

$$R_d = \frac{2marc-s/yr}{0.5marc-s/yr} = 4 \qquad \text{15-12-13}$$

This discrepancy says "Space time is not curved as Einstein's general relativity predict."

Scientists of old age need recognize about this fact, because they don't know what means result from accuracy of GP-B.